SICA, VINCENT P., Ph.D. Applications of Mass Spectrometry Surface Sampling Techniques towards Natural Products Research. (2016)
Directed by Dr. Nicholas H. Oberlies. 180 pp.

Since the pharmaceutical industry has experienced a decline in output over the past decade, natural products research has regained interest. The complexity and molecular diversity seen in nature remains unmatched, even against combinatorial chemistry. However, this re-approach to natural products will look different from our predecessor's, since advancements in technology provide higher-throughput screening, innovative structure-guided fractionation, and chemical visualization. The recent development of ambient ionization techniques for mass spectrometry can assist in the revival and sustainability of natural products research for drug discovery. The goals of the project sought to explore natural products *in situ* using ambient ionization mass spectrometry in three ways: (1) visualize the chemical ecology, (2) implement higher-throughput screening while maintaining high content analysis, and (3) elucidate the chemical entities.

Aim 1 was achieved by utilizing desorption electrospray ionization (DESI) and the droplet-liquid microjunction-surface sampling probe (droplet-LMJ-SSP) by performing mass spectrometry imaging and mapping experiments to understand the spatial and temporal distributions of secondary metabolites. This information, which is lost through the traditional extraction protocols, can provide deep insight into the chemical ecology that takes place between organisms. The effects that herbicidal and fungistatic metabolites have on their environment were visualized via mass spectrometry imaging and mapping experiments.

Aim 2 was achieved by coupling the droplet-LMJ-SSP with UHPLC–PDA–HRMS/MS, thus regaining the mutually supportive data that is typically lost through ambient ionization, such as UV data, retention time, and chromatographic separation. The pre-existing database of over 300 fungal secondary metabolites was implemented at least six weeks earlier in the drug discovery process by screening fungal cultures directly from the Petri dish. This new methodology sacrificed none of the data that would be lost using other ambient techniques.

Aim 3 was achieved by exploring a suite of analytical techniques to characterize secondary metabolites *in situ*. Techniques such as post-column lithium infused chromatography, HRMS/MS fragmentation patterns, and mass defect filtering were all possible, since the droplet–LMJ–SSP incorporates liquid chromatography and traditional electrospray ionization. The structural class known as acetogenins was used to highlight this ability by differentiating between analogues and isomers, while elucidating their structures *in situ*.

APPLICATIONS OF MASS SPECTROMETRY SURFACE SAMPLING TECHNIQUES TOWARDS NATURAL PRODUCTS RESEARCH

by

Vincent P. Sica

A Dissertation Submitted to
the Faculty of The Graduate School at
The University of North Carolina at Greensboro
in Partial Fulfillment
of the Requirements for the Degree
Doctor of Philosophy

Greensboro
2016

Approved by

Nicholas H. Oberlies
Committee Chair

To my loving
wife, Erica. I truly could
not have done any of
this without
you

APPROVAL PAGE

This dissertation, written by VINCENT P. SICA, has been approved by the following committee of the Faculty of The Graduate School at The University of North Carolina at Greensboro.

Committee Chair Nicholas H. Oberlies

Committee Members Nadja B. Cech

Norman H. Chiu

Mitchell P. Croatt

Date of Acceptance by Committee

May 19, 2016
Date of Final Oral Examination

ACKNOWLEDGMENTS

This research was supported in part by the Biotechnology Research Grant from the North Carolina Biotechnology Center (2011-BRG-1206) and a grant from the United States Department of Agriculture (NIFA 2012-33610-19523).

Drs. Vilmos Kertesz and Gary Van Berkel, for inspiration and guidance with the droplet-LMJ-SSP. Drs. Nadja Cech, Norman Chiu, and Mitchell Croatt, for serving as my committee. Drs. Daniel Todd and Brandie Ehrmann, for mass spectrometry training and advice. Tyler Graf, for training in operating and repairing instrumentation. Drs. Huzefa Raja and Cedric Pearce, for mycological assistance and support. Drs. Tamam El-Elimat and Mario Figueroa, for general laboratory training and mentoring. Dr. Nicholas Oberlies, for providing me the opportunity to conduct this research, and for his endless advice and support

TABLE OF CONTENTS

Page

LIST OF TABLES

Page

LIST OF FIGURES

Page

CHAPTER I

INTRODUCTION

Background

The rewards from natural products research for drug discovery over the past 30 years are well established,[1] including 50% of all small molecule new chemical entities, 79% of new small molecule anticancer drugs, and 68% of the small molecule anti-infectives. In spite of these statistics, natural products remain underexplored with combinatorial chemistry and genome sequencing still prominent, even though there are major issues with combinatorial chemistry, such as the lack of structural diversity, solubility issues, and poor selectivity. However, despite this trend towards new, innovative discovery methodologies, there has been a growing concern in the decreased pharmaceutical output.[2]

In addition to the combinatorial chemistry issues mentioned, the recent decreased output of successful drug discovery can be, in part, attributed to the shift from the 'function-first' to the 'target-first' methodologies in the pharmaceutical industry, the former being part of the natural product approach.[2] The 'Function-first' approach revolves around finding active compounds, and then understanding the mechanism of action, while 'target-first' screens compounds that bind or inhibit a target, then tests for activity later. The latter approach has led to attrition in marketable drugs being produced.[3,4] Unlike synthesized compounds, natural products often possess highly

selective and specific biological activities stemming from the hypothesis that essentially all natural products have some receptor-binding activity.[5]

Natural products are often viewed as a tapped resource, but this continues to be proven untrue. Fungi alone are a testament as to how much potential remains in nature. Conservative estimates are that at least 1.5 million fungal species exist with estimates as high as almost 10 million,[6] yet only 75,000 have been described in literature.[7] Drugs such as caspofungin[8] and fingolimod[9] continue to breathe new life into fungal natural products research, but they only touch the surface of the true potential of this field. Our recent research of fungi has already proven fruitful with several new classes of compounds discovered.[10,11] This continued success could persuade industry to refocus some energy back into natural products, since more and more new, bioactive compounds are identified daily.

Importance

Fungi are an opportunistic avenue of natural product drug discovery. Most fungi are phylogenetically affiliated to the phylum Ascomycota, the most speciose members within the fungal kingdom,[12] and are among the most prolific producers of bioactive natural products.[13,14] As of 2005, these fungi generated about 8,600 (38%) of the roughly 22,500 bioactive secondary metabolites isolated from microorganisms.[15,16] From an ecological standpoint, fungal communities are also widely diverse, even in a micro-scale setting,[17] resulting in many fungal interactions.[18] The aims of this project sought to support this notion and provide a visualization of the interactions between the bioactive compounds of fungi.

Species richness is another important factor in finding diverse classes of compounds, and therefore, obtaining a large number of isolates increases the likelihood of discovering new chemistry. A single fungal species will often produce of the same metabolites.[19] For example, 85 isolates of *Penicillium expansum* were examined and all produced the compounds chaetoglobosin A, roquefortine C, and communesin along with many other compounds with high percentage isolation rates.[20] Since diversity of fungal isolates is important to increasing the opportunity for new compound discovery, the selected fungal cultures for this project stemmed from two main sources covering a wide range of diversity: the Mycosynthetix library (55,000+ strains) and the UNCG library (800+ strains).

Experimental

Desorption electrospray ionization (DESI) is a mass spectrometry technique that facilitates the detection of compounds under ambient conditions.[21,22] By spraying charged droplets onto a sample, compounds are desorbed from the surface, ionized, and then sent into the MS for analysis.[23] By ionizing with little destruction, the sample can not only remain in its native environment, but it can also be reanalyzed repeatedly.[24] Since the inception of DESI, the applications to utilize this technique have grown substantially, including the high-throughput screening of pharmaceuticals,[25,26] environmental analysis,[27] food safety testing,[28] forensics,[29-31] and biological analyses. [32,33] In the realm of natural products, DESI-MS is becoming a prominent technique for the detection of compounds directly on the surface.[34] A notable early account displayed the detection of the anticancer drug, camptothecin, directly from the bark of *Nothapodytes nimmoniana*.[35]

Mass spectrometry imaging has become a popular technique in natural products due to its ability to visualize the spatial distribution of secondary metabolites across an organism [36]. Historically, matrix assisted laser desorption/ionization (MALDI) has been the prominent technique for this purpose. MALDI imaging has been applied towards the study of plants,[37] marine cyanobacteria,[38] sponges,[39] and fungi.[40] More recently, the shift towards ambient, less abrasive techniques, such as DESI has grown in popularity. The works of Janfelt and Kubanek have displayed mass spectrometry imaging (MSI) of secondary metabolites on terrestrial[41,42] and marine[43,44] organisms through indirect and direct surface analysis via DESI, while the accomplishments of Dorrestein have demonstrated the ability to directly analyze metabolites in microbiota via nanoDESI.[45-47]

However, direct fungal culture analysis via DESI-MS has been very limited,[48] and none have directly analyzed an unaltered culture. This may be due to the challenges that must be overcome for effective DESI-MSI on direct fungal cultures. First, pressures from the solvent spray and gas can manipulate the surface of the media. Therefore, a firm and flat surface is required for effective and consistent ionization, something that the media does not provide naturally. Second, the fungal topography is naturally uneven and often contains mycelium and spores that freely move. Finally, DESI-MS, as with other direct mass spectrometry techniques, loses the mutually supportive information that is collected via traditional LC-MS, such as retention time and UV data.

The droplet–liquid microjunction–surface sampling probe (droplet–LMJ–SSP) overcomes many of these issues by being less abrasive, amenable to surface sampling of uneven planes, and incorporates chromatography. This technique performs

microextractions on the surface of a sample causing little damage to the culture itself, therefore affording spatial and temporal studies of fungal interactions. The inclusion of chromatography allows for the separation of complex mixtures that can be found in fungi and plants. Furthermore, it allows the identities of the detected compounds to be confirmed with standards using retention time, UV data, HRMS, and MS/MS fragmentation patterns.

Both techniques were explored with the intent of understanding the chemical ecology that takes place in situ via mapping experiments. A prominent example of can be seen in literature by Dorrestein and colleagues. A bacterial strain that produces antifungal metabolites was co-cultured with various fungi. Using MALDI mass spectrometry imaging, the fungal secondary metabolites can be seen decreasing in areas where the fungi and bacteria are adjacent, while the bacteria continue to grows in all directions regardless of the adjacent fungi.[49] The work herein used similar studies but using less destructive techniques such as DESI and the droplet–LMJ–SSP.

Conclusion

To date, few mass spectrometry mapping experiments have been performed to examine fungi, whether it be standalone cultures or interacting co-cultures. This dissertation examined this underexplored kingdom by focusing on the imaging of filamentous fungi utilizing DESI-MS and the droplet–LMJ–SSP. With the ability to analyze direct cultures under ambient conditions, investigating interesting cultures goes beyond what is learned though the traditional extraction, isolation, characterization processes. The DESI-MS and droplet–LMJ–SSP delve deeper into the biological

understanding of secondary metabolite production and fungal interactions. The ability to understand where compounds are produced, how they change biosynthetically, and how they interact with the environment provides insight into an otherwise underexplored realm.

CHAPTER II

MASS SPECTROMETRY IMAGING OF SECONDARY METABOLITES DIRECTLY ON FUNGAL CULTURES

This chapter has been published in the journal *RSC Advances* and is presented in that style. Sica, V.P., Raja, H.A., El-Elimat, T., Oberlies, N.H. *RSC Adv*. **2014**, *4*, 63221-63227.

Introduction

Desorption electrospray ionization (DESI) is a mass spectrometry (MS) technique that allows for the detection of compounds under ambient conditions.[21] Charged droplets are sprayed on the sample, inducing the compounds to be desorbed from the surface, such that they can be vacuumed into the MS for analysis.[23] By ionizing in a minimally destructive manner, the sample can not only remain in the culture environment, but it can also be reanalyzed repeatedly. DESI-MS can be used to image a surface and create a 2D map of the detected compounds. These maps can be superimposed on photos of the initial sample, so as to visualize, determine the location, and estimate the relative concentration of key compounds.[22]

The popular techniques used for the MS analysis and imaging in microbiology include matrix assisted laser desorption ionization (MALDI), laser ablation electrospray ionization (LAESI), DESI and nanoDESI.[50] Both MALDI [51] and LAESI[9] incorporate

lasers to assist in the ionization process, thereby ablating the samples during analysis, preventing repetitive analysis over time. Since DESI and nanoDESI[52] rely on the solventsystem for ionization, they are minimally abrasive, permitting the repetitive analysis of the same sample. This can be applicable when selected-ion monitoring (SIM), MS/MS, and/or ionization optimization are desired post the initial run, as well as, when instrument limitations prevent simultaneous ionization in both positive and negative modes.

Despite these benefits, DESI is not without challenges. First, high spatial resolutions as those of MALDI and nanoDESI are difficult to achieve with DESI.[50] Also, there are many physical parameters that must be in place to effectively ionize a compound. The height, distance, and angle of the spray emitter relative to the sample must be optimized and remain precise and consistent throughout a scan. Therefore, an ideal sample should be flat, as to not alter these measurements, and firm, as to not be distorted by the spray and gas pressure coming from the source.[47] Additionally, the solvent system must be optimized to allow for sufficient desorption. Finally, the charge applied and flow rate of the droplets are also important considerations for optimizing a DESI-MS experiment.

Due to its versatility, DESI-MS has generated great interest in several fields, including the high-throughput screening of pharmaceuticals,[25] environmental analysis,[27] food safety testing,[28] forensics,[29] and biological analyses.[33] In the realm of natural products, DESI-MS is becoming a prominent technique for the detection of compounds directly on the surface.[53] Recent studies have demonstrated MS imaging of secondary

metabolites on terrestrial[41,42] and marine[44] organisms through direct surface analysis. Additionally, Dorrestein and colleagues have been leaders[54] for the direct cultural analysis of microorganisms. However, their research has focused primarily on metabolic exchanges in bacteria[45] often using nanoDESI.

Although microorganisms, such as bacteria, have been imaged using DESI and nanoDESI, members of the fungal kingdom have only undergone limited investigation.[55] Taxa that belong in the phylum Ascomycota are the most speciose[12] and are among the most prolific producers of bioactive natural products.[13] From an ecological standpoint, fungal communities are also diverse, even in a mircoscale setting,[17] resulting in many fungal interactions. Inhibition zones, color alteration of mycelia, and sporulation are examples of the physical changes that can occur when fungi grow together,[18] but the chemical interactions that take place are poorly understood. Therefore, DESI-MS presents an opportunity for profiling fungal cultures *in situ* to examine spatial and temporal distribution patterns of secondary metabolites.

The imaging of fungi with DESI-MS raises several issues that are not encountered with plants or bacteria.[56] For instance, plant tissues, such as leaves, stems and seeds, are typically firm and more defined than a fungal culture.[35,53] Fungal cultures also differ from bacteria, since fungal surfaces often contain topography due to the presence of aerial hyphae, and can, therefore, be dynamic due to the movement of the mycelium and spores. Additionally, organisms grown on media are disadvantageous, since the media can be affected by the gas and spray pressures from the DESI source, which can form divots in the media, altering the distances and angles that are required for consistent and efficient

ionization.[23] With bacterial cultures, which grow relatively flat, nanoDESI is often utilized, since it is a less abrasive technique than DESI, thus minimizing distortion of the medium's surface. However, the typical surfaces observed with fungal cultures can be more detrimental to nanoDESI than to DESI. Not only can nanoDESI be hampered by physical issues (i.e. topography), since the fused capillaries are fragile and susceptible to breaking if not carefully monitored, but also, viscous materials (i.e. guttates[55]) can lead to clogging of the secondary capillary.[57] In short, fungal cultures present many challenges for DESI-MS that may not be an issue when analyzing natural products from other kingdoms of life.

A key advantage to direct culture ionization is the ability to perform mass spectrometry imaging (MSI) experiments. MSI could become an important tool for mycologists interested in the spatial and temporal distribution of secondary metabolites of fungal cultures. Furthermore, visualizing the chemical distribution of metabolites in mixed or co-cultures may provide an understanding of the interactions and chemical communications between organisms. Direct fungal cultures have been imaged using DESI-MS on a limited scale,[55] and most examples of direct culture analysis involve bacterial samples using nanoDESI.[47] Therefore, the methodology developed in this study opens up new avenues for studying the chemistry of fungal interactions *in situ*.

Results and Discussion

Development of desorption electrospray ionization methodology for direct fungal analysis

A freshwater fungal strain, coded G100, was identified via ITS sequencing[58] as *Clohesyomyces aquaticus* (Pleosporales, Dothideomycetes, Ascomycota). It was selected for the initial DESI-MS studies due to the biosynthesis of phomopsinone A (**1**), a previously reported antifungal compound.[59] Another culture, coded G3, was also selected because of its observed cytotoxic activity; it displayed 100% cytotoxicity at 10 and 100 ppm in the brine shrimp lethality test.[60] G3, an endophytic fungal strain, was isolated from surface sterilized seeds of *Asimina triloba* (L.) Dunal (Annonaceae) and identified via ITS as *Fusarium* sp. (Hypocreales, Sordariomycetes, Ascomycota). This fungal strain biosynthesized the mycotoxin, T-2 toxin (**2**)[61] (Figure 1), which has been reported to cause alimentary toxic aleukia and Kashin-Beck's disease. Both fungal strains were deposited in the GenBank (G100: KM589855, G3: KM589854). Both phomopsinone A and T-2 toxin were isolated and identified via traditional natural product protocols and fully characterized by NMR and MS (Figure S1-S2).[55]

We hypothesized that these two fungi would make an interesting test case, because we could image the interaction of an antifungal compound producing fungus (G100) and a mycotoxin producing fungus (G3). However, such experiments were predicated upon the development of an effective DESI-MS methodology. The initial stages of DESI-MS required optimizing the conditions for these two fungal secondary metabolites. Pure aliquots of **1** and **2** were spotted on Teflon coated slides and sprayed

with the DESI emitter. Several solvent systems were tested, including various ratios of CH_3CN:H_2O, CH_3CN:CH_3OH, CH_3CN:CH_3OH:H_2O, and CH_3OH:H_2O (all with 0.1% formic acid). While all permitted ionization at some level, the system comprised of CH_3OH:H_2O (70:30) led to the greatest intensities of the targeted peaks. Furthermore, adjustments to the tube lens voltage had great effects on the classes of compounds that were ionized, coinciding with previous reports suggesting that small molecules ionized best at 100V, while peptides were best at 250V.[29]

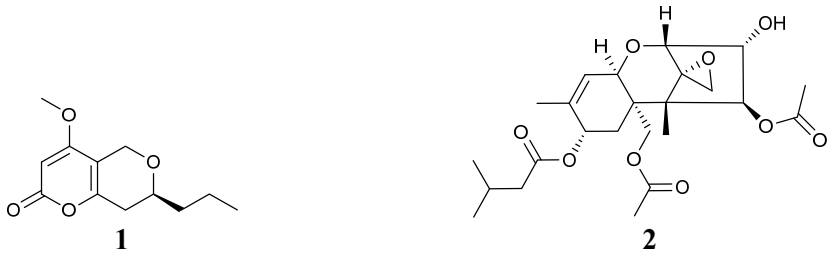

Figure 1. Structures of Phomopsinone A (1) and T-2 Toxin (2).

When the 70:30 CH_3OH:H_2O (0.1% formic acid) system was tested initially on a culture of G100 in a Petri dish, compound **1** was detected. However, the signals disappeared rapidly, as the gas pressure from the DESI source molded a divot on both the fungus and the surrounding agar. It became clear that agar did not provide the firm, flat surface necessary for optimal ionization in the 2D mapping experiments. Since agar is pliable, it was hypothesized that the incorporation of an insert would provide for a surface that was less malleable by the DESI spray and gas pressure (Table 1). Moreover, since fungi play a role in cycling carbon in the environment, cellulosic inserts were

explored, so as to provide a nutrient-rich substrate for the test fungus that could be removed easily for analysis. [62]

The first two trials did not yield positive results. Initially, G100 was grown on a cheesecloth insert, so that it could be removed from the agar for DESI-MS analysis. The cheesecloth's porous nature allowed the fungus to grow on top while still gaining additional nutrients from the agar. Unfortunately, the fungus decomposed the cheesecloth, leaving shreds with only trace amounts of fungus remaining on it. Next, filter paper (Ahlstrom Chromatography Blotting Paper Grade 222) was attempted, as its thickness would prevent complete deterioration while still being easily removed from the agar. While that was largely the case, a second problem developed. The sample did not ionize well when imaged by DESI-MS. It was hypothesized that during the analysis, the filter paper absorbed some of the solvent, thereby preventing desorption of secondary metabolites.

Based on those initial failures, cardboard (Staples®, item # 521401) was examined as an insert, since it provided a firm growth substrate that was less absorbent than filter paper. Fortunately, compound **1** was easily ionized off of the surface of G100 grown on cardboard, and the DESI source did not distort the surface. As DESI rastered across the cardboard (Figure 2), **1** was detected readily, thereby permitting relative quantification, i.e. the higher the peak (Figure 2B), the higher the relative abundance of **1** (Figure 2C). Moreover, even in the development stage of the methodology, an unanticipated benefit of the DESI-MS emerged; the biosynthesis of **1** was minimal and

inconsistent until three weeks of growth. This temporal observation factored into the experimental design of the co-culture experiments.

Table 1. Methods Tested for Direct Imaging of Fungal Cultures from a Petri Dish. Cellulosic Inserts were Used, Since They Would Provide a Nutritious Surface for Fungal Growth. The Key Goals Were Both to Minimize Sample Preparation and to Limit Alterations of the Fungal Culture by the DESI Source

Insert Type	Hypothesis	Results
None	Analysis of unaltered fungal cultures directly from Petri dish	Pressure from spray and gas distorted the agar, causing an uneven surface that was not ideal for DESI-MS imaging
Cheesecloth	Allows fungal culture to interact with agar medium but could be removed for DESI-MS imaging	Fungal culture deteriorated the cheesecloth
Filter Paper	Thicker insert would minimize deterioration and would allow the fungal culture to be easily removed from the medium	Solvent did not desorb ions effectively off of this absorbent surface
Cardboard	A less absorbent insert could increase ion desorption and provide a firm, flat surface for ionization	Compounds ionized effectively and the fungal culture grew relatively flat on the firm cardboard
Balsa Wood	Wood inserts better simulate the natural environment of the fungus	Fungal cultures grew inconsistently, often uneven, thus decreasing the chances that a culture could be analyzed via DESI
Insert in liquid media	Inserts inoculated in liquid media would better simulate a more natural habitat	Culture surfaces were uneven and medium on insert created a malleable surface

Balsa wood was also explored as an insert, since some of the test fungi were isolated from submerged woody debris in freshwater habitats.[63] It was hypothesized that balsa wood could provide a more natural substrate to test the spatial distribution of secondary metabolites from aquatic fungi. Unfortunately, the fungal growth patterns on balsa wood were inconsistent. Sometimes they grew raised and bulbous (Figure S3A) and other times they were transparently thin (Figure S3B). The fungal culture often exhibited

a higher preference for agar than remaining on the insert, an issue that was not observed with cardboard.

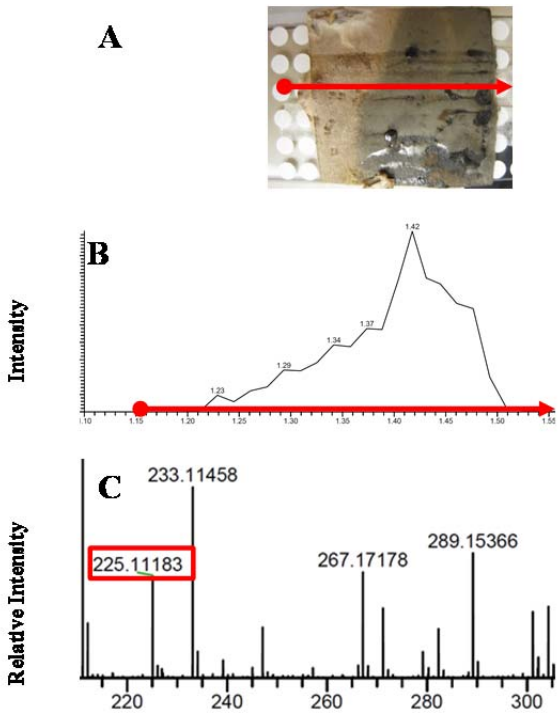

Figure 2. Analysis of 1 in Fungal Culture G100. (A) Culture Grown on Cardboard with Visible Scan Lines from DESI. (B) Extracted Ion Chromatogram (XIC) of **1** Showing the Intensities of Secondary Metabolites During a Single Scan Across the Sample. (C) At 1.42 Minutes, the Accuracy for $[M+H]^+$ of **1** Between the Observed and Calculated was 1.3 ppm (225.1118 VS 225.1121 for $[C_{12}H_{16}O_4+H]^+$

Another approach to mimic a more natural environment included incubating G100 on the cardboard or balsa wood submerged in liquid media for 7-10 days, followed by placing onto the agar (Figure S4). Since G100 was isolated from submerged wood in an aquatic habitat, it was hypothesized that this method would better simulate a more natural environment. However, this method resulted in growth that was uneven (Figure S4A). Additionally, a malleable agar layer between the fungal culture and the insert was

formed, thus negating the firmness provided by the insert (Figure S4B). The submerged inoculation also prevented making correlations between location and age. Younger areas of the culture were indeterminable, and therefore, they could not be paired with the biosynthesis or timing of specific compounds when performing the imaging experiments.

Application of mass spectrometry imaging to fungal cultures

Since cardboard provided the best surface for DESI-MS of fungal cultures, both G100 and G3 were subjected to this methodology, and 2D mapping experiments were applied in an attempt to observe and quantify the production of compounds **1** and **2**, respectively. For the fungal culture of G100, there were two points of inoculation on a single piece of cardboard, as indicated by the yellow dot (Figure 3A). Compound **1** was observed at the point of inoculation and increased in concentration towards the edge of its growth, but not at the immediate edge. This radial distribution of **1** in cultures of G100 on cardboard was observed from both inoculation points.

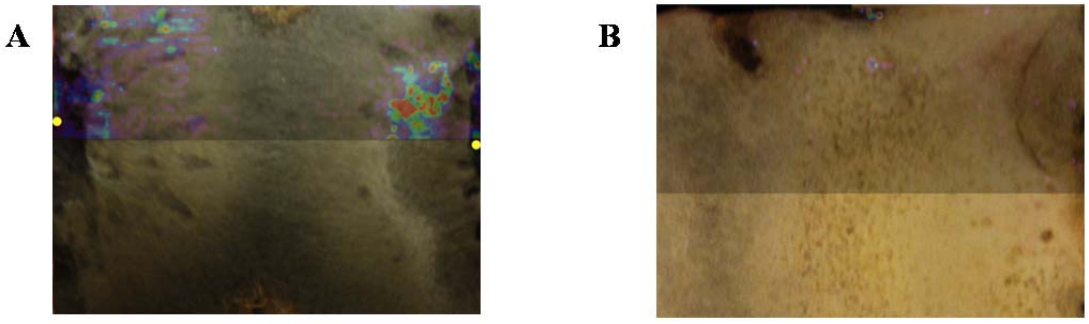

Figure 3. (A) G100 and (B) G3 Grown on Cardboard Inserts with the DESI-MS Image Overlaid on the Upper Half of the Photo for Phomopsinone A (1) and T-2 Toxin (2), Respectively. The DESI-MS Illustrates the Detection of **1** on the Surface of G100, While **2** was not Observed on the Surface of G3. The Yellow Circles (A) Indicate the Points of Inoculation. The Darker Red the Spot, the Higher the Relative Concentration of **1.**

Conversely, when the identical experiment was performed to monitor **2** on the surface of G3, little to zero **2** was observed (Figure 3B). To further analyze G3 and determine why compound **2** wasn't detected, a cross-section of G3 with agar was analyzed. As is characteristic of *Fusarium* sp., the G3 culture had white aerial hyphae (surface) with a mycelial mat[64] (inner body) color that was pink to purple.[65] Upon DESI-MS analysis of the cross-section, compound **2** was detected, but only in the areas where the culture was pink/purple in color (Figure 4). Therefore, it was determined that **2** was located in the body of the fungal culture, and not on the surface.

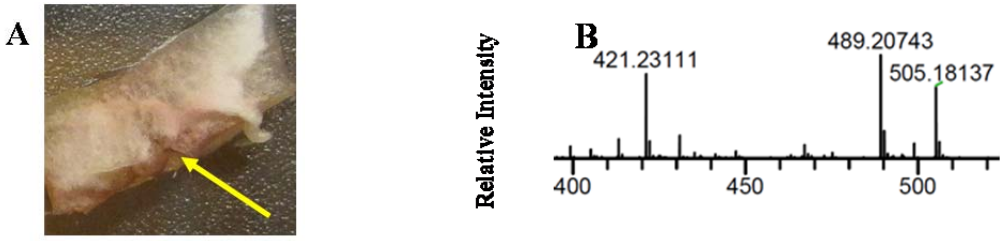

Figure 4. Analysis of 2 in a Fungal Culture of G3 Grown on Agar and Cross-Sectioned, Showing the Characteristic Pink Body Color of *Fusarium* sp. (A) Upon DESI-MS Analysis of the Cross-Section, the Na-Adduct of the Molecular Ion of **2** Was Observed Only in the Pink Area as Indicated by the Yellow Arrow. (B) The Accuracy Between the Observed and Calculated Was 4.3 ppm (489.2074 Observed VW 489.2095 Calculated for $[C_{24}H_{34}O_9+Na]^+$

These studies demonstrated that external compounds were readily desorbed by DESI but internal compounds were not. Thus, a different method of preparation was required to achieve a firm, flat surface to facilitate imaging of internal compounds (Figure 5, bottom). Hole-punches were made into the cultures, effectively removing circular cross-sections of fungus on agar. By flash freezing and vacuum drying the removed pieces of culture, the internal compounds were exposed as a ring around the edges. The crude analogy of squishing and flattening a "jelly donut" can be used to

visually explain the process. The middle of the excised piece would constitute the surface of the "donut", while the outside edges would contain the "jelly" as it is extruded from the inside. Thus, the compounds on the fungal surface remained intact, while the metabolites on the inside were extruded to the edges as the culture dried under vacuum.

Cross sectioning of tissue samples (i.e. brain, lung, spinal cord, etc.) to facilitate DESI-MS imaging of internal compounds has been reported, particularly in combination with a cryotome. Unfortunately, fungal cultures are often too thin for cryotome sectioning. Thus, freezing and desiccating represented a rapid, effective procedure to obtain a similar outcome with delicate fungal cultures.

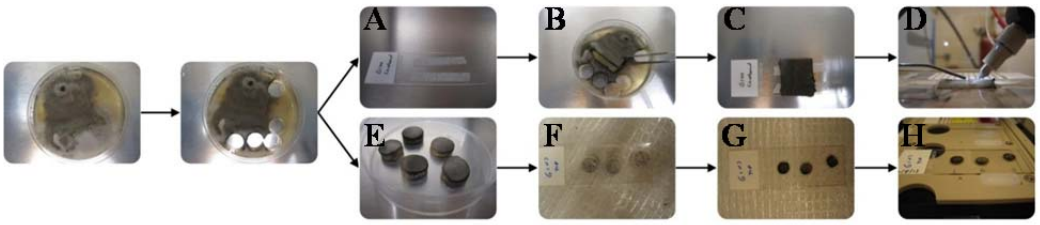

Figure 5. The General Sample Preparation Steps for DESI-MS Analysis of Fungal Cultures. The Top Figures Show the (A) Prepared Slide, (B) the Removal of the Insert, (C) Its Application to the Slide, and (D) the Analysis of the Fungus via DESI-MS. The Bottom Figures Show (E) the Hole-Punches That Are Then (F) Frozen and (G) Vacuum Desiccated Prior to (H) DESI-MS Analysis

This procedure was applied to cultures of G100 and G3 (Figure 6). Once again, compound **1** was observed on the surface of the fungal disc. When analyzing G3, compound **2** was detected, but only on the outer, pink/purple edges. This supported the hypothesis that the mycotoxin was located inside the body of the fungus, rather than on the surface. While mycotoxins have been well studied in literature,[61] their location within the body of a fungal culture has not been reported.

Figure 6. DESI-MS Imaging of 3 in G100 (A) and 4 in G3 (B) After the Flash Freeze and Vacuum Dry Procedure Was Applied. The DESI-MS Image Showed **3** on the Surface of G100, While **4** Was Only Observed Inside the Culture of G3, Evident by Detection on the Edges. The Darker Red the Spot, the Higher the Relative Concentration. However, Intensities Between Images Do Not Relate in Concentration

To evaluate the applications of this technique and to visualize secondary metabolite biosynthesis in co-culture, G100 was grown against G3 and then imaged. This experiment tested the antifungal activity of G100, as monitored by DESI-MS for the biosynthesis of **1**, in the context of growth against the mycotoxin producing fungus (G3). For the initial tests, G3 and G100 were inoculated at the same time. On one Petri dish they were inoculated on agar, and on another Petri dish they were inoculated with G3 on the agar and G100 on cardboard. This would allow for surface analysis of **1** on G100 using the cardboard technique and the analysis of **2** from G3 using the freeze/dry procedure. Unfortunately, due to the rapid growth of G3, it quickly overtook the entire plate (Figure S5); this is a common challenge with cultures of *Fusarium* sp.[65]

As noted earlier, the biosynthesis of **1** was not observed at two weeks or earlier. Therefore, the experiment was repeated with a time delay between inoculations. This time, G100 was inoculated three weeks prior to the inoculation of G3 (Figure 7), and then both cultures were grown for two weeks before DESI-MS analysis. G100 visibly prevented the growth of G3 in both Petri dishes (with and without cardboard).

Figure 7. Two Week Old Co-Cultures of G100 on (A) Agar or (B) Cardboard Grown Against G3 on Agar. G100 (Gray Mycelium) Was Inoculated 21 Days Prior to G3 and Inhibited G3 Growth. The Reddish Rectangle (Noted by Arrow) Seen in the Images is From the Initial Inoculation of G3

The cardboard insert of G100 was removed and imaged (Figure 8) showing the presence of **1** in similar fashion to when it was grown by itself. However, **2** was unable to be detected in the surrounding areas of where G3 was inoculated. Further analysis via the "jelly donut" method was not performed due to the absence of any visual G3 growth. Unfortunately, further exploration into the chemical interactions between these two fungi was hindered due to the attenuation of phomopsinone A (**1**) production. As is often the case with fungi, successive subculturing often leads to decreased biosynthesis of certain metabolites.[66]

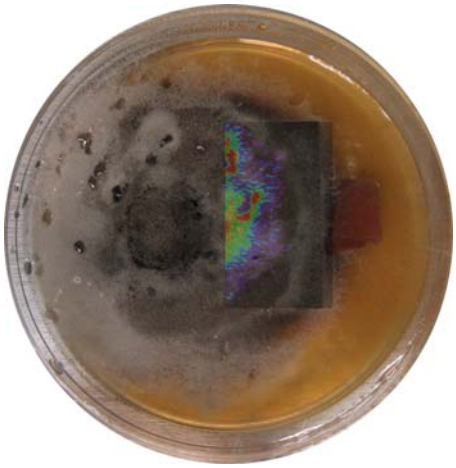

Figure 8. G100 (Left) on Cardboard Against G3 (Right) on Agar with the MSI of 1 Superimposed.

Conclusion

In conclusion, two methods were developed for the mass spectrometry imaging of fungal cultures. The cardboard insert was an effective and inexpensive way to prepare the fungal culture for imaging of compounds on the surface. Using this, we observed the biosynthesis of **1** at approximately three weeks. This was supported by the observed antifungal properties of G100 in co-culture experiments. Moreover, a second technique was developed to image compounds within the body of a fungal culture. By excising and then freezing and drying a hole-punch from the culture, the mycotoxin (**2**) was observed for the first time in the body of a culture. Studies are ongoing to expand these techniques to other co-culture experiments with a goal of imaging *in situ* the chemical signals between fungal cultures.

Materials and Methods

General experimental procedures

For DESI-MS, a Prosolia OS-3201 DESI source was used with a Thermo LTQ Orbitrap XL system with the following settings: positive mode ionization; capillary temperature, 200 ºC; source voltage, 3.00 kV; capillary voltage, 46 V; tube lens, 100 V; scan time, 150 ms; flow rate, 1.20 µL/min; nitrogen gas pressure, 180 psi; spray angle, 55°; inlet height, 1-2 mm. The solvent was CH_3OH:H_2O (70:30) with 0.1% formic acid, and the mass range was set to optimally pass ions from m/z 150-700. A spatial resolution range between 200-300 µm was used for the imaging experiments. Thermo Xcalibur 2.1 software was used to run the queues for mass spectrometry imaging, as well as, to examine the raw data. The raw files were converted to image files via Thermo FireFly

2.1. The image files were opened with BioMAP 3 software and used to create the MS images. Adobe Photoshop CS6 version 13.0 x32 was used to superimpose the MS images over the pictures of the fungal cultures.

DESI inoculation methodology

Fungal cultures were inoculated initially on potato dextrose nutrient agar (PDA, Difco) in 50 × 9 mm sterile Petri dishes to provide stock cultures for subsequent experiments. After 7–10 d of growth, the test fungus was grown on an autoclaved insert. Inserts used included cheesecloth, filter paper, cardboard, and balsa wood, all of which were sterilized via autoclaving. Two methods for inoculating an insert were used. First, a small piece of agar with the fungus was 2-point inoculated on a small segment of sterile insert (40 mm × 20 mm) placed on a newly prepared Petri dish with PDA media. In a second method, the fungus was grown in liquid media containing 2% soy peptone, 2% dextrose, and 1% yeast extract (YESD media) with a segment of sterile insert and incubated for (7–10 d) at 22 °C with agitation (shaken at 100 rpms). After 7–10 d, the segment of insert with fungal colony growing on its surface was aseptically transferred onto a Petri dish with PDA media; only cardboard and balsa wood were tested via the second method. The first method using cardboard (40 mm × 20 mm × 1 mm, Staples, item # 521401; Figure S6) yielded the best surface of the explored options for DESI-MS analysis.

Sample preparation for imaging experiments

The samples grown on inserts (i.e. cardboard and wood) required very little additional preparation (Figure 5, top). Double-sided tape was placed on a microscope

slide. While working in a laminar flow hood, the cardboard/wood was removed from the Petri dish using forceps and placed onto the taped area with minimal pressure, so as to not compromise the surface. In some cases, the inoculant was too elevated relative to the fungal growth, and therefore, was carefully removed using forceps to provide a more even, flat surface. The microscope slides were then placed directly onto the DESI platform for analysis. This method was ideal for analyzing metabolites on the surface of the cultures

To analyze the internal metabolites, fungal cultures were grown directly on media (Figure 5, bottom). Circular sections were made using a 5 mm hole-puncher and placed into a separate, empty plastic Petri dish. Liquid nitrogen was then poured into the Petri dish to flash freeze the sections. Using forceps, the pieces were removed and placed on an unaltered microscope slide. The slide was then placed under vacuum in a desiccator and left overnight. The resulting samples were shriveled, relatively flat, and stuck to the slide. Finally, the slide was then removed from the desiccator and placed onto the DESI platform for analysis.

Acknowledgments

The DESI source was acquired via partial support of a Biotechnology Research Grant from the North Carolina Biotechnology Center (2011-BRG-1206). The authors thank Dr. B. Ehrmann in the Triad Mass Spectrometry Laboratory for helpful discussions.

CHAPTER III

DEREPLICATING AND SPATIAL MAPPING OF SECONDARY METABOLITES FROM FUNGAL CULTURES IN SITU

This chapter has been published in the journal *Journal of Natural Products* and is presented in that style. Sica, V.P., Raja, H.A., El-Elimat, T., Kertesz, V., Van Berkel, G.J., Pearce, C.J., Oberlies, N.H. *J. Nat. Prod.* **2015**, *78*, 1926-1936.

Introduction

In the drug discovery realm of natural products, strategies to increase the output of new, bioactive compounds, while decreasing the isolation of previously known structures, are continually evolving. To achieve these goals, researchers strive to profile samples as early as possible in the isolation/identification procedures by utilizing LC–UV,[67] LC–MS,[68] LC–NMR,[69] or a combination of these techniques.[70] This identification of known compounds, which was coined 'dereplication',[71] allows for the early detection of known metabolites, thus saving time, effort, and cost.[72] Our methodology for the dereplication of fungal metabolites involves analyzing mutually supportive data by screening fungal culture extracts via an ultra–performance liquid chromatography–photodiode array–high resolution tandem mass spectrometry (UPLC–PDA–HRMS–MS/MS) protocol and comparing the retention time, UV/VIS data, HRMS and MS/MS fragmentation patterns with a database.[73,74] Presently, the method is used routinely to

dereplicate fungal extracts from a growing library of over 300 secondary metabolites, particularly mycotoxins, in approximately 30 min. However, that time frame starts once the extract has been generated and does not take into consideration the 4-12 weeks that the culture was growing in solid phase culture prior to extraction. The main goal of this study was to dereplicate fungal cultures with four stipulations: (1) eliminate the need to extract the fungal sample, (2) conduct the analysis directly from the culture dish, (3) avoid optimizing growth conditions to facilitate ambient ionization, and (4) include the acquisition of mutually supportive data.

Ambient ionization techniques for MS allow for direct culture analysis without the need for extracting the sample or extended fungal growth times.[34,54,75-77] Our team has explored desorption electrospray ionization—mass spectrometry (DESI–MS)[21] as a method for examining fungal cultures directly from Petri dishes.[77] DESI–MS has many advantages over other direct ionization techniques, such as MALDI, due to its ambient, minimally destructive nature. For instance, the ability to analyze and identify known metabolites using DESI–HRMS and MS/MS without destroying the culture was beneficial, as repeat analyses were possible. However, to optimize the DESI setup for fungal cultures, a few challenges must be overcome, particularly due to the dynamic topography of a fungal culture, which is not flat.[78] In a scenario that draws from the analysis of biological tissues,[79] a cryotome was used to afford thin, flat cross–sections of the desired culture.[55] Alternatively, an imprint of the culture could be made and then scanned by DESI–MS.[55] Moreover, we developed methods to grow a fungal culture on an insert, so as to afford a firm, flat surface that was desired for DESI–MS analysis.[77] While

these techniques worked for MS imaging experiments, they were not universally applicable to the goals of dereplication. They each required optimization of the individual fungal culture, which would be impractical for the analysis of hundreds of cultures annually. Moreover, none of them permitted the collection of mutually supportive chromatographic or UV/VIS data, all being based solely on MS measurements.

Innovative MS techniques, such as molecular networking, have emerged that utilize ambient ionization sources to dereplicate cultures directly.[76] This technique involves creating a web of connectivity between compounds by plotting the HRMS and fragmentation patterns. The spectra are converted into unit vectors, and the cosine of the angle between vectors creates a similarity score.[76] This method works well as a complement to the traditional dereplication protocols, but the loss of chromatographic separation prevents the differentiation of isomers and limits the amount of mutually supportive data that can be generated concomitantly. The importance of these ancillary data should not be overlooked. For example, even in 2015, the UV/VIS spectrum of a fungal metabolite can be valuable data for rapid dereplication, especially with compounds that were discovered prior to the common use of NMR and MS in structure elucidation.[80]

Recently, a droplet—liquid microjunction—surface sampling probe (droplet–LMJ–SSP) system was reported for analysis of drug–dosed animal thin tissue sections.[81-84] With this system, a droplet of 2–4 μL is employed to perform a microextraction on the surface of a sample, which can then be injected directly into LC and any additional inline detectors, such as PDA, ELSD, and/or MS (Figure 9).[85] By coupling the droplet–LMJ–SSP with UPLC–PDA–HRMS–MS/MS, dereplication[73] can take place by sampling a

culture directly, thereby gaining chromatographic separation and obtaining retention time and UV/VIS data. The retention time alone acts as a key identifier for specific metabolites, such as isomers (or isobars), which are often indistinguishable without chromatography. For the purpose of dereplication, the acquisition of mutually supportive data highlights a major advantage of the droplet–LMJ–SSP over other ambient ionization techniques (Table 2), while saving much time over the traditional protocol of performing dereplication on extracts (Figure 9).

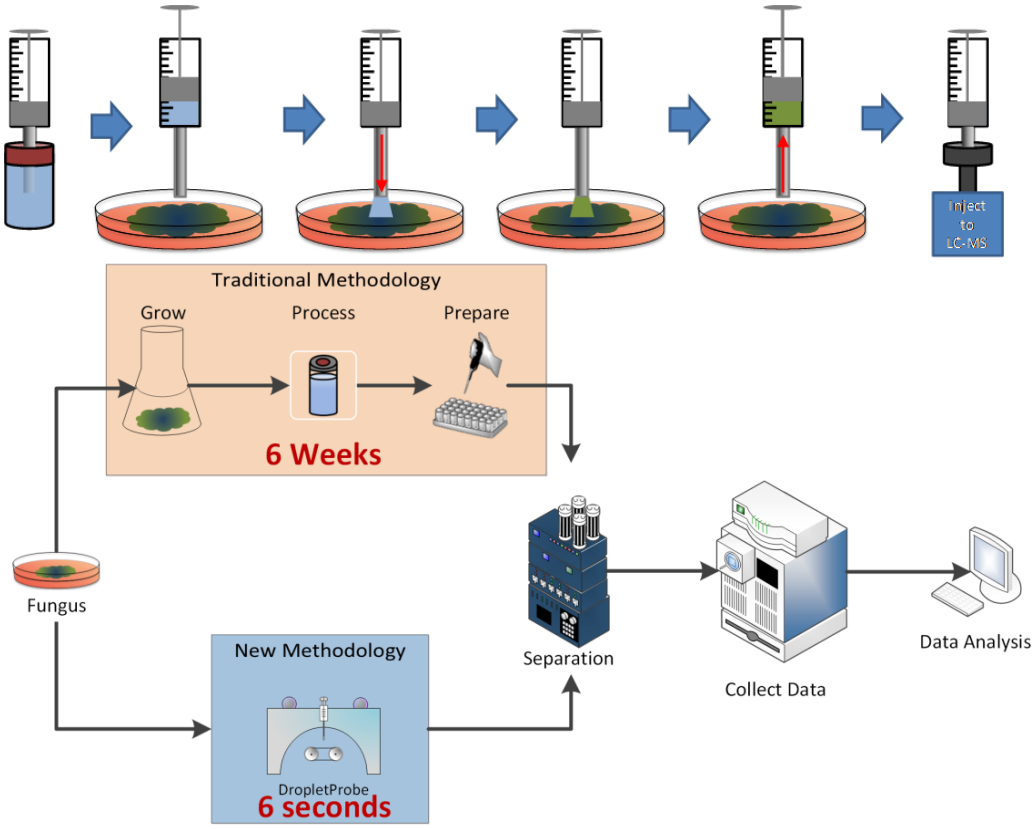

Figure 9. (A) The Droplet–LMJ–SSP Can Extract Secondary Metabolites Directly Off the Surface of a Culture, Including Compounds Exuded into the Agar, and Inject the Extract into the LC–MS Instrument for Analysis. (B) Comparison of the Current Dereplication Protocol (Orange) and the Streamlined Methodology (Blue)

Table 2. Comparison of Direct Ionization Sources (DESI, nanoDESI, MALDI, LAESI, and LESA) to Droplet–LMJ–SSP Functionalities for Direct Sample Analysis						
Applications[a]	DESI[86]	nanoDESI[87]	MALDI[88]	LAESI[89]	LESA[90]	droplet–LMJ–SSP[81]
Direct Culture Analysis	✓	✓	✓	✓	✓	✓
Repeat analysis	✓	✓	✗	✗	✓	✓
Accurate Mass	✓	✓	✓	✓	✓	✓
Tandem MS	✓	✓	✓	✓	✓	✓
Imaging/Heat Mapping	Imaging	Imaging	Imaging	Imaging	Heat Mapping	Heat Mapping
Sample Preparation	Minimal	None	Matrix	None	None	None
Separation of Isomers*	✗	✗	✗	✗	✗	✓
Points of Identification						
HRMS	✓	✓	✓	✓	✓	✓
MS/MS	✓	✓	✓	✓	✓	✓
Retention time	✗	✗	✗	✗	✗	✓
UV/VIS absorbance	✗	✗	✗	✗	✗	✓
[a]Gas-phase separation techniques (i.e. ion mobility) lack sensitivity and resolution compared to liquid-phase separation techniques (i.e. LC). Hence this table is only comparing solution based processes.						

Mass spectrometry imaging (MSI), or mapping, has become increasingly popular in the natural products community.[34] Mapping the locations of metabolites to the sample's surface has created opportunities to analyze the chemical interactions that take place between cultures.[49] Like many other ionization techniques, droplet–LMJ–SSP has the ability to map the location of compounds on a sample; however, it does so in a different format, termed heat mapping. Heat mapping shows the relative intensity of a compound at specific locations, rather than as a continuous image (Figure 10).[82] Heat mapping with the current system configuration has some limitations, compared to imaging, due to the low spatial resolution (0.7–1.0 mm).[85] However, it does have benefits, such as the ability to obtain LC separation, analyze by more than one detection

type, and use various ionization sources (i.e. ESI, APCI and APPI). Furthermore, high spatial resolution is not necessarily required for the analysis of fungal cultures, as the general trends are often just as informative as the minute differences obtained with high spatially resolved locations.

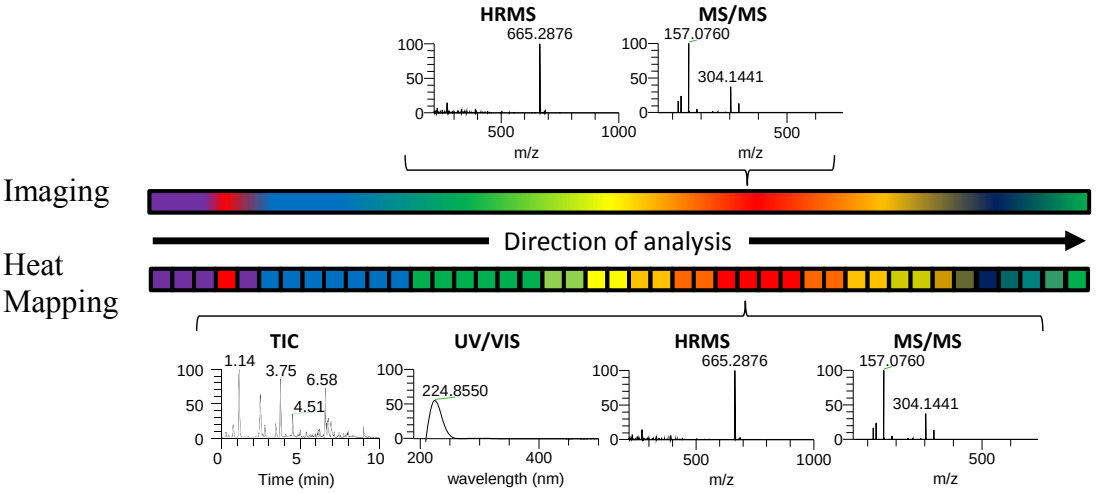

Figure 10. Conceptual Comparison of MSI (Top) and Heat Mapping (Bottom) Experiments as They Scan a Sample from Left to Right. Imaging Experiments Have a Continuous Flow of Data, While Heat Maps Are of Specified Locations. However, for Each Specific Location in the Heat Map, There Is Chromatographic Separation and UV/VIS Data Associated with it. In This Hypothetical Example, the Color Scale Indicates the Relative Amount of Signal Detected for the Given Analytes

Results and Discussion

Dereplication of fungal cultures

An in–house database of over 300 fungal secondary metabolites, encompassing a diverse range of structural classes such as polyketides, terpenoids, and peptides,[91] had been assembled, recording the chromatographic retention times, UV/VIS data, full–scan HRMS, and MS/MS spectra in both positive and negative electrospray ionization (ESI) modes.[73] Once extracts were analyzed, these data were processed utilizing the ACD

IntelliXtract software, which scans the data and reports molecular ions that match the database. The matches were investigated further by comparing the fragmentation pattern of the sample to that of the standard. However, for this study, there were two slight differences. First, the original database was built using collision–induced dissociation (CID) with a normalized collision energy (NCE) of 30 on an LTQ Orbitrap XL, thereby generating low–resolution fragmentation data; at the time, that presented a more efficient way to process the data. In contrast, this study used a QExactive Plus, and therefore used high–energy collision dissociation (HCD) with a NCE of 35, which had the benefit of having high–resolution fragmentation. Although the resulting fragments were mostly similar between HCD and CID, there were some differences, making it important to rerun the standards using HCD. Secondly, the QExactive Plus has the ability to perform polarity switching, thus allowing for the collection of both positive and negative ionization modes in a single run. The use of the QExactive Plus also provided increased sensitivity and the option of higher resolution (140,000 vs 100,000) as compared to the LTQ Orbitrap XL.

Initially, a representative 10% of the compounds from the fungal library[73] were spotted on Teflon coated slides and sampled via the droplet–LMJ–SSP (Table S1, Supporting Information). Although our traditional drug discovery projects focus on metabolites soluble in organic solvents (such as $CHCl_3$—MeOH), a droplet comprised of 50:50 MeOH—H_2O was used for two reasons. First, MeOH was chosen because of its compatibility with LC-MS systems and had the added benefit of mimicking the typical extraction process; CH_3CN worked in an equivalent manner. Also, an equal volume of

H_2O was added to maintain droplet formation and integrity, as reported previously.[83] Polyketides, cyclic peptides, terpenoids, and peptides, as well as commonly dereplicated compounds, such as equisetin (**22**), aerofusarin (**25**), and alternariol analogues (Table S1), were all readily detected. For each standard, the HRMS, MS/MS, UV/VIS data, and retention times were all reacquired and recorded to account for any changes to the retention times and fragmentation patterns due to the droplet–LMJ–SSP setup. Over a mass range of 225 to 1963 amu, complications of extraction and ionization were not observed with any of the compounds (Table S1, Supporting Information), suggesting that it would work for the entirety of the library. Subsequently, 12 fungi[66,77,92-96] (Table S1) were selected that were known to biosynthesize those standards from traditional natural product studies, and each were dereplicated readily from cultures on Petri dishes using the droplet–LMJ–SSP (Table S1).

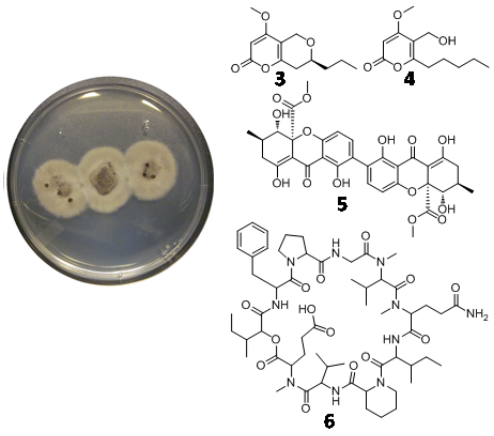

Figure 11. Fungal Culture G100 and the Structures of the Identified Metabolites Using the Droplet–LMJ–SSP

Briefly, the first fungus selected for dereplication *via* the droplet–LMJ–SSP was a culture identified as *Clohesyomyces aquaticus* (Pleosporales, Dothideomycetes, Ascomycota) and coded G100 (Figure 11). Phomopsinone A (**3**) and three other metabolites (compounds **4**–**6**) were all detected and identified by their retention time, UV/VIS data, HRMS, and MS/MS data (Figure 12).

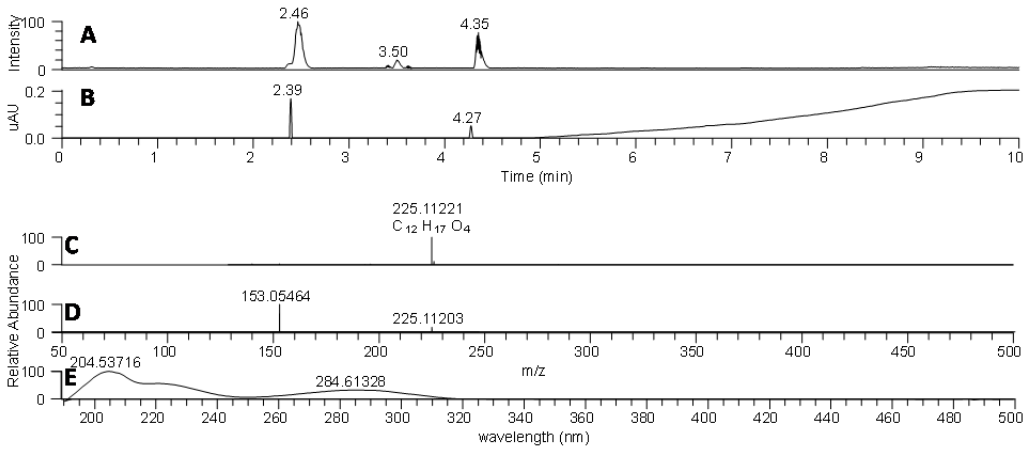

Figure 12. The Droplet–LMJ–SSP Coupled to UPLC–PDA–HRMS–MS/MS Was Used to Sample Fungus G100 Thereby Generating (A) the Total Ion Chromatogram and (B) the UV/VIS (190–500 nm) Chromatogram (0.08 min Delay Between PDA and MS). At 4.35 min, (C) the HRMS spectrum, (D) the HCD fragmentation pattern, and (E) the UV/VIS spectrum can be observed, all corresponding to **3**. The mass accuracy of **3** was -0.6 ppm (225.1120 observed vs 225.1121 calculated for $[C_{12}H_{16}O_4 + H]^+$).

An important aspect of the droplet–LMJ–SSP was its tolerance of diverse fungal topographies and its ability to analyze specific features of a fungal culture, such as guttates (i.e. liquid droplets).[55] While many fungi produce guttates, ambient techniques, such as DESI and nanoDESI, have reported the difficultly of analyzing such liquids on a culture's surface.[57,77] Previously, guttates on the surface of a fungus were explored using DESI–MS.[55] This required imprinting the culture onto Teflon coated slides and analyzing with DESI–MS, rather than directly sampling the culture's surface.[55] However, the

droplet–LMJ–SSP was able to extract liquid droplets off the surface of a fungal culture without any sample preparation. To showcase this ability, the droplet–LMJ–SSP sampled both a guttate and the outer mycelium on a fungal culture of G100. The antifungal compound **3** was observed in significantly larger amounts (over two magnitudes) on the guttate than on the outer edge of the fungus (Figure S7). This interesting observation would be impossible with a standard natural products protocol that extracts the entire sample. Moreover, it allows us to now postulate and test questions about where, when, and why this fungus concentrates an antifungal compound in guttates.

Separation of isomers

Isomers are often encountered in natural products research.[92] One of the most powerful advantages of the droplet–LMJ–SSP over other ambient ionization techniques is the ability to differentiate between isomers using LC. Ion mobility has tried to alleviate this issue but has several limitations, such as decreased sensitivity, low ion mobility resolution, and requires a mass spectrometer that has ion mobility capabilities.[97] Currently, ion mobility works best as a complimentary technique with LC, rather than as the sole source of separation.[98] The separation that LC provides has a greater ability to resolve compounds due to the abundance of chemically diverse columns and chromatographic conditions available. Moreover, chromatography is likely more familiar to most specialists in natural products chemistry.

To display the separating ability of the droplet–LMJ–SSP coupled with LC–MS, a fungus, identified as *Halenospora* sp. and coded G87 (Figure 13), was reported previously to biosynthesize two sets of isomeric resorcylic acid lactones (compounds **7/8**

and **9/10**).[92] To apply the droplet–LMJ–SSP, the fungus was sampled in a Petri dish and had three peaks with an accurate match (±5 ppm) for *m/z* 381.1099 (Figure 14). Standards were analyzed for compounds **7** and **8**, and these displayed matching retention times (4.03 and 4.21 min, respectively), HRMS, and MS/MS fragmentation patterns (Figure S8) for two of the peaks.

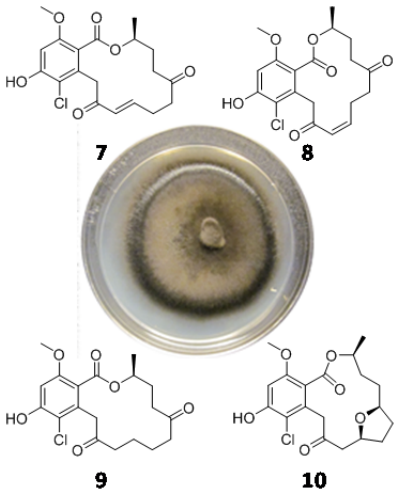

Figure 13. Fungal Culture G87 and the Structures of the Identified Metabolites Using the Droplet–LMJ–SSP.

Interestingly, none of the previously isolated compounds from G87 matched the peak on the extracted ion chromatogram (XIC) at 3.46 min.[92] This was perplexing at first given its relative abundance, but upon further inspection, the mass was identified as a loss of water on the precursor ion at 399.1204 (Figure S9). This observation further highlights two important benefits to sampling a fungal culture directly with the droplet–LMJ–SSP. First, the chromatographic separation allows for the assignment of multiple adducts, such as assigning $[M+H]^+$, $[M–H_2O+H]^+$, and $[M+Na]^+$ to a compound. With ambient

ionization techniques that directly infuse into the mass spectrometer, it is difficult to differentiate whether observed masses (i.e. 399.1204 and 381.1098) are analogues that differ by 18 amu or if one of them is a loss of water from the other (i.e. $[M+H]^+$ and $[M–H_2O+H]^+$). Without chromatography, the two isomers (**7** and **8**) may have been presumed to be $[M–H_2O+H]^+$ to the mass at 399.1204, rather than the presence of three unique metabolites. By gaining chromatographic separation, adducts can be differentiated from analogues, eliminating this concern. Second, because the proposed metabolite that eluted at 3.46 min (Figure S9) was not encountered in the original study, which identified fourteen new resorcylic acid lactones,[92] its detection with the droplet–LMJ–SSP indicated a suite of interesting possibilities. For example, the fungus might not have biosynthesized this compound when grown on rice in solid phase culture, the fungus might only have biosynthesized it early in the growth of the fungus, or the compound decomposed during the initial extraction/isolation processes. Performing a microextraction of the culture directly from the Petri dish, such as afforded by the droplet–LMJ–SSP, could be used to probe these and related questions.

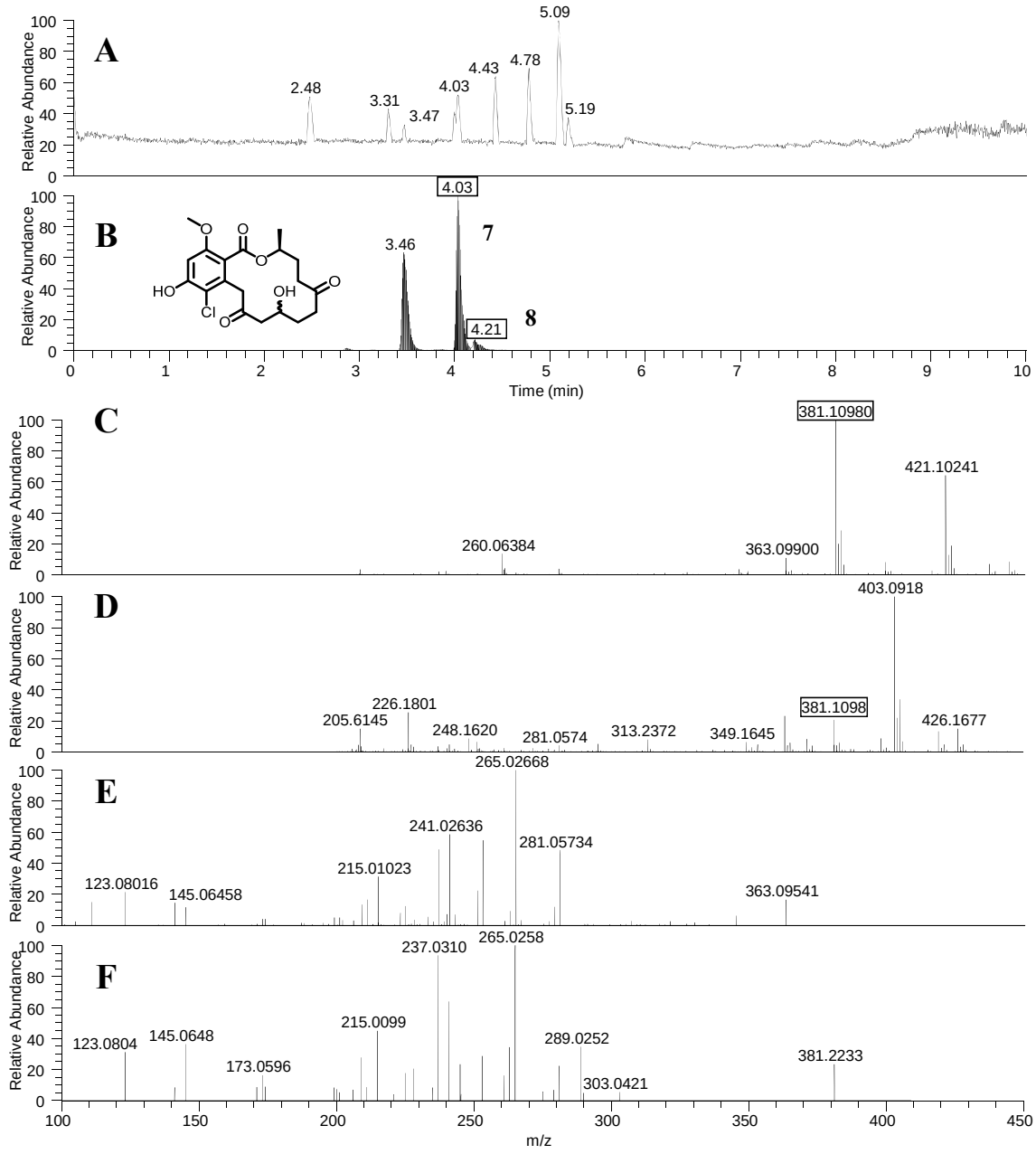

Figure 14. (A) The Base Peak Chromatogram for Fungus G87 Sampled by the Droplet–LMJ–SSP. (B) The XIC of *m/z* 381.1099 (± 5ppm) displays matching retention times (boxed) for compounds **7**, **8**, and a potential analogue. The full scan MS at (C) 4.03 and (D) 4.21 min and the tandem MS of 381.11 at (E) 4.03 and (F) 4.21 min match the standards for compounds **7** and **8**, respectively.

Identification of fungal culture

An interesting circumstance arose while testing the ability of the droplet–LMJ–SSP as a dereplication tool. Four secondary metabolites (**11**–**14**) from a fungal strain, coded MSX19583 (Figure 15), had been isolated, characterized, and added to the dereplication database.[93] However, when a regrowth of this culture was requested in order to identify its genus and species via ITS sequencing,[99] it was discovered that there was a contaminant in fungal strain MSX19583 (Figure S10). To identify which fungus was the contaminant and which one biosynthesized the isolated metabolites, both fungi were isolated and subjected to analysis *via* the droplet–LMJ–SSP. The XIC of masses for the four previously isolated metabolites were compared for each fungus against the pure standards. Matches of retention time, accurate *m/z* match (±5 ppm), and tandem MS for compounds **11–13** were present in the green colored fungus (Figures 16, S11, and S12), while the matches for these compounds were not observed in the purple colored fungus. Initially, compound **14** appeared to be detected in the green colored fungus. However, the retention time and MS/MS data demonstrated that this was a spurious observation and not the same compound (Figure 17), further exemplifying the benefits of mutually supportive data afforded by the droplet–LMJ–SSP. From this, culture MSX19583 and the contaminant were later identified as *Aspergillus sydowii* (green) and a *Chaetomium* sp. (purple), respectively.[93]

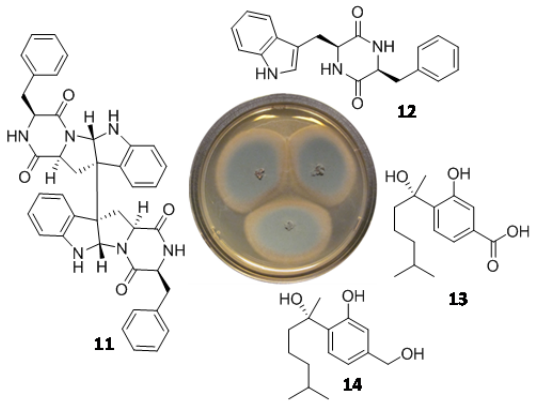

Figure 15. Fungal Culture MSX15983 and the Structures of the Isolated Metabolites.

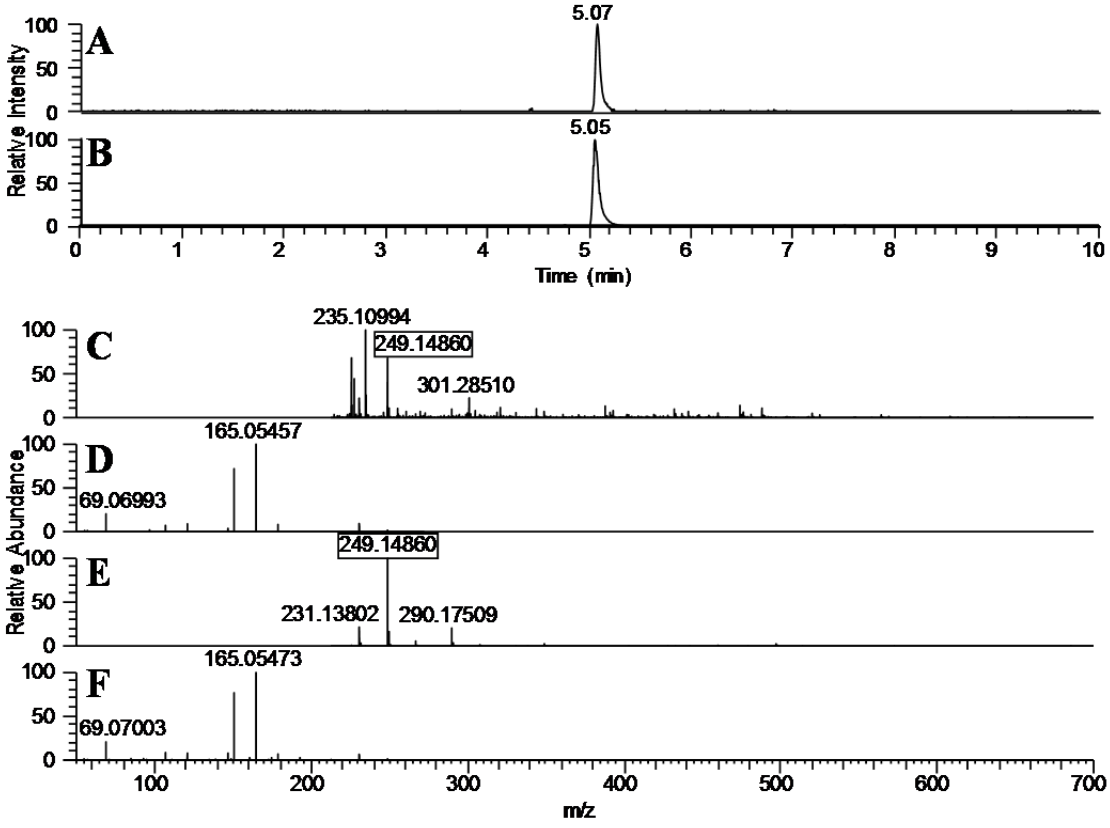

Figure 16. Compound 13 Was Previously Isolated from Fungal Culture Coded MSX19583. Matches in retention time can be observed by comparing the XIC of 249.1485 ± 5ppm from (A) the fungal culture and (B) the standard. Furthermore, the HRMS data for (C) the fungus and (E) the standard both matched, and the MS/MS spectra for (D) the fungus and (F) the standard have matching fragmentation patterns.

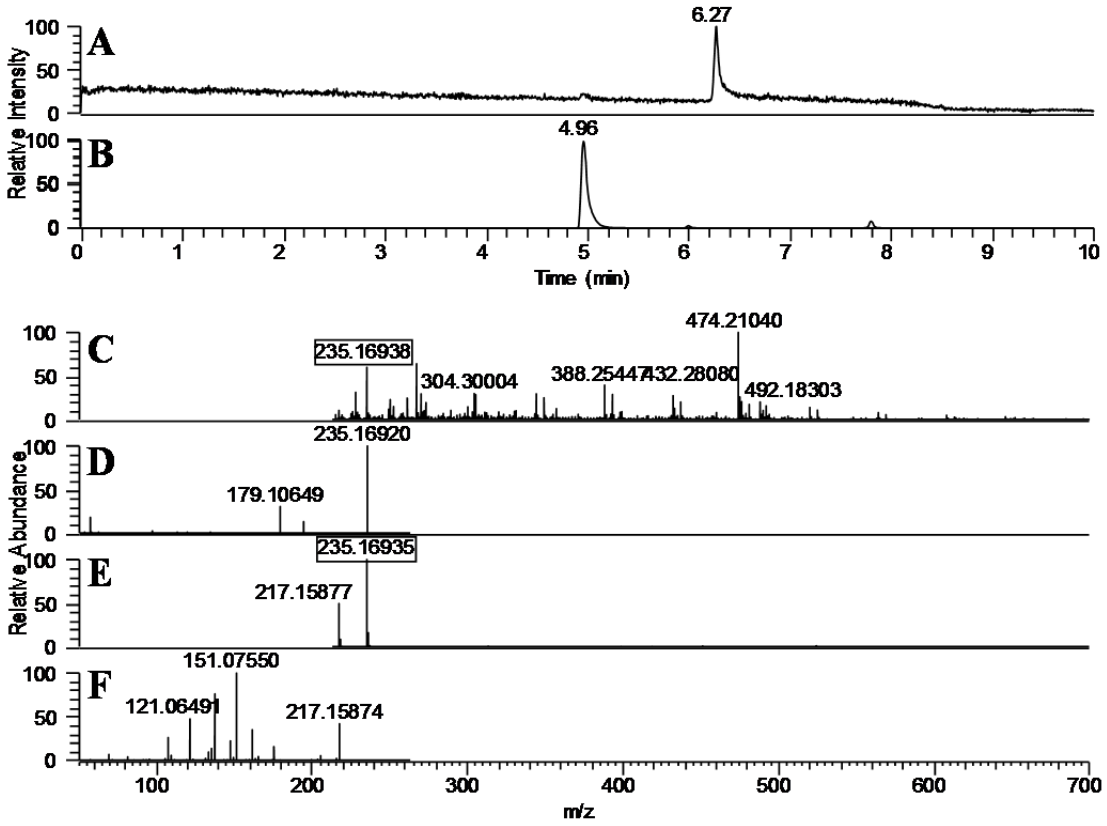

Figure 17. Compound 14 Was Previously Isolated from Fungal Culture Coded MSX19583. A difference in retention time can be observed by comparing the XIC of 235.1693 ± 5ppm from (A) the green colored fungal culture and (B) the standard. The MS spectra display the difficulties of solely using MS for this metabolite identification. The HRMS spectrum for (C) the fungus and (E) the standard both matched $[C_{15}H_{23}O_2–H_2O+H]^+$ within a 5 ppm mass tolerance, but the MS/MS spectra showed differences between (D) the fungus and (F) the standard in fragmentation patterns.

Mapping of secondary metabolites

Similar to MSI, the droplet–LMJ–SSP also has the ability to map the relative intensities of selected molecular ion peaks. The fungus coded MSX19583 was used to map the location of two of the key metabolites, compounds **11** and **12**. As mentioned earlier, this culture was originally contaminated. Initially, the impure culture was analyzed, mapping a straight line from the contaminant (purple) to the desired fungus

(green), and back to the contaminant (Figure 18). It was observed that compound **11** was detected primarily on the body of the fungus, while compound **12** was predominantly exuded into the surrounding media. This experiment was repeated on another culture of MSX19583, once the contaminant (purple) was removed. The results were the same, showing that compound **11** remained on the body of the fungus while compound **12** was exuded into the surrounding media (Figure S13, Supporting Information). This was an important observation, as we initially pondered if the purple fungus had been either responsible for the biosynthesis of **12** or stimulated its biosynthesis by the green colored culture. These sorts of measurements are impossible with extracted cultures, as all spatial information would be lost in the context of the entire extract. Moreover, sampling the agar region could be challenging in other MSI experiments, as we observed the formation of divots from the gas and spray pressure when attempting a similar experiment with a DESI source.[77]

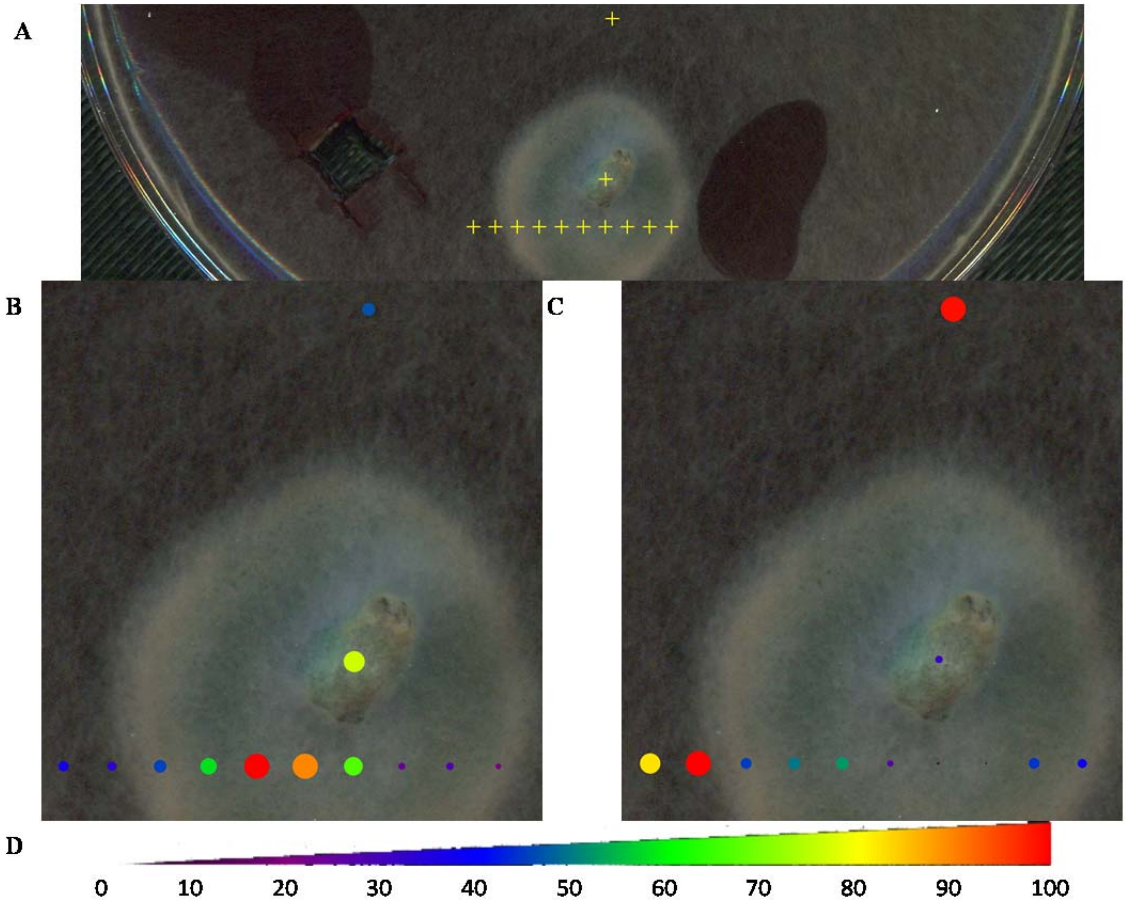

Figure 18. (A) Culture MSX19583 (Greenish/Gray) with the Contaminant (Purple); crosshairs illustrate location of sampling points. (B) Heat map of compound **11** as sampled from the contaminant to the culture. (C) Heat map of compound **12** as sampled from the contaminant to the culture. (D) The color scale and diameter of spot indicate the relative amount of signal detected for the given analytes.

Challenges and Conclusions

There are many questions and challenges that one could envision for the utilization of the droplet–LMJ–SSP for fungal culture analysis. First, there were concerns about whether the fungal culture would absorb the droplet rather than forming a liquid microjunction between the fungus and syringe. In working with 12 cultures, the amount of droplet loss was considered negligible for most fungi. However, significant droplet loss was an issue for two fungi, coded G87 and MSX59553 (Figure 19). Interestingly,

visual inspection of the fungus was not an adequate predictor of droplet loss. For example, G100 and G87 (Figures 11 and 13) were similar looking and covered in mycelia (i.e. a hair–like surface), yet G100 permitted droplet—liquid microjunction formation readily, while G87 would absorb the droplet. A possible explanation of this could be due to the presence of hydrophobins that are often contained in the conidia/spores. Strains that produce conidia/spores on the surface of aerial mycelium tend to be hydrophobic (i.e. G100), while aerial mycelium that lack conidia/spores are more hydrophilic (i.e. G87).[100] Additionally, MSX59553 and MSX57715 (Table S1) resembled each other with flat, spore covered surfaces, yet MSX59553 would absorb most of the droplet and MSX57715 would not. For the challenge concerning MSX59553, the droplet–LMJ–SSP still recovered some of the solvent from the sampled area. In this case, it was enough to generate data for dereplication, but would result in poor spatial resolution (3–5 mm) for mapping. Fortunately, these challenges for G87 and MSX59553 could be alleviated by resampling the same position several hours later. After the sub–optimal sampling area dried, a hardened surface was created that was amenable to liquid microjunction formation. By resampling this area, the droplet was recoverable and multiple extractions could take place with the single droplet (i.e. sampling three or more times before injecting into the UPLC–PDA–HRMS–MS/MS).

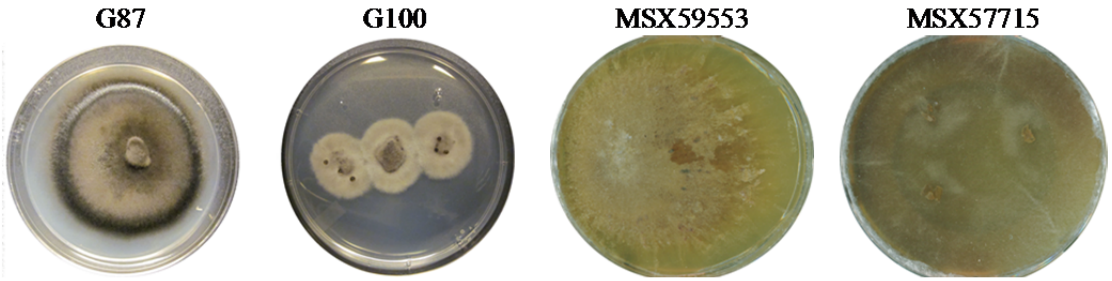

Figure 19. Comparison of the Topography of Fungal Cultures that Resembled Each Other Superficially, but Either Had Challenges (i.e. G87 and MSX59553) or Were Amenable (G100 and MSX57715) with the Droplet–LMJ–SSP.

Besides absorbency issues, occasionally a droplet was simply unrecovered. This typically happened in one of the following instances: (1) when sampling cultures with steep topography, or (2) if repeated sampling eventually resulted in considerable droplet loss. Of the two scenarios, and given our previous studies with DESI–MS,[77] the steep topography was surprisingly not a prevalent issue, but could occur in a few instances, particularly with fungi covered in mycelia. It was also not a consistent issue, as immediately resampling the same steep location would often result in a successful microextraction. For repeated sampling with the droplet–LMJ–SSP, droplet loss could be minimized by utilizing three or less microextraction cycles, with the exception of the fungal cultures with absorbent surfaces, as noted above.

When working with solid–phase cultures for isolation studies, our typical protocol involves an overnight extraction, largely out of convenience.[55,92,96] Thus, another concern that arose was the amount of material a microextraction could absorb *via* a 4 μL droplet during the two seconds of contact with the culture. This was addressed by repeating the microextraction three times with the same droplet before injecting the sample into the

UPLC–PDA–HRMS–MS/MS system. This gave the droplet a higher concentration of fungal metabolites, while minimizing the risk of losing the droplet to the fungal surface. As previously reported,[83] several short microextractions were more effective for this application than a single long extraction. In fact, when designing the experiments, a QExactive Plus (with enhanced resolution) was used with this concern in mind. However, after experimenting, a less sensitive instrument should also suffice. With the various types of structural classes tested (Table S1), limitations were not encountered with this method for secondary metabolite detection for both pure standards and direct fungal culture analysis.

A question that arose during peer review was how this process compared to rapid plug extractions, which were first described in the late 1990s.[101,102] In this, a 6 mm plug is excised by hand from the fungal culture (including agar) in the Petri dish. The entire plug is extracted, and the effluent can then be analyzed by HPLC. While that method has corollaries with some of the droplet–LMJ–SSP benefits (such as sampling across a culture, the space between co-cultures, etc.), it requires more human power for the sample manipulation/processing. The possibilities for *in situ* analysis are not quite the same, particularly in a temporal manner, as those afforded by the droplet–LMJ–SSP, which has the added benefit of automation and integrated heat mapping capabilities. Nevertheless, rapid plug extractions likely probe the chemistry of fungal cultures in a similar manner.

An advantage of the droplet–LMJ–SSP is that the fungal culture survives the analysis, except in the immediate area of the microextraction (typically ~ 1 mm). Hence,

a promising application for the droplet–LMJ–SSP is examining the timing of secondary metabolite biosynthesis, particularly for the optimization and eventual scale up of drug leads. One concern, particularly from the mycologist on our team, was contamination from fungal spores in the air that could arise when the Petri dish was exposed repeatedly. In sampling dozens of fungal cultures, this occurred in only one instance. Approximately a week after the culture G87 was sampled, a contaminant appeared in the Petri dish. For the purposes of dereplication and heat mapping experiments, this was not an issue, as the cultures were analyzed immediately after opening. However for temporal studies, this must be considered. Indeed, our current protocol involves first opening a plate in a laminar flow hood, such that fungi that sporulate prolifically do not contaminate the MS facility and instruments; for non-sporulating fungi (i.e. hyphal/mycelia forms) this is not a major concern. Moreover, the plates are only exposed immediately prior to analysis. Since the droplet–LMJ–SSP is a separate instrument from the LC–MS, a possible solution if contamination (either of the sample or of the facility) was a serious concern would be to place the droplet–LMJ–SSP in a laminar flow hood, coupling the instruments together with longer tubing.

Finally, although heat mapping experiments obtain a large amount of information, they are not a replacement for MS imaging experiments. For instance, heat mapping experiments take a longer period of time due to the addition of chromatography. More importantly, the resolution (0.7–1.0 mm) of the current droplet–LMJ–SSP is not as high as it is for other imaging techniques (20–200 μm) that must be considered when looking for precise changes in distribution of secondary metabolites, or biomarkers in other

matrices. However, the droplet–LMJ–SSP has the ability to map the spatial distribution of isomers, something not currently possible with other imaging platforms. Also, because heat mapping is not a continuous flow, it has the ability to re–adjust to the various topographies that are encountered, which is a particular challenge with routine sampling of fungal cultures.[77] Additionally, heat mapping provides semi-quantitative results, as its true potential as an analytical technique has been neither evaluated nor optimized due to challenges, such as consistency in droplet recovery. Thus, MS imaging and heat mapping experiments should be viewed as complementary techniques, rather than a substitution for one another.

In conclusion, coupling a droplet–LMJ–SSP with a UPLC–PDA–HRMS–MS/MS system advances ambient ionization techniques with the inclusion of chromatography. Secondary metabolites were characterized with more confidence due to the mutually supportive data that were obtained. Furthermore, cultures were dereplicated directly, with no time spent on sample preparation, seamlessly integrating the current database of retention times, PDA, HRMS, and MS/MS at the level of the extract. The robustness and simplicity of using the droplet–LMJ–SSP makes it a powerful and effective tool for natural products research. Besides our immediate needs in natural products drug discovery, we can envisage applications to probe questions of biosynthesis and chemical ecology.

Experimental

General experimental procedures

The droplet–LMJ–SSP[81-85] capabilities were acquired via collaboration with the Organic and Biological Mass Spectrometry Group at Oak Ridge National Laboratory, who assisted in the conversion of a CTC/LEAP HTC PAL auto–sampler (LEAP Technologies Inc.) into an automated droplet–LMJ–SSP system by using in–house developed software dropletProbe Premium. Extractions were performed using Fisher Optima LC/MS grade solvents consisting of 50:50 MeOH—H_2O. Variations of tested solutions included 30:70 CH_3CN—H_2O, 50:50 CH_3CN—H_2O, 30:70 MeOH—H_2O, and 50:50 MeOH—H_2O. There was no discernable difference in metabolite extraction between the CH_3CN and MeOH mixtures, therefore all experiments proceeded with 50:50 MeOH—H_2O. Higher organic ratios often resulted in unsuccessful liquid microjunction formation, as previously reported.[83] An initial 5 μL of solvent was drawn into the syringe. Droplets of 4 μL were dispensed onto the surface of the sample at a rate of 2 μL/s, held on the surface for 2 s, and withdrawn back into the syringe at the same rate. This extraction process was repeated a total of three times for a single spot prior to injection into the UPLC–MS system.

The droplet–LMJ–SSP was coupled with a Waters Acquity ultra–performance liquid chromatography (UPLC) system (Waters Corp.) to a MS. The initial testing of the applicability of the droplet–LMJ–SSP on fungal cultures was coupled to an AB Sciex TripleTOF 5600+ at Oak Ridge National Laboratory, but the majority of the analyses was performed on a Thermo QExactive Plus MS (ThermoFisher) at UNCG. The

QExactive Plus was adjusted to collect data from 150 to 2000 *m/z* at a resolution of 70,000. The HCD fragmentation used a normalized collision energy of 35 for all compounds. The voltage for both positive and negative ionization modes were set to 3.7 kV, with a nitrogen sheath gas set to 25 arb, and an auxiliary gas set to 5 arb. The S–Lens RF level was set to 50.0 with a capillary temperature at 350 °C. The flow rate of the UPLC was set to 0.3 mL/min using a BEH C18 (2.1 × 50 mm × 1.7 μm) equilibrated at 40 °C. The mobile phase consisted of Fisher optima LC–MS grade CH_3CN—H_2O (acidified with 0.1% formic acid), starting at 15% CH_3CN and increasing linearly to 100% CH_3CN over 8 min. It was held at 100% CH_3CN for 1.5 min before returning to starting conditions for re–equilibration. The PDA was set to acquire from 200–500 nm with 4 nm resolution.

Fungal strain identification

For the identification of strains used in this study, the internal transcribed spacers, ITS region and a portion of the 28S rRNA gene of the nuclear RNA operon were sequenced. Amplicons and sequences for ITS1–5.8S–ITS2 region were generated using primers ITS1F/ITS5 and ITS4, and 28S rRNA gene sequence data were obtained for the first two divergent domains (D1/D2) using primers LROR and LR3. Methods used for strain identification and phylogenetic analysis have been detailed previously.[66,92] [55,95,96,103]

The ITS region was used for barcoding of fungal species by searching against nBLAST with RefSeq database as well as the regular NCBI database; uncultured/environmental sequences were excluded from the BLAST search. The ITS

region was used for species identification, while a portion of the 28S was used for phylogenetic analysis.

Software

Images of each culture were acquired using an Epson Perfection v370 scanner controlled by dropletProbe Premium. The location of the sampling area and the scanned images were calibrated to correlate the X and Y coordinates, and dropletProbe Premium automatically marked the scanned images with a crosshair at the spots where extraction sampling occurred. The creation of heat maps was also performed using the dropletProbe Premium software by correlating the intensities of specified molecular ions (±5 ppm) and retention times to the selected spots on the scanned images.[84,85] ACD MS Manager with add–in software IntelliXtract (Advanced Chemistry Development Inc.) was used for the primary analysis of the LC–MS data for dereplication. This software was used as detailed previously.[73]

Custom sample trays

A customized tray was designed using SketchUp Make (Trimble Navigation Limited), sliced using Simplify3D (Simplify3D LLC), and printed out of polylactic acid (PLA) using a F306 3D printer (Fusion3 Design LLC). The design held a small or large size Petri dish, a solvent vial, and had a needle block position (Figure S14, Supporting Information).

Funding sources

This research was supported by Program Project Grant P01 CA125066 from the National Cancer Institute/National Institutes of Health, Bethesda, MD, USA. Endophytic

fungi from milk thistle were acquired via a Biotechnology Research Grant from the North Carolina Biotechnology Center (2011-BRG-1206). Advancement of the droplet–LMJ–SSP surface sampling technology at ORNL was supported by funding provided through a Cooperative Research and Development Agreement (CRADA NFE-10-02966) with AB Sciex. ORNL is managed by UT-Battelle, LLC for the U.S. Department of Energy under contract DE-AC05-00OR22725.

Acknowledgments

The authors thank Dr. A. Kaur (UNCG) for her contributions to our understanding of the chemistry of several fungal species. We also thank Drs. N.B. Cech and L.M. Duffy (both of UNCG) for helpful discussions pertaining to MS and 3D printing, respectively.

CHAPTER IV

SPATIAL AND TEMPORAL PROFILING OF GRISEOFULVIN PRODUCTION IN XYLARIA CUBENSIS USING MASS SPECTROMETRY MAPPING

This chapter has been published in the journal *Frontiers in Microbiology* and is presented in that style. Sica, V.P., Rees, E.R., Tchegnon, E., Bardsley, R.H., Raja, H.A., Oberlies, N.H. *Front. Microbiol.* **2016**, *7*, 544.

Introduction

For decades, griseofulvin (Figure 20) has been well studied, imparting a rich history in mycology, structure elucidation, and biological activity.[104] For mycologists, its initial discovery from *Penicillium griseofulvum*[105] and subsequently *P. janczewskii*[106,107] proved noteworthy as these griseofulvin-producing cultures induced abnormal development of fungal hyphae. Essentially, griseofulvin triggered other fungal hyphae to "curl" imparting the name "curling factor" as its original descriptor.[106,107] From the perspective of organic chemistry, the characterization of griseofulvin details how the structure elucidation of fungal metabolites evolved in the 20th century. Initially, an ensemble of IR and UV spectroscopy, coupled with combustion analysis of derivatives or degradation products, was employed.[105,108,109] Ultimately, ^{1}H NMR[110] and X-ray crystallography[111] were used to support the previously proposed structures. From a biological activity standpoint, griseofulvin was originally noted to have a unique effect

on molds.[108] Griseofulvin has been employed to treat fungal infections,[112,113] notably dermatophytosis (ringworm), and ultimately became a commercialized product in 1975 (e.g. Fulvicin, Gris-PEG, Grifulvin V). More recently, griseofulvin has shown potential by inhibiting the proliferation of cancer cells but with low general toxicity.[114-116]

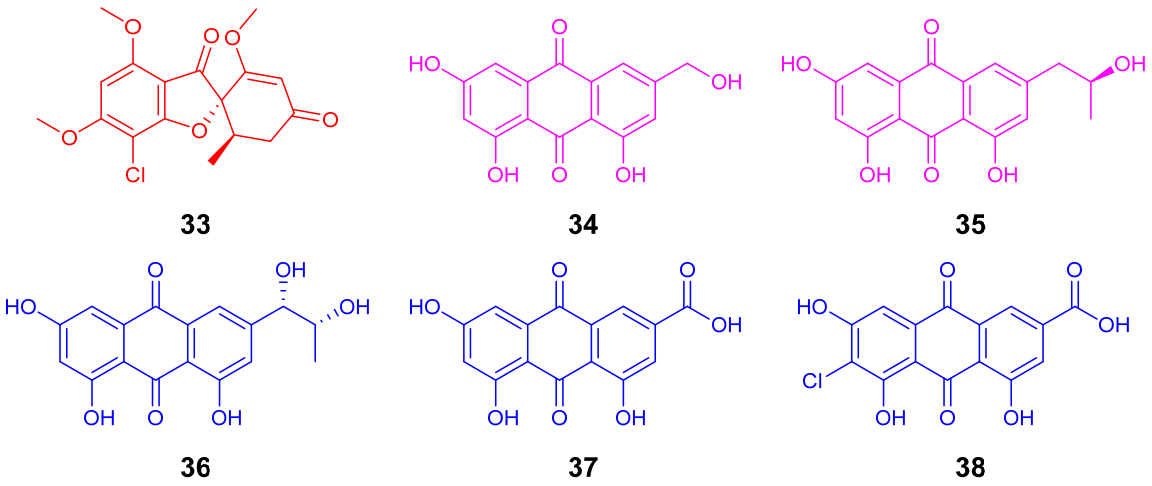

Figure 20. The Structure of the Antifungal Agent, Griseofulvin (33; Red), from *Xylaria cubensis* (G536). The polyhydroxyanthraquinones (**34**–**38**) from Penicillium restrictum (G85) were grouped into two categories (purple and blue) based on their distributions in co-culture.

As an antifungal agent, griseofulvin is fungistatic[117,118] as opposed to fungicidal. This denotes that it inhibits fungal growth, rather than kills competing fungi. While this inhibition has been observed biologically via agar-based disk diffusion assays,[119] the spatial and temporal distribution of its chemistry has never before been visualized. Advances in ambient mass spectrometry techniques, such as mass spectrometry imaging, have allowed for the mapping of secondary metabolites *in situ*.[34,56] However, only a few recent studies have explored mass spectrometry mapping experiments of fungi *in*

situ,[77,120] and even fewer have attempted to understand the chemical interactions between competing microbial cultures.[49]

The popular ambient ionization mass spectrometry techniques include matrix assisted desorption electrospray ionization (MALDI), desorption electrospray ionization (DESI), and nanoDESI to achieve surface sampling and mapping of metabolites directly on fungal cultures. While effective, each of these techniques is not without limitations. Comparatively, MALDI provides superior spatial resolution, but it often requires the application of a matrix to the sample, which can cause ion suppression when dealing with small molecules. Also, it destroys the sample during the laser desorption/ionization process, thus limiting repeat analysis of a growing fungal culture. DESI is less destructive, but the gas and solvent pressures used for this system can manipulate the surface of the fungal culture and its surrounding environment, making it difficult to analyze directly.[77,121] NanoDESI overcomes some of these issues by forming a liquid microjunction with the surface of the culture. This technique is even less abrasive than DESI and more amenable for surface sampling of a fungus and its surrounding agar. However, certain characteristics, such as aerial fungal hyphae and guttates (liquid droplet),[55] have been known to clog the system.[57] Furthermore, both DESI and nanoDESI are not amenable to the natural heterogeneous topography of a fungal culture.[77,120]

To overcome these issues, a droplet–liquid microjunction–surface sampling probe (droplet–LMJ–SSP)[81,82] was optimized to sample and map the secondary metabolites of fungal cultures *in situ*.[120] This technique is robust and provides a non-destructive sampling system that is tolerant of the topography that fungal cultures possess.

Additionally, it has great ionization efficiency and reliability due to its use of electrospray ionization (ESI). The incorporation of liquid chromatography is also beneficial, since it provides mutually supportive data, including retention time and UV data, when analyzing fungal metabolites. The summation of these data, and the ability to separate complex mixtures via chromatography, imparts a high degree of confidence when assigning structures.

Previously, griseofulvin was discovered from xylariaceous endophytes, an important taxonomic group of fungi.[122,123] Endophytes of the *Xylaria* generate morphologically distinct stromatic outgrowths, but the spatial distribution of secondary metabolites throughout the stroma is poorly understood.[124-126] Recently, fungal endophytes from the tree *Asimina triloba* were isolated and revealed several species of xylariaceous fungi, one of which biosynthesized griseofulvin. Mapping the chemical entities of this fungus as it interacts with a competing fungus *in situ* can begin to answer a series of ecological questions that may be lost through a traditional natural products extraction protocol: *where* are the metabolites distributed (spatial), *when* is each metabolite formed (temporal), w*hat* metabolites are interacting (qualitative), *how much* of each metabolite is produced (quantitative), *why* do the fungi produce them (function), and *which* fungus is most affected by the interaction (target). This project sought to probe these questions by using the droplet–LMJ–SSP for direct analysis of a griseofulvin-producing endophytic fungus.

Materials and Methods

Isolation of fungal cultures

Both fungal species employed in this study were isolated as endophytes from surface sterilized plant tissue segments. Fungal strain G536 was isolated from surface sterilized twigs of pawpaw (*Asimina triloba* (L.) Dunal, Annonaceae) collected from Pfafftown, North Carolina, USA (36°09'58.8"N 80°24'18.6"W). Fungal strain G85 was isolated from surface sterilized stems of a milk thistle (*Silybum marianum* (L.) Gaertn. Asteraceae).[55] Isolation of fungal endophytes was performed using methodology described previously.[94,103]

Identification of fungal cultures

Both strains were identified via morphological and molecular methods. Since the former could only provide information regarding the genus of the fungal isolates, molecular data were used to obtain a more accurate identification.

For strain G536, the partial ribosomal polymerase II subunit 2 (*RPB2*) gene was amplified using primers RPB2-5f and RPB2-7cR primers.[127] DNA extraction, PCR amplification and Sanger sequencing was performed using protocols outlined previously.[55,128] Typically, we acquire genomic DNA from two week old cultures on PDA; [55,92] however, this proved challenging for culture G536 and each attempt to acquire DNA from two week old cultures proved unsuccessful. Interestingly, to overcome this challenge, DNA was acquired from a younger (one week) culture grown on 10 ml of YESD. Methods utilized for the molecular identification of strain G85 have been outline previously.[55]

Two forward and reverse contigs of the partial *RPB2* regions were obtained for strain G536 and were assembled and edited using Sequencher v5.3 (Gene Codes Corporation, Ann Arbor, MI). The consensus sequence was then submitted to NCBI GenBank database via BLAST search to obtain matches with identical sequences for subsequent phylogenetic analysis. The BLAST search revealed *Xylaria cubensis* (GQ848365, GQ848364, GQ848366, and GQ853017), as the top match with high coverage and percent identity values. Therefore, these sequences, along with other *RPB2* sequences of *Xylaria* obtained for a recent multi-gene phylogenetic evaluation of Xylariaceae,[129] were downloaded and incorporated into a multiple alignment for Maximum Likelihood (ML) analysis with RAxML using previously described methods.[130]

In addition, to the *RPB2* gene, the entire ITS region was PCR-amplified using primer combinations ITS5 and ITS4[99,131] using PCR amplification protocols defined previously.[55] A forward and reverse contig was obtained as above using Sequencher. The ITS sequence was then subjected to a BLAST search using NCBI GenBank database. Based on this, the closest hits were members of the genus *Xylaria cubensis,* Ascomycota [*Xylaria cubensis* (Mont.) Fr., GenBank GU991523; Identities = 386/392 (98%); Gaps = 0/392 (0%), *Xylaria cubensis* GenBank AB625440; Identities = 383/392 (98%); Gaps = 0/392 (0%)]. In addition, our ITS sequence also showed high coverage and percent identity values with 26 unidentified sequences of Sordariomycetes, Ascomycota [GenBank JQ761856, JQ761796, JQ761749, JQ761744, JQ761693, JQ761562, JQ761423, JQ761405, JQ761381, JQ760963, JQ760763, JQ760481, JQ760128,

JQ761454, JQ760138, JQ761695, JQ761549, JQ761384, JQ761371, JQ761326, JQ761317, JQ760708, JQ760193, JQ761847, JQ761823, JQ761727; Identities = 391/392 (99%); Gaps = 0/392 (0%)]. Interestingly, these ITS sequences were isolated as endophytes from lichen fungi (endolichenic) collected from Highlands Biological Station, North Carolina,[132] which was within 200 miles from where fungal culture G536 was collected. The top BLAST matches were downloaded and incorporated into a multiple alignment for Maximum Likelihood (ML) analysis with RAxML as above.

Fermentation of fungal cultures

In preparation for chemical extraction, G536 was grown on rice, as this has been shown to be an efficient medium for the production of secondary metabolites in culture.[94] To make seed cultures for inoculating rice, a piece of fresh culture grown in Potato Dextrose (PD) (Difco) or 2% Malt Extract (ME) (Difco) media was excised from the leading edge of the colony and transferred to a liquid seed medium containing 2% soy peptone, 2% dextrose, and 1% yeast extract (YESD; 5 g of yeast extract, 10 g of soy peptone, and 10 g of D-glucose in 500 ml distilled water). Following incubation for 7 days at 22°C with agitation, the culture was used to inoculate 10 g of rice media prepared using 30 ml of distilled H_2O and autoclaved in a 250 ml Erlenmeyer flask. This screener scale fermentation was incubated at 22°C for 14–21 days prior to chemical extraction. For large-scale production of fungal cultures, four 250 ml Erlenmeyer flasks containing 10 g of rice were inoculated using one seed culture for each flask.

Extraction of fungal culture

The fungal culture, coded G536, was extracted using a previously reported procedure.[92,133,134] Briefly, the fungus was extracted by adding 60 ml of MeOH–$CHCl_3$ (1:1) to a 125 ml flask containing 10 g of rice with endophytic fungal growth. The fungus was chopped with a spatula before shaking overnight (~16 h) at ~100 rpm at room temperature. Using vacuum filtration, the sample was filtered, and the remaining residue was washed with MeOH. To the filtrate, 90 ml of $CHCl_3$ and 150 ml of H_2O were added. The mixture was stirred for 30 min and then transferred into a separatory funnel. The organic layer was drawn off and evaporated to dryness. The dried organic extract was re-constituted in 100 ml of MeOH–CH_3CN (1:1) and 100 ml of hexanes and transferred to a separatory funnel. The biphasic solution was shaken vigorously. The MeOH–CH_3CN layer was evaporated to dryness under vacuum (69 mg).

Isolation and identification of griseofulvin

The extracted material (69 mg) was dissolved in $CHCl_3$, adsorbed onto Celite 545, and fractionated via normal phase flash chromatography on a CombiFlash Rf system using a 4 g RediSep Rd Si-gel Gold column (Teledyne-Isco, Lincoln, NE, USA). The gradient solvent system was hexane–$CHCl_3$–MeOH at a flow rate of 18 ml/min with 72.9 column volumes over 19.4 min. This afforded three fractions: fraction 1 (0.8 mg), fraction 2 (10 mg) and fraction 3 (50 mg). Fraction 2 was subjected to preparative HPLC using a gradient system of 40% to 100% CH_3CN in H_2O (acidified with 0.1% formic acid) over 30 min at a flow rate of 21.1 ml/min on a Kinetex C_{18} column (Phenomenex, Torrance, CA, USA; 5µm; 250 × 21.2 mm). Griseofulvin eluted at 6.9 min and yielded

1.06 mg. The structure of griseofulvin was verified (Figure S15 & Table S2) via NMR on a JEOL ECS-400 NMR spectrometer (400 MHz; JEOL Ltd., Tokyo, Japan) and HRMS on a QExactive Plus (Thermo Fisher Scientific, San Jose, CA, USA) in positive ionization mode coupled to an Acquity UPLC system (Waters Corp., Milford, MA, USA); literature values were compared for structural confirmation.[109,110,135] The ^{1}H and ^{13}C NMR data are included to update the literature (Figure S15 & Table S2), and this material was used as a standard for the mapping experiments.

LC-MS methodology

The QExactive Plus mass spectrometer was scanned across a range from 225 to 2000 m/z at a resolution of 70,000. The voltage for both positive and negative ionization modes were set to 3.7 kV, with a nitrogen sheath gas set to 25 arb, and an auxiliary gas set to 5 arb. The S–Lens RF level was set to 50.0 with a capillary temperature at 350 °C. The flow rate of the UPLC was set to 0.3 ml/min using a BEH C18 (2.1 × 50 mm × 1.7 μm) equilibrated at 40 °C. The mobile phase consisted of Fisher Optima LC–MS grade CH_3CN–H_2O (acidified with 0.1% formic acid), starting at 15% CH_3CN and increasing linearly to 100% CH_3CN over 8 min. It was held at 100% CH_3CN for 1.5 min before returning to starting conditions for re-equilibration. The PDA was set to acquire from 200–500 nm with 4 nm resolution.

Solid media co-cultivation

Fungal cultures of *Xylaria cubensis* (G536) and *Penicillium restrictum* (G85) were transferred separately from PDA solid media with antibiotics onto three plates of MEA separately to act as controls. Simultaneously, six plates of MEA were prepared for

co-cultivation of *X. cubensis* (G536) and *P. restrictum* (G85). *X. cubensis* was transferred first and allowed to grow for 10 days because *P. restrictum* grows relatively fast compared to *X. cubensis.* After initiating the co-culture experiments, the plates were then parafilmed and allowed to grow for 30 days, until the cultures began to grow towards each other. Concomitantly, the same experiment was performed using PDA and SDA (Sabradoud Dextrose). Visually, the zone of inhibition was most notable in the MEA plates (data not shown). Thus, the co-cultures grown on MEA were subsequently sampled by droplet–LMJ–SSP.

Surface sampling and mapping

The dropletProbe Premium software converted a CTC/LEAP HTC PAL auto–sampler (LEAP Technologies Inc.) into a droplet–liquid microjunction–surface sampling probe (droplet–LMJ–SSP).[81,82,120] This probe performs 5 μl microextractions using Fisher Optima LC–MS grade MeOH–H_2O (1:1). Droplets were dispensed onto the surface of the fungal cultures at a rate of 2 μl/s, held on the surface for 2 s, and withdrawn back into the syringe at the same rate. This extraction process was performed in triplicate using the same droplet. The droplet was then injected into the UPLC-MS system. The relative concentrations of the metabolites, calculated using the dropletProbe Premium software via the area of the exact mass chromatograms for each metabolite at their specific retention times, were mapped, resulting in a visualization of their spatial distribution. The heat mapping experiments focused on griseofulvin (*m/z* 353.0792 ± 5 ppm), which eluted at a retention time of 4.49±0.05 min when using the droplet–LMJ–SSP–UPLC–MS system.

Stroma sectioning

The fungal culture G536 was inoculated in 10 ml liquid YESD media for 7 days then poured into an autoclaved Petri dish containing autoclaved rice. The Petri dish was then placed inside a sterile plant tissue-cultivating container (Plant Con®), and sealed with parafilm. The plant container provides a sterile environment for the stroma producing fungus to grow on rice-based media. Stroma began appearing after 2-3 weeks, but the cultures were allowed to grow for 5.5 weeks (Figure 21).

Figure 21. Image of G536 Grown in a Glass Petri Dish and Placed in a Sterile Plant Tissue-Cultivating Container (Plant Con) to Maintain Sterile Conditions While Providing Room for Stroma Growth.

Stroma were then cut and removed from the Petri dish using a sterile scalpel and forceps. Three individual stroma (one thin [~40×2 mm], one medium [~50×4 mm], and one thick [~50×6 mm]) were removed from the fungal culture G536. Each stroma was cut into three segments: tip, middle, and base (Figure 22 & Figure S16). The three white tips, the three mid-sections, and the three bases were combined and placed into separate

vials and weighed. This procedure was repeated two more times resulting in three groups that sampled a total of nine stromata (Table S3).

Figure 22. A Representative Group (Group 3) of Three Stroma and Their Respective Segments. Each segment ranged from 9 to 20 mm.

To each vial, 5 ml of MeOH–H_2O (1:1) were added and shaken overnight (~16 h). The supernatant was then drawn off, placed in a weighed vial and dried under a stream of nitrogen. An aliquot of each dried extract was prepared in MeOH–H_2O (1:1) to a concentration of 2 mg/ml and subjected to LC-MS analysis.

Results

Molecular analysis

Stromata were examined for sporulating structures, but we were unable to observe any ascospores, asci or conidia. Thus, species delimitation based on morphological characters in cultures of endophytic *Xylaria* was difficult because of a lack of diagnostic characters; therefore, molecular data were used for species identification.

Based on RAxML analysis using *RPB2* sequences (Figure S17), the strain G536 was identified as *Xylaria cubensis. RPB2* sequences of strain G536 were nested within the *X. cubensis* aggregate[129] with 80% RAxML bootstrap support. *X. cubensis* (G536) is sister to GQ848365, a *X. cubensis* isolate collected from the Great Smoky Mountains National Park, and forms a monophyletic clade with 100% RAxML bootstrap support with other collections of *X. cubensis* from different geographical locations, including Russia, French West Indies, and Papua New Guinea (Figure S17). The phylogenetic tree obtained using ITS sequences supported the *RPB2* results. Strain G536 was nested in a clade containing other identified *X. cubensis* sequences, including authenticate voucher sequences of *X. cubensis* (GU373810 and GU991523) (Figure S18). The sequence data were deposited in the GenBank (KU560914, KU560915, KU560916).

Spatial distribution of griseofulvin on *X. cubensis*

The griseofulvin-producing fungus, *X. cubensis*, was subjected to surface sampling analysis via the droplet–LMJ–SSP, and the spatial distribution of griseofulvin was mapped. *X. cubensis* was grown on MEA for 2.5 weeks. The culture was then sampled at nine locations, transecting the culture both horizontally and vertically (Figure 23A). The first sampling was taken at the point of inoculation (center), followed by four spots towards the right end of the culture and another four spots towards the bottom of the culture (Figure 23A). The map shows a higher concentration of griseofulvin towards the edges of the culture. A second culture was simultaneously inoculated and grown for 5.5 weeks. Similarly, this culture was sampled from the center to the edge. However, griseofulvin displayed a more even distribution across the culture (Figure 23B).

Furthermore, liquid droplets containing high concentrations of secondary metabolites, termed guttates, were formed on the surface of the 5.5 week old culture (Figure 23B).[55,136]

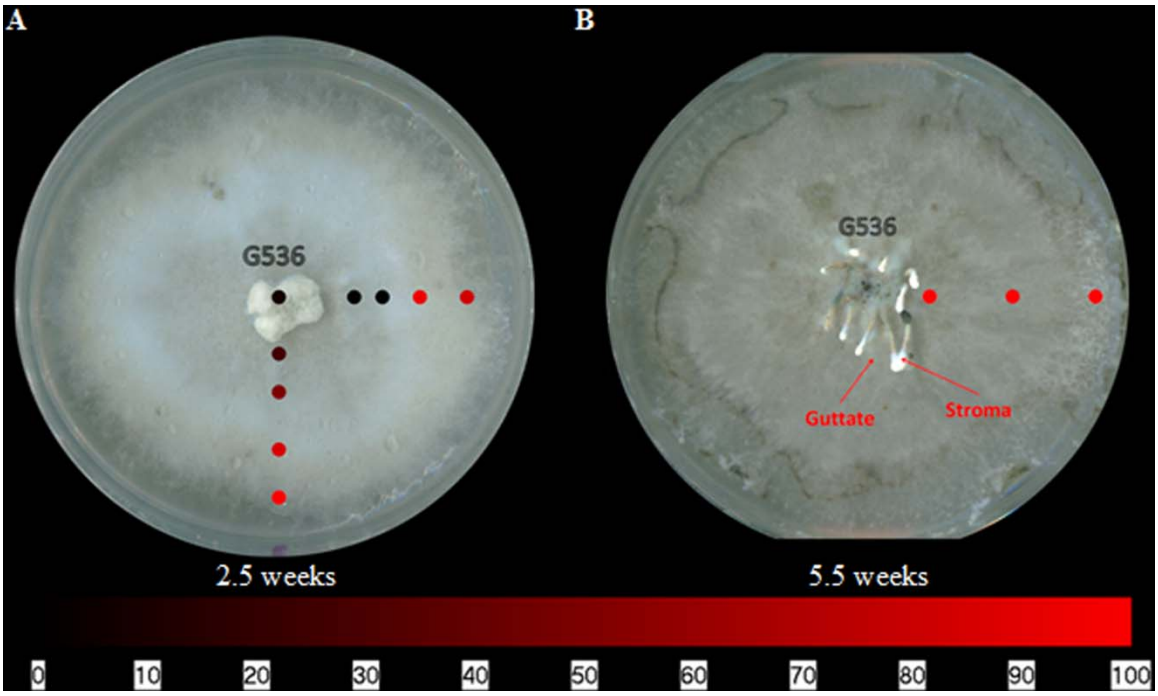

Figure 23. The Spatial Distribution of Griseofulvin on *X. cubensis* (G536) Grown on MEA at (A) 2.5 Weeks and (B) 5.5 Weeks of Growth Displaying the Locations of Guttate and Stroma Formations. Each circle represents a sampled location. Griseofulvin was most intense where the circles are bright red. The bottom bar indicates the relative amount of signal as measured via mass spectrometry.

Spatial distribution of griseofulvin in stroma of *X. cubensis*

Xylariaceous fungi often grow morphologically-distinct 'finger-like' protrusions called stroma (Figure 23B). Mapping of the spatial distribution of griseofulvin on stroma was originally planned via the droplet–LMJ–SSP, but black, mycelium-covered portions of the stroma were too absorbent to recover the micro-extraction droplet. This experiment was repeated several times to no avail, likely due to the absence of hydrophobins, since

aerial mycelium that lack conidia/spores are more hydrophilic.[100,120] Therefore, an alternative methodology was performed. *X. cubensis* was grown in a sterile plastic container for 5.5 weeks to promote stroma growth. The stroma were then segmented, grouped (Figure S16), extracted, and then subjected to LC-MS analysis. Griseofulvin was most abundant at the base of the stroma and less abundant as sampled vertically towards the white tip (Figure S19 & Table S3). For groups 1 and 2, the concentration of griseofulvin in the middle was less than a magnitude greater than the tip, while the base was over three magnitudes greater than the tip. Group 3 varied from this trend with the middle being about three magnitudes greater than the tip, yet the base was only about two magnitudes greater. This discrepancy for group 3 was likely due to the uncharacteristically large mid-section for the thick stroma. Regardless, all three groups displayed increased griseofulvin in the black, mycelium-covered portion of the stroma compared to the white, spore-covered tip.

Spatial distribution of griseofulvin in co-culturing experiments

A benefit of mass spectrometry heat mapping experiments of secondary metabolites is not only the ability to provide visualization of the chemical entities, but also, to gain insight into the role that the entities play when interacting with the environment. Mapping the spatial distribution of griseofulvin in a co-culture experiment provides an understanding of the chemical ecology that takes place when the fungus interacts with another fungus. To achieve this, the griseofulvin producing culture, *X. cubensis*, was simultaneously inoculated with a culture of *Penicillium restrictum*, which was chosen due to our knowledge of its chemistry via previous research.[55,137]

When mapping griseofulvin in the co-culturing experiments, griseofulvin was only detected on the surface of the fungus in which it was produced; it was neither in the surrounding agar nor on the other fungus, *P. restrictum* (Figure 24). This distribution was evident after 2.5 weeks and 3.5 weeks of co-cultured fungal growth. While there was a clear inhibition zone between the two fungi, griseofulvin was not detected in this area (Figure 24). It remained on the surface of *X. cubensis*, similar to its spatial distribution when grown in isolation (Figure 23). Furthermore, *X. cubensis* did not display any physical changes to its growth patterns, besides the inhibition zone.

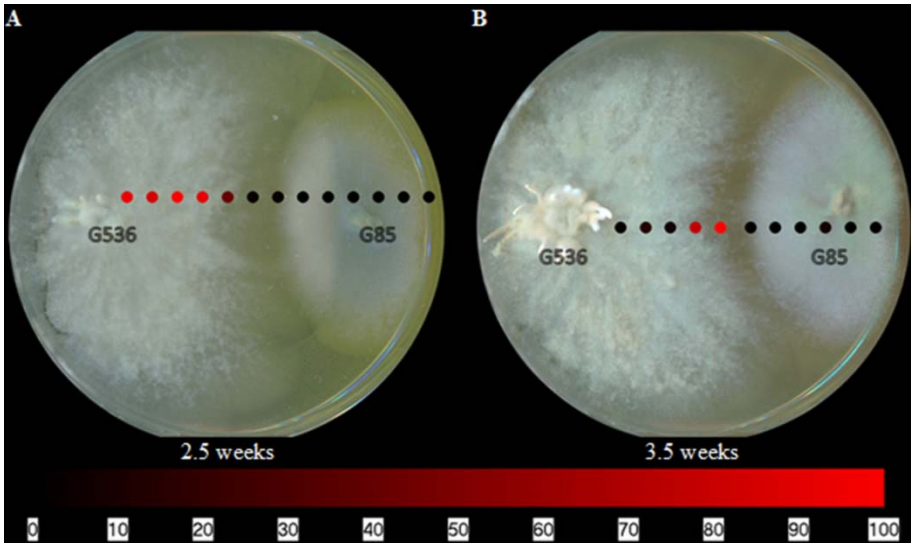

Figure 24. The Spatial Distribution of Griseofulvin from *X. cubensis* (G536) While Grown in Co-Culture with *P. restrictum* (G85) at (A) 2.5 Weeks and (B) 3.5 Weeks. Each circle represents a sampled location. Griseofulvin was most intense where the circles are bright red. The bottom bar indicates the relative amount of signal as measured via mass spectrometry.

The co-culturing effects on the competing *P. restrictum* culture

In addition to mapping the spatial distribution of griseofulvin, it is important to understand the toll that is taken on the other fungal culture. By mapping the metabolites

of *P. restrictum*, the inhibitory effects of griseofulvin can be further understood. In a previous study of *P. restrictum*, a series of polyhydroxyanthraquinones were identified.[55,137] In this study, *P. restrictum* was grown on agar for 2.5 weeks, and five of its secondary metabolites (compounds **34**-**38**) (Figure 20) were readily detected on the surface using the droplet–LMJ–SSP (Figure 25A). While the metabolites were detected on the surface of the mycelium, their signals were a magnitude greater on the surface of the agar (Figure S20). Furthermore, another plate of this culture was grown for 5.5 weeks, and similar distributions (Figure 25B) and magnitude differences (Figure S21) were observed.

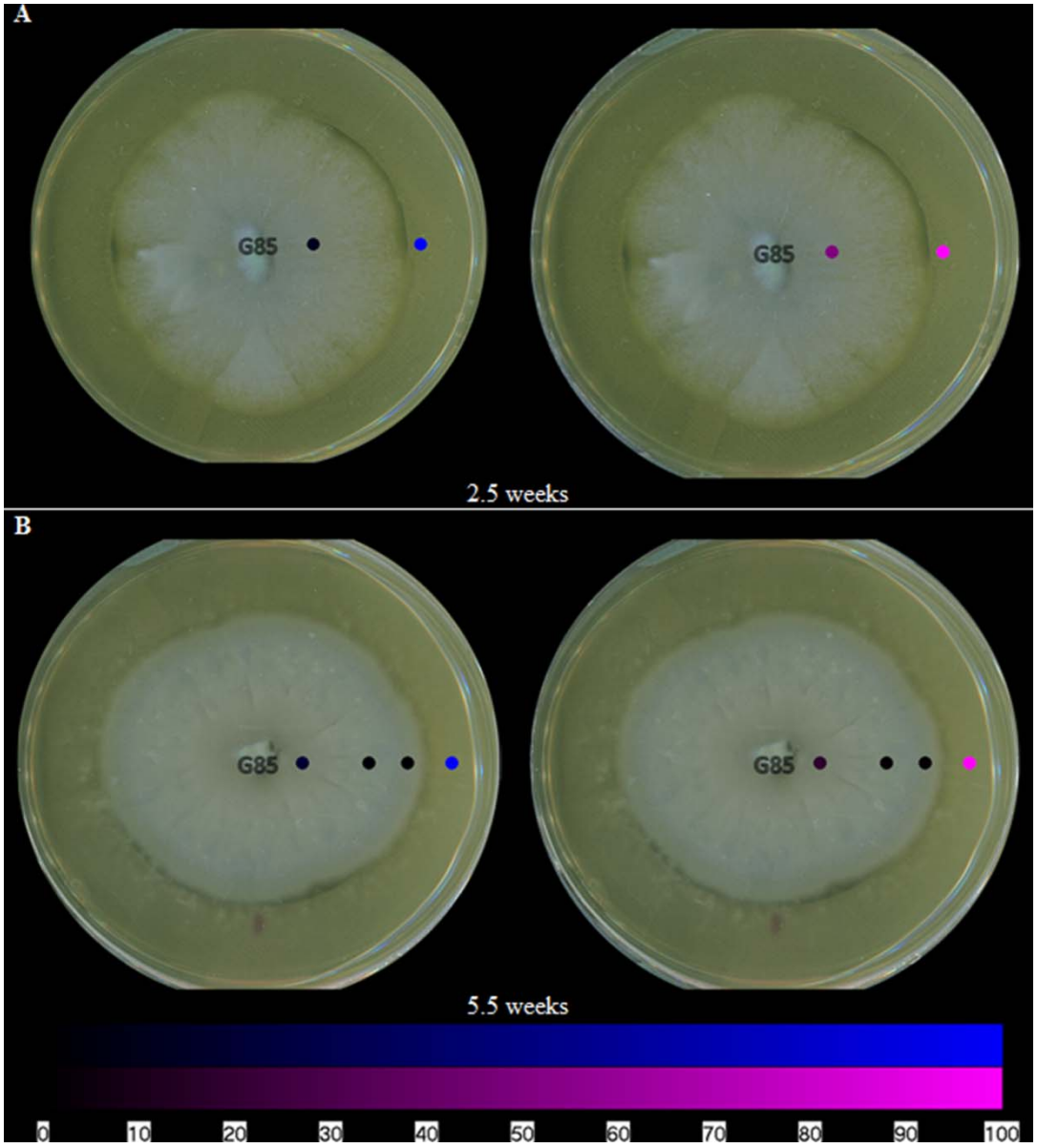

Figure 25. The Spatial Distribution of Both Groups of Polyhydroxyanthraquinones on Fungal Isolates of *P. restrictum* (G85) at (A) 2.5 Weeks and (B) 5.5 Weeks. The color coding (blue and purple) corresponds to the structures in Figure 20. Each circle represents a sampled location. The polyhydroxyanthraquinones were most intense where the blue or purple circles were brightest. The bottom bar indicates the relative amount of signal as measured via mass spectrometry.

Visualizing the secondary metabolites from *P. restrictum* in isolation created a baseline of how this fungal culture distributes its metabolites. Subsequently, by mapping

the metabolites of *P. restrictum* in co-culture with *X. cubensis*, the effects of griseofulvin on a competing fungus could be probed. The five compounds from *P. restrictum* were grouped into two categories (compounds **34**–**35**; purple and compounds **36**–**38**; blue) (Figure 20) that were determined by their distribution patterns in co-culture (Figure 26). As a fungal isolate, *P. restrictum* metabolites (**34**–**38)** were exuded into the surrounding agar (Figure 25); however, in co-culture with *X. cubensis*, only three of the five compounds (**36**–**38**; blue) continued this trend by being detected on both sides of the colony (Figure 26A). The other two metabolites (**34**–**35**; purple) were not detected in the interaction zone, but still remain exuded into the media on the side of the colony farthest from the griseofulvin-producing fungus (Figure 26B).

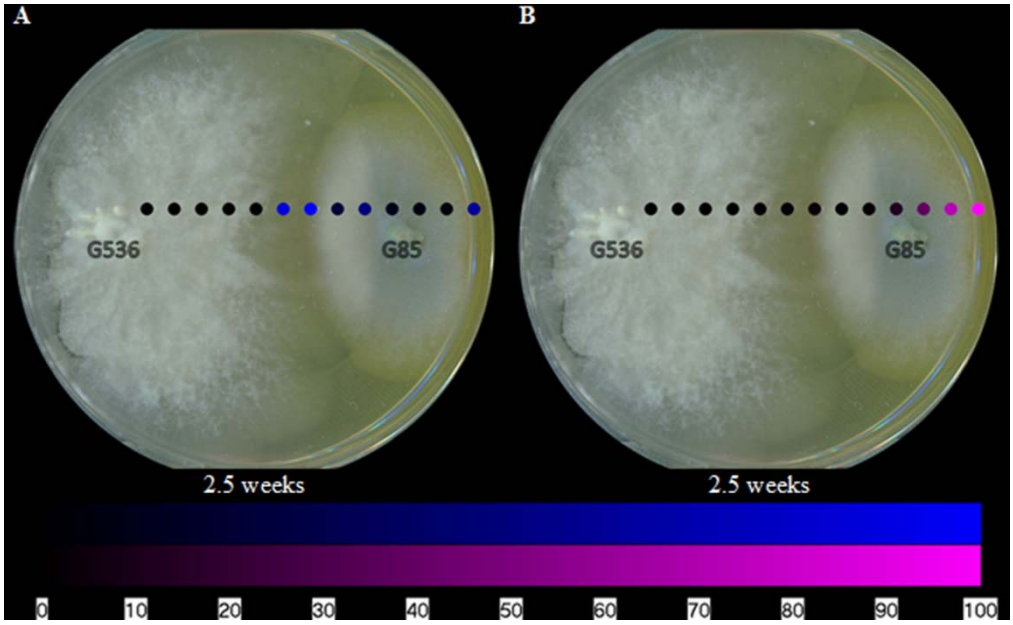

Figure 26. The Spatial Distribution of Both Groups of Polyhydroxyanthraquinones on Fungal Isolates of *P. restrictum* (G85) While Grown in Co-Culture with *X. cubensis* (G536) at 2.5 Weeks. The color coding (blue and purple) corresponds to the structures in Figure 20. Each circle represents a sampled location. The polyhydroxyanthraquinones were most intense where the blue or purple circles were brightest. The bottom bar indicates the relative amount of signal as measured via mass spectrometry.

As the co-cultures continued to grow for another week to a total of 3.5 weeks, the pattern continued (Figure 27A). Griseofulvin still remained primarily on *X. cubensis*, while some of the *P. restrictum* (G85) metabolites were no longer detectable (**34**–**35**; purple). By 5.5 weeks, griseofulvin was detected on both the original *X. cubensis* colony and where the original *P. restrictum* colony was inoculated (Figure 27B). This was attributed to the observation that new growths of *X. cubensis* had begun to grow where the original *P. restrictum* colony was, as indicated by the formation of guttates and stroma containing griseofulvin. This suggests how griseofulvin may be used by *X. cubensis* to outcompete other fungi and then propagate.

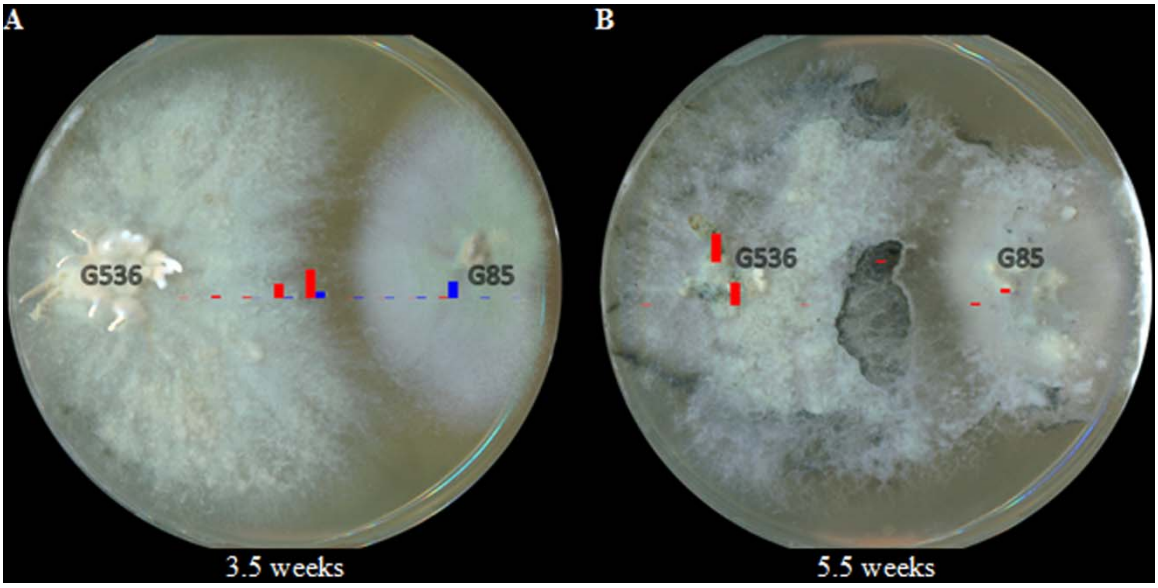

Figure 27. Heat Map of Griseofulvin (Red) and the *P. restrictum* (G85) Metabolites (Blue Group Only; Purple Metabolites Were Undetectable) at (A) 3.5 Weeks and (B) 5.5 Weeks. The heights of the bars are relative to their intensity from the HRMS data.

Visually, the growth of the competing culture, *P. restrictum*, began to lose color after 2.5 weeks. (Figure 28A). The left most edge of *P. restrictum* began to turn white, something that was not observed when this fungus was grown in isolation. The discoloration continued to grow, eventually turning the entire *P. restrictum* colony white after 3.5 weeks of co-culturing (Figure 28B). After 5.5 weeks, the *P. restrictum* culture failed to grow further and the griseofulvin-producer, *X. cubensis*, began to grow new colonies on top of *P. restrictum* (Figure 28C). Guttates formed on both the original and the new growths of *X. cubensis*. Furthermore, the formation of stroma, morphological characteristics of fungi of this family, were visible on both colonies as well. By 8 weeks, the stromata from *X. cubensis* were prevalent on both the original colony and the new growths that were on top of the presumed dead *P. restrictum* colony (Figure 28D).

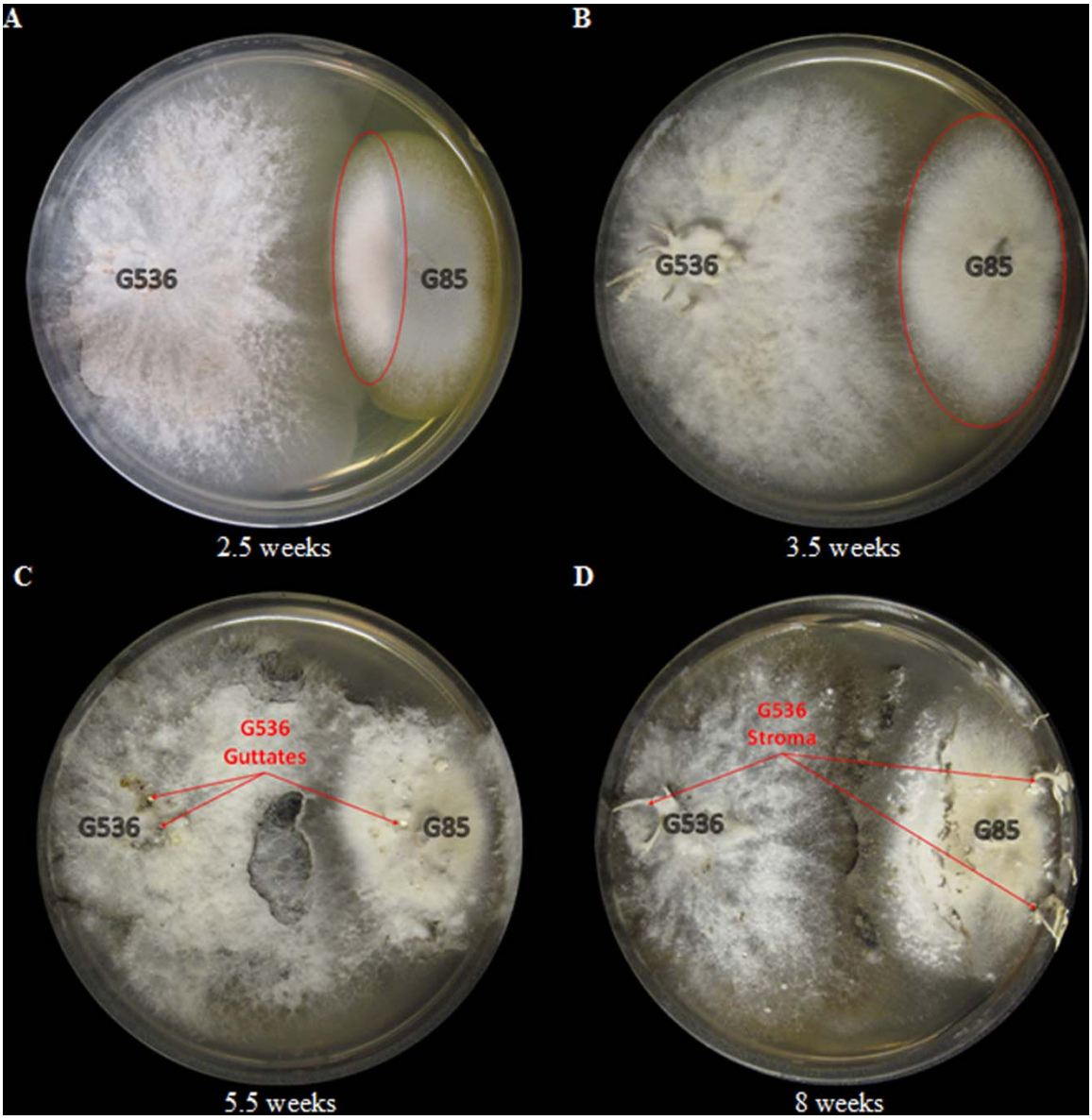

Figure 28. The Visible Discoloration of *P. restrictum* (G85) While in Co-Culture with the Griseofulvin-Producer, *X. cubensis* (G536), at (A) 2.5 Weeks and (B) 3.5 Weeks. The discolored regions of *P. restrictum* (G85) are circled in red. The visible expansion of *X. cubensis* (G536) while in co-culture with *P. restrictum* (G85) at (C) 5.5 weeks and (D) 8 weeks. The guttates were attributed to *X. cubensis* (G536) due to the detection of griseofulvin. The stroma were attributed to X. cubensis (G536) since *P. restrictum* (G85) does not produce stroma.

Discussion

Spatial distribution of griseofulvin on *X. cubensis*

The heat mapping experiments of the griseofulvin-producer, *X. cubensis* (G536), showed a relative concentration of griseofulvin towards the edges after 2.5 weeks of growth (Figure 23A). As the culture grew for 5.5 weeks, the distribution appeared more uniform across the culture (Figure 23B). It is hypothesized that griseofulvin is most abundant in the younger sections of a colony (i.e. the outer edges) to facilitate continued growth, but evens out when the culture is no longer growing laterally.

Additionally, at 3.5 weeks, the culture began to form stromata and produce guttates (i.e. liquid droplets)[55,136] on its surface. On a culture at 5.5 weeks, surface sampling analysis was performed using the droplet–LMJ–SSP to analyze the stromata and guttates. The signal of griseofulvin on a guttate was over two magnitudes greater than that of a stroma (both base and tip) and about half a magnitude greater than on the mycelium (Figure 29 & Figure S22). This finding continues to support a previous hypothesis that guttates are concentrated droplets of metabolites exuded into their environment.[120,138,139] In this culture, the stroma were immature, thus the black, mycelium-covered body was not as hydrophilic as it was for the older stroma. As such, the droplet–LMJ–SSP was able to carry out the analysis *in situ*.

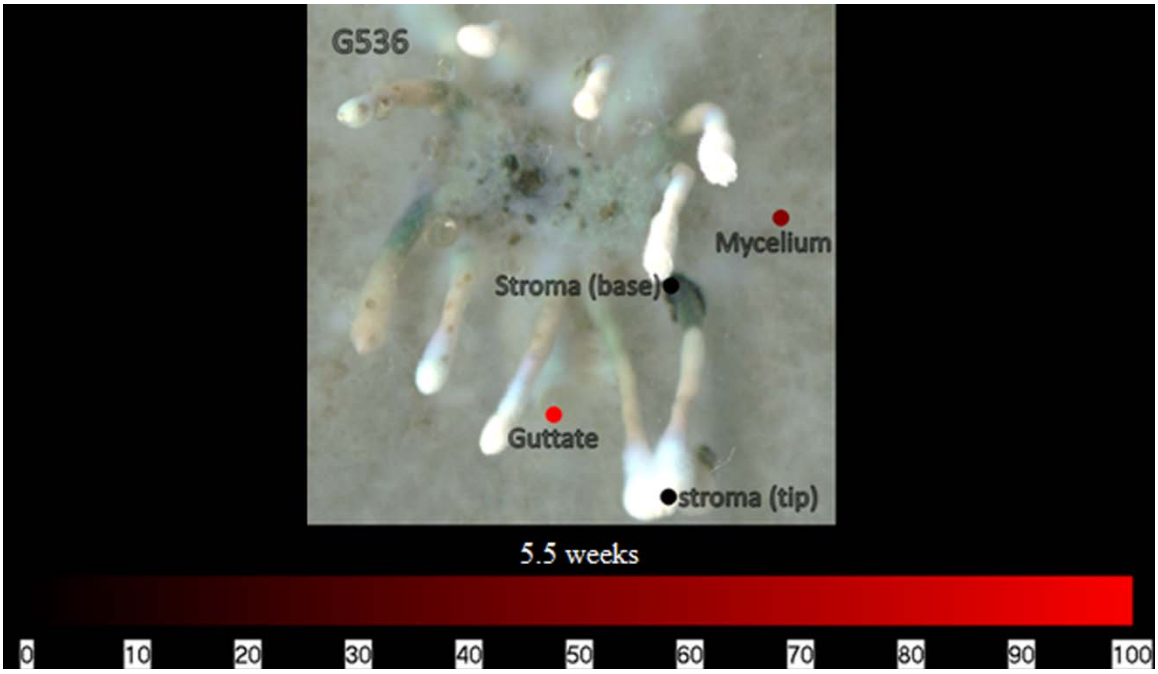

Figure 29. The Spatial Distribution Indicating the Relative Intensities of Griseofulvin on Fungal Culture *X. cubensis* (G536) for the Stroma, Mycelium, and Guttates at 5.5 Weeks. Each circle represents a sampled location. Griseofulvin was most intense where the circles are bright red. The bottom bar indicates the relative amount of signal as measured via mass spectrometry.

Spatial distribution of griseofulvin in stroma of *X. cubensis*

Initially, the stroma were to be analyzed via the droplet–LMJ–SSP to give a heat map from the base of a stroma to the tip. However, upon sampling the black, mycelium-covered portions of the stroma, the droplet was quickly absorbed in the stroma, rendering the droplet unrecoverable. The white tips of the stroma were amenable to droplet recovery, but not the black regions of the stroma, which were more heavily covered by mycelium. Various methods were explored in an effort to directly sample the stroma using the droplet–LMJ–SSP but all proved unsuccessful. Three of these stroma modifications included: (1) freezing stroma in liquid nitrogen, (2) drying stroma in a desiccator, or (3) cutting stroma open longitudinally. None of these methods worked and

all resulted in the droplet being absorbed into the stroma. Combinations of all of these methods were also attempted with no success. This led to the more traditional procedure of cutting the stroma into three segments, extracting, and then analyzing via LC-MS. The results indicated that griseofulvin was most abundant at the base compared to the tip. Since griseofulvin was concentrated towards the edges of the mycelial growth (Figure 23A), compounded with the observation that griseofulvin was concentrated towards the base of the stroma, we hypothesized that the stroma were basipetal (i.e. youngest at the base of the stromata).

Spatial distribution of griseofulvin in co-culturing experiments

Since griseofulvin is known to be fungistatic and not fungicidal, we hypothesized that griseofulvin would reside mostly on the surface of *X. cubensis*, rather than actively being exuded into its surroundings. This would effectively inhibit the growth of other fungi, rather than kill them. This contrasts a phenomenon that was previously reported when mapping the spatial distribution of the fungicidal compound, iturin,[140] from a coral microbe[49] in co-culture with a fungus. In this case, iturin was exuded into the media, thus similarly inhibiting the fungal growth and the production of fungal secondary metabolites.[49]

The spatial distribution patterns of griseofulvin as an isolated fungal culture (Figure 23) and as part of a co-culture experiment (Figure 24) displayed minimal changes. Griseofulvin appeared to remain on the surface of *X. cubensis*, rather than exuding into the surrounding media or on the competing fungus. These mapping

experiments support the fungistatic ability of griseofulvin by remaining on the griseofulvin-producing fungus.

The fungistatic ability of griseofulvin was explored further by growing *X. cubensis* along with another fungus. The fungus selected was a non-xylariaceous endophyte from *Silybum marianum* (milk thistle) and was previously identified as *Penicillium restrictum*, coded G85.[55] *P. restrictum* was selected for three reasons: (1) the secondary metabolites of this fungal culture were defined;[55] (2) the key secondary metabolites were explored previously using mass spectrometry imaging experiments;[55] (3) the secondary metabolites were shown to play a role in inhibiting the quorum sensing pathways for bacteria,[137] hence we suspected that they would also be found exuded into the environment.

The co-culturing effects on the competing *P. restrictum* culture

The spatial distribution of the metabolites from fungal culture G85 were mapped using the droplet–LMJ–SSP. The metabolites were exuded into the surrounding agar of *P. restrictum* (Figure 25). This behavior was not unexpected since we presumed that these compounds would be exuded into the environment due to our understanding of their biological activity as microbial quorum quenching metabolites.[55,137] However, while in co-culture with *X. cubensis*, some of the *P. restrictum* metabolites (purple) were not observed in the interaction zone between fungal cultures *P. restrictum* and *X. cubensis* (Figures 26 & 27), indicating inhibition of secondary metabolite biosynthesis in *P. restrictum*. Interestingly, the two compounds (**34**–**35**; purple) most affected by the co-

culturing experiment were the same two compounds that were most active in the bacterial quorum sensing inhibition bioassay.[55,137]

From an ecological standpoint, the growth of the competing culture, *P. restrictum*, was clearly inhibited as observed by its loss of color over time. Ultimately, this discoloration was attributed *P. restrictum* dying, since the culture never continued to grow in the direction where the white was present. However, griseofulvin is reported to be fungistatic rather than fungicidal,[117,118] therefore, it was questioned whether or not *X. cubensis* truly killed *P. restrictum* prior to growing over it. An experiment, coined the Lazarus experiment (John 11:1-44 (Common English Bible), was performed to test if *P. restrictum* survived the co-culture experiment with *X. cubensis*. Therefore, *P. restrictum* was subsequently transferred from the co-culture Petri dish to a new Petri dish without any competing fungal cultures. Within a week, *P. restrictum* began to grow a new colony, thus confirming that it wasn't killed by the griseofulvin from *X. cubensis*, supporting the fungistatic properties of griseofulvin.

***Xylaria cubensis* lives a dual mode of life**

Xylaria cubensis is widely distributed in tropical, subtropical, and temperate regions of the world, where it is usually found in decaying angiosperm wood.[141,142] Additionally, there is growing evidence in the literature where *X. cubensis* has been reported as an endophyte from various healthy tissue types (twigs and foliage).[143-147] The production of griseofulvin by the endophytic stage of *X. cubensis* has an ecological advantage to the fungus. Similarly, other studies of endophytic *Xylaria* have also reported griseofulvin as a major secondary metabolite.[122] By producing griseofulvin, *X. cubensis*

can stunt the growth of other fungi in the host in an endophytic state or on decaying substrates in the saprobic state. The production of secondary compounds is a common characteristic of many endophytic fungi and provides a basis for selection supporting the symbiosis in the host plant.[148] Thus, by inhibiting the growth of other fungi, *X. cubensis* ensures it can spread its mycelium throughout the host when its host senesces, at which time it can begin to sustain as a saprobe by decomposing cell wall materials;[149,150] griseofulvin biosynthesis likely imparts a competitive advantage in the saprobic state as well.

Mass spectrometry mapping experiments enabled the visualization of how griseofulvin biosynthesis imparts an ecological advantage to a fungus, which can lead dual (endophytic/saprobic) modes of life. The measurements of the spatial and temporal production of griseofulvin by endophytic *Xylaria* sp. when in competition with another endophyte demonstrated how endophytes might use secondary metabolites against other microorganisms in nature. Our chemistry data lend support to the hypothesis that *Xylaria* endophytes are quiet colonizers of their host. Presumably, they use secondary metabolites, such as griseofulvin, to keep other microbes at check. This allows them to spread within the host, so it can decompose the plant when it begins to senesce.[149,150]

In conclusion, ambient mass spectrometry mapping techniques provided an understanding of the chemical ecology that took place between two fungal cultures. For *X. cubensis,* it was revealed that griseofulvin was concentrated in the younger tissues of the fungus, typically around 2-3 weeks of development, towards the edges of the mycelial growth and at the base of the stroma. Conversely, *P. restrictum* excreted the secondary

metabolites, polyhydroxyanthraquinones, into the surrounding environment with only trace amounts detected on the mycelium. When *X. cubensis* was grown in co-culture with *P. restrictum*, the spatial and temporal distributions of griseofulvin remained the same, but there was a noticeable effect on the distribution of polyhydroxyanthraquinones from *P. restrictum*. The biosyntheses of two of the five polyhydroxyanthraquinones were greatly hindered. Eventually, the growth of *P. restrictum* was inhibited and *X. cubensis* began to overtake the culture. Griseofulvin displayed clear signs of having a fungistatic effect on competing fungi as visualized via mass spectrometry mapping experiments. By exploring the temporal and spatial distributions of fungal secondary metabolites through these co-culturing experiments, the questions of – *where* (spatial), *when* (temporal), w*hat* (qualitative), *how much* (quantitative), *why* (function), and *which* (target) – were probed in detail.

Acknowledgments

Fungal culture G85 was first isolated via support from a Biotechnology Research Grant (2011-BRG-1206) from the North Carolina Biotechnology Center. The authors thank Drs. Vilmos Kertesz and Gary J. Van Berkel (Mass Spectrometry and Laser Spectroscopy Group, Chemical Sciences Division, Oak Ridge National Laboratory) for inspiration and guidance with the droplet-LMJ-SSP.

CHAPTER V

OPTIMIZING PRODUCTION AND EVALUATING BIOSYNTHESIS IN SITU OF AN HERBICIDAL COMPOUND, MEVALOCIDIN, FROM CONIOLARIELLA SP.

This chapter has been published in the journal *Journal of Industrial Microbiology and Biotechnology* and is presented in that style. Sica, V.P., Figueroa, M., Raja, H.A., El-Elimat, T., Darveaux, B.A., Pearce, C.J., and Oberlies, N.H. *J. Ind. Microbiol. Biotechnol.* **2016**.

Introduction

Organic farming had seen exponential growth over the past decade. According to the USDA, certified organic acreage in 2008 was over 2.6 million in the United States alone,[151] and global organic sales reached $54.9 billion in 2009.[152] With these numbers steadily increasing, the need for a natural product herbicide has grown as well. The use of herbicides for organic farming is extremely restricted,[151] leaving few options available for weed control, other than manual labor. No new, unaltered natural product herbicides or farming bioherbicides have been introduced to the market in over 15 years.[153]

Natural products have yielded some herbicides, but they have typically required synthetic modifications to create an effective product. Phytotoxic allelochemicals produced by microorganisms make up one class of commercialized natural product

herbicides.[154] The tripeptide, bialaphos, was isolated originally from *Streptomyces hygroscopicus*.[153] Introduced to the market (Japan) in 1984 as a post-emergent herbicide, bialaphos is not phytotoxic itself, but rather, becomes phytotoxic when the targeted plant converts it metabolically to phosphinothricin.[155] Synthetically, phosphinothricin is made into an ammonium salt, termed glufosinate. While bialaphos is marketed as an herbicide in Japan (as Herbiace), only glufosinate is commercially available globally (i.e. Basta, Ignite, and Liberty). Triketones, another class of naturally derived herbicides,[153] were discovered in 1977 via the isolation of leptospermone from *Callistermon citrinus*. Various derivatives were synthesized to optimize the herbicidal properties, yielding the commercialized products mesotrione (Callisto), topramezone (Armezon), and tembotrione (Laudis). However, only the derivatives were found to be viable herbicides, thus eliminating the potential application towards organic farming.

From an organic farming perspective, the post-emergent natural product herbicides that are available lack in many areas. Aqueous acetic acid (20% v/v), sold as horticultural vinegar, often requires continual treatment to be effective and is typically used on non-cropland areas due to its burn down, non-selective method of weed management.[156] Fatty acids have been used, as well, but they also require repeat treatment, since there is no residual activity after the initial burn down effect.[157] Other natural products that are similarly ineffective include cornmeal with clove oil,[158] lemongrass oil, and D-limonene.[159]

Dow AgroSciences in collaboration with Mycosynthetix discovered mevalocidin[160] (Scheme 1) from two, now patented[161], fungal strains, MSX56446 and

MSX92917, originally identified as *Fusarium* sp. and *Rosellinia* sp., respectively using only the D2 region of the nuclear large subunit (nLSU/28S), which was approximately 320 bp; the identification of these organisms has been revised using both the internal transcribed spacer region of the rRNA gene (ITS) as well as the D1/D2 region. Mevalocidin (**39**) has shown promise in filling the need as an effective herbicide for organic farming, since it is produced naturally from fungi. It has displayed strong post-emergent activity with greater than 50% injury to all of the broadleaf and grass species tested at 4 kg/ha after 16 days and lethality after 21 days.[160] Perhaps more importantly, mevalocidin displays the rare, yet desirable, attribute of being phloem and xylem mobile, allowing distribution throughout the plant, including the meristems. Hence, this study determined the growth conditions for optimal mevalocidin production in support of efforts to commercialize these fungal strains as organic bioherbicides for the farming industry. Furthermore, mass spectrometry mapping experiments were employed to examine the potential ecological role of mevalocidin in these fungi.

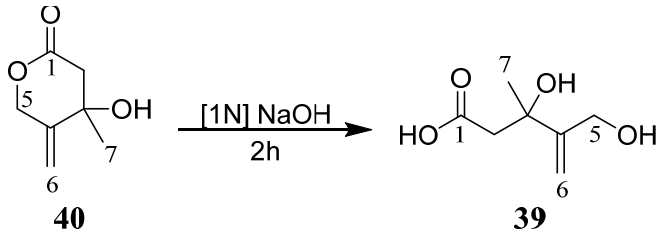

40 **39**

Figure 30. Conversion of Methylidene Mevalonolactone (40) to Mevalocidin (39).

Materials and Methods

Fungal strain and fermentation

Mycosynthetix fungal strain MSX92917 (*Coniolariella* sp.; Figure S23 and S24, Supporting Information) was isolated from twigs and wood collected in 1998, while fungal strain MSX56446 (*Coniolariella* sp.; Figure S23 and S24) was isolated from oak and sweetgum leaf litter. The strains were deposited at the NRRL culture collection of the National Center for Agricultural Utilization Research (Peoria, IL) under the accession numbers NRRL 30882 (for DA056446/MSX56446) and NRRL 30883 (DA092917/MSX92917),[160] respectively. A fresh culture of each isolate was grown on a malt extract slant, and a piece was transferred to a medium containing 2% soy peptone, 2% dextrose, and 1% yeast extract (YESD media). After incubation at 22 °C for 7 d (with agitation), the culture was used to inoculate 50 mL of rice medium [containing rice, vitamin solution, and water (twice the volume of rice)] in a 250-mL Erlenmeyer flask. The cultures were incubated at 22 °C until sufficient fungal growth (~14 d) was observed. The scaled-up cultures were grown in a 2.8-l Fernbach flask containing 150 g of rice and 300 mL of H_2O and inoculated using a seed culture grown in YESD medium followed by incubation at 22 °C for 14 d. For the time variable experiments, the growths were stopped at the indicated time points by freezing the entire culture prior to processing in parallel. For the temperature variable experiments, the cultures were grown at either 25 °C, 30 °C, or 35 °C for 14 d. For the comparison of the liquid vs solid YESD media experiments, the above YESD formula was used in both cases, with the addition of 1.5% agar for the latter; in both cases rice was not added. For the experiments where the amount of

dextrose was varied, each fungal strain was inoculated in 50 mL of medium containing 1% malt extract and 1% agar with incremental amounts of dextrose (Table 4) and grown at 22 °C.

Molecular identification of the fungal strains

For molecular identification and phylogenetic analysis of the fungal strains employed in this study, the ITS region was sequenced using primers ITS5 and ITS4 [99,131] and PCR amplification methods outlined previously.[66,162] The ITS region has been proposed as a barcoding marker for members of the kingdom fungi.[163] Two portions of ribosomal genes were sequenced to get an indication of where the strains belonged using BLAST search. Since there were no other genes sequenced (e.g. beta tubulin) for *Coniolariella* in NCBI GenBank, our phylogenetic analyses relied on ribosomal genes (ITS + LSU) for identification purposes. After obtaining the complete ITS region for both the strains MSX56446 and MSX92917, the individual ITS sequences were aligned using MUSCLE, which was implemented in the program Seaview.[164] The sequences from the two strains were then analyzed with PAUP* 4.0b10[165] to calculate the uncorrected p-distances. P-distance compares the two sequences by calculating the proportion of nucleotide sites at which the sequences are different; uncorrected p-distances can be obtained by dividing the number of nucleotides by the total number of nucleotides in the sequences being compared.

A BLAST search was implemented in GenBank with the ITS sequences obtained from the two stains. Sequences from the top BLAST search were downloaded and analyzed using PHYML[166] to obtain the closest phylogenetic disposition for the MSX

strains. BLAST search was employed using nucleotide collection (nr/nt) with uncultured/environmental samples sequences excluded. The BLAST search was also performed with RefSeq database.[167] In addition, for one of the strains (MSX56446), a portion of the D1/D2 region of the Large Subunit, 28SrDNA (LSU) was also sequenced using primers LROR and LR3.[168] The LSU sequences of other *Coniolariella* spp. from a recently published study on this genus[169] were downloaded and analyzed using PHYML. The sequence data obtained for both the MSX strains were deposited in the GenBank (MSX56446: KT835371; MSX92917: KT835372).

Extraction and isolation

The initial processing of fungal cultures was derived from well established procedures (Figure S25).[133,170] To each flask of the fungus grown on specific media were added 80 mL of $CHCl_3$, 20 mL of MeOH, and 100 mL of deionized H_2O, adjusted to pH ~3 with formic acid. The samples were mixed/chopped with a large spatula before being shaken overnight (~16 h) at room temperature. Then, the samples were filtered *in vacuo*, and the eluents were transferred to separatory funnels. The aqueous phases (~100 mL) were partitioned against water-saturated *n*-butanol (2 × 100 mL). The separated layers were dried.

The resultant aqueous and *n*-butanol fractions were dissolved in H_2O and H_2O/MeOH (2:1 v/v), respectively, and purified via reverse phase flash chromatography (C18) using a gradient solvent system of H_2O-MeOH at a 64 mL/min flow rate and 12.5 column volumes over 25.3 min to afford several fractions. These fractions were dried, and the presence of methylidene mevalonolactone (**40**) was detected via NMR. $CHCl_3$

was added to the identified fractions; compound **40** is soluble in this organic solvent, facilitating its isolation (>98% pure; Figure 30). Of the two, the n-butanol fraction had a higher relative concentration of the target compounds, and this facilitated the chromatographic purification step, particularly for gram-scale quantities needed for this stage of development.

Conversion of compound 40 to compound 39

To a vial containing **40** (11.44 mg, 0.08 mmol), 1N NaOH (80.4 μL, 0.08 mmol) and deionized H_2O (0.7 mL) were added and stirred with a magnetic stir bar for 2 h at 25 °C [160]. The product was dried to afford **39** (Figure 30).

Quantification

Calibration curves (Table 3) were prepared using standards isolated from fungal strain MSX92917. Identification of both **39** and **40** was performed by NMR (Figure S26) (JEOL ECS 400 MHz) and HRMS (Figure S27) (Thermo LTQ Orbitrap XL) analyses. Both compounds were isolated and purified (ISCO flash chromatography), and UPLC-HRMS was used to verify the purity (>98%). These standards of **39** and **40** were dissolved in deionized H_2O or MeOH, respectively, and analyzed 0.5 to 75 ppm for **39** and from 0.5 to 50 ppm for **40** (Table 3). Aqueous and *n*-butanol dried fractions were dissolved in deionized H_2O or MeOH, respectively, to a concentration of 1 mg/mL.

Table 3. The Calibration Curve Data Used for the Quantitative Analysis of Mevalocidin (39) and Methylidene Mevalonolactone (40)		
	(**39**)	(**40**)
Retention time (min)	3.20	3.68
Observed Mass	161.08057	143.06972
Calculated Mass	161.08084	143.07027
Linear equation	y = 3078692x - 1500577	y = 61765810x + 138182908
R^2	0.999	0.995
Range (ppm)	0.5-75	0.5-50

A UPLC Acquity system equipped with a BEH C18 (1.7 mm; 50 × 2.1 mm) column heated to 40 ºC was run at a flow rate of 0.2 mL/min with a solvent system of CH_3CN-H_2O [0.1% formic acid] (0-1.0 min, 0:100; 1.0-6.0 min, from 0:100 to 25:75; 6.0-6.1 min, from 25-75 to 100% CH_3CN and hold for 1 min; 7.0-7.1 min, return to initial conditions and hold for 1 min). PDA (190-400 nm) and HRMS (Thermo LTQ Orbitrap XL system) were used to analyze the samples. Compound **39** eluted at 3.20 min and compound **40** eluted at 3.68 min. The standards of **39** and **40** were run in triplicate and the areas under the curves were calculated to create the calibration curve. Similarly, extracts were run in triplicate, the areas were averaged, and the concentrations of **39** and **40** were extrapolated from the calibration curve.

Surface sampling

A droplet–liquid microjunction–surface sampling probe (droplet–LMJ–SSP) was a converted from a CTC/LEAP HTC PAL auto–sampler (LEAP Technologies Inc.) using in–house developed software dropletProbe Premium.[81-85] Microextractions were performed using Fisher Optima LC/MS grade H_2O. An initial 5 μL of H_2O was drawn into the syringe and 4 μL droplets were dispensed onto the surface of the sample at a rate

of 2 μL/s, held on the surface for 2 s, and withdrawn back into the syringe at the same rate. This extraction process was repeated a total of three times using the same droplet, then injected in a UPLC-MS system using the same chromatographic conditions as above except into a Thermo Q QExactive Plus mass spectrometer. Heat mapping experiments showed the relative concentration of mevalocidin (**39**) at a particular location directly on the fungal culture. The area was calculated for the chromatographic peak of **39** (*m/z* 161.0808 ± 5 ppm) at 3.53 min. Retention times are shift compared to those for the quantitative study due to the incorporation of the droplet–LMJ–SSP.

Results and Discussion

Molecular identification of the fungal strains

Results from uncorrected p-distance using ITS data suggested that the two MSX strains were 99% identical. Based on a BLAST search of NCBIs GenBank nucleotide database, the closest hits using the ITS sequence were *Coniolariella limonispora* (basionym: *Rosellinia limonispora*) (strain CBS 283.64) (GenBank KF71998; Identities = 502/518 (97%), Gaps = 8/518 (1%), followed by *Coniolariella hispanica* (strain ATCC MYA-4453) (GenBank FJ172294; Identities = 503/524 (96 %), Gaps = 10/524 (1 %)).

Maximum Likelihood analysis of the ITS and LSU regions indicated that the MSX strains are phylogenetically related to the genus *Coniolariella* D. García, Stchigel & Guarro [171]. The two strains were clustered within the clade containing most species of *Coniolariella* [169,172] including the type species, *C. gamsii* (Asgari & Zare) Garcia, Stchigel & Guarro (Figure S23, S24). Based on both ITS BLAST search as well as ML analysis using portions of ITS and LSU regions, the MSX strains were identified as

belonging to *Coniolariella* (Xylariales, Ascomycota). In an earlier study, Gerwick et al.[160] identified MSX56446 (which they termed as DA056446) as *Fusarium* and MSX92917 (which they termed as DA092917) as *Rosellinia* sp, respectively. We compared the D2 region of GenBank accession no: KF698738 for DA092917, and it matched the D2 region of MSX56446 with 100% identity. Thus it is likely that both the strains MSX92917 and MSX56446 are congeneric (Figure S24), but Gerwick et al. used a different name due to erroneous interpretation of BLAST search data, especially since Coniolariella shows a close phylogenetic relationship with *Rosellinia*-like genera within the Xylariales.[169]

Purification protocol

Due to its H_2O solubility, mevalocidin (**39**) was difficult to isolate directly using the traditional protocols common for natural products discovery.[92,95] To overcome this, the isohypsic ability to rearrange between the open and closed forms was exploited. After drying the reverse phase flash chromatography fractions, they were screened for methylidene mevalonolactone (**40**) using NMR. Compounds **39** and **40** can be clearly distinguished from each other through ^{1}H NMR (Figure S26). Due to the rigidity of the lactone, the proton signals are coupled at the C-5 position resulting in a very distinct differentiation between the two compounds (Figure 31). Furthermore, isolation of compound **40** was readily achieved by dissolving the chromatography fractions in $CDCl_3$. Once isolated, compound **40** was opened to **39** by introducing a base. This methodology was utilized for the isolation of the standards for the quantitation study.

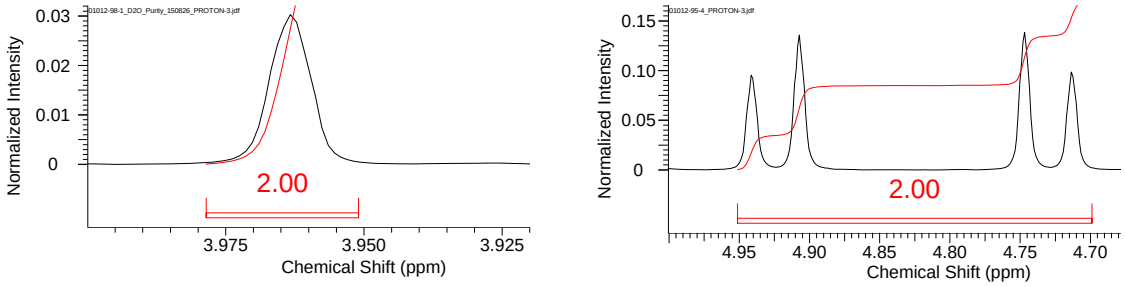

Figure 31. The Zoomed in NMR Spectra for the H-5 Signals of Mevalocidin (Left, D_2O) and Methylidene Mevalonolactone (Right, $CDCl_3$) Display the Identifying Signals for Each Compound.

Mevalocidin production optimization

Fungal strains MSX92917 and MSX56446 were tested for their viability for producing these compounds as bioherbicides for organic farming. Large scale rice cultures were extracted using the traditional protocol incorporating $CHCl_3$, MeOH, and H_2O;[133,170] however, partitioning the aqueous layer with *n*-butanol was performed to concentrate mevalocidin and remove it from the abundance of sugars present in the aqueous layer. While both layers contained significant proportions of **39** and **40** (Table 2), the more concentrated *n*-butanol fraction was more amenable for the gram quantity isolation of each compound needed for future testing. The productions of compounds **39** and **40** were compared for both cultures, ultimately determining the yields to be higher in MSX92917 by approximately a factor of two (Table 4). Therefore, subsequent analyses were performed only on MSX92917.

To optimize mevalocidin production, the fungus was subjected to a series of altering conditions, including media nutrient levels, media phase (liquid or solid), growth time, and incubation temperature. First, the nutrition levels of the media were examined to understand if production of mevalocidin would change as the sugar levels in the media

changed. Incremental amounts of dextrose (0-12.5%) were added to liquid media, since dextrose was shown to be a readily utilized; it was also an inexpensive carbon and energy source. The yields of **39** and **40** were highest at 2.5% dextrose (Table 4). This was evident when combining the calculated mass from both the *n*-butanol and aqueous partitions.

Solid and liquid media were compared by growing the fungal strain in two separate flasks of the same medium, but one with agar (solid) and the other without (liquid). The presence of agar displayed an increase in production for both compounds (Table 4).

Optimization of the growth time was performed by comparing the production over increments of five days before freezing. The combined calculated masses of **39** and **40** increased steadily until 20 days (Table 4). After 20 days, the rate of mevalocidin production began to slow, therefore approximately 20 days was considered the preferred growth time for commercial production.

Additionally, the temperature in which the fungus was grown had an effect (Table 4). Cultures of MSX92917 were grown on rice, but the temperature for each culture varied (25 °C, 30 °C, or 35 °C). The cultures at 30 °C showed the highest production of **39** and **40** with a significant drop-off at 35 °C (Table 4).

As mevalocidin progresses into commercial development, further optimization may be required. While all of these data are based on single growths, the goal of these experiments was to gauge relative trends, so that we could choose the best culture conditions. This may include a combination of the above conditions, as well as, probing

additional conditions, such as the FERMEX methods,[173] particularly for kg or larger scale production. Studies on the efficacy of mevalocidin as an organic herbicide are ongoing, as well.

Table 4. The Concentrations of Mevalocidin (39) and Methylidene Mevalonolactone(40) for Each Partition (*n*-Butanol and Aqueous) Were Determined by the LC-MS Calibration Curve. The Concentrations of **1** and **2** Obtained from the Quantitation Study Were Converted from ppm to mg and then Combined as a Total Mass. This was then Subsequently Converted to (mg of Total Compound)/(g of Rice) to Effectively Represent the Optimal Production Conditions. Highlighted Cells (Gray) Indicate the Highest Total for Each Individual Study.

Fungal Code	**39** (mg)[a]			**40** (mg)[a]			Combined Total (mg)[b]	Concentration for Commercial Production (mg/g)[c]
	n-Butanol	Aqueous	Total **1**	*n*-Butanol	Aqueous	Total **2**		
MSX92917	28.48 ± 2.97	147.81 ± 8.51	176.29	48.40 ± 4.51	110.06 ± 4.52	158.46	334.75	2.2
MSX56446	29.11 ± 3.85	38.92 ± 6.83	68.03	58.36 ± 2.24	34.61 ± 6.18	92.97	161.00	1.1
MSX92917								
Dextrose (%)	**39** (mg)[a]			**40** (mg)[a]			Combined Total (mg)[b]	Concentration for Commercial Production (mg/g)[d]
	n-Butanol	Aqueous	Total **1**	*n*-Butanol	Aqueous	Total **2**		
0.0	0.13 ± 0.01	0.84 ± 0.07	0.97	0.51 ± 0.02	0.42 ± 0.02	0.93	1.90	0.16
2.5	0.48 ± 0.03	3.43 ± 0.30	3.90	2.41 ± 0.08	2.42 ± 0.01	4.83	8.74	0.73
5.0	0.71 ± 0.03	1.54 ± 0.07	2.25	3.14 ± 0.07	1.43 ± 0.10	4.57	6.82	0.57
7.5	0.45 ± 0.05	2.37 ± 0.18	2.82	2.47 ± 0.12	1.72 ± 0.09	4.19	7.01	0.58
10.0	0.49 ± 0.05	2.65 ± 0.05	3.14	2.51 ± 0.03	0.65 ± 0.08*	3.16	6.30	0.53
12.5	0.59 ± 0.05	3.17 ± 0.06	3.76	1.71 ± 0.17	1.85 ± 0.18	3.56	7.32	0.61
MSX92917								
Media Phase	**39** (mg)[a]			**40** (mg)[a]			Combined Total (mg)[b]	Concentration for Commercial Production (mg/g)[d]
	n-Butanol	Aqueous	Total **1**	*n*-Butanol	Aqueous	Total **2**		
YESD	0.06 ± 0.00	0.49 ± 0.11	0.55	0.01 ± 0.00*	0.04 ± 0.05*	0.05	0.60	0.050
YESD + 1.5% Agar	0.06 ± 0.00	0.64 ± 0.04	0.70	0.04 ± 0.00	0.20 ± 0.03*	0.24	0.94	0.078
MSX92917								
Grow Length (days)	**39** (mg)[a]			**40** (mg)[a]			Combined Total (mg)[b]	Concentration for Commercial Production (mg/g)[d]
	n-Butanol	Aqueous	Total **1**	*n*-Butanol	Aqueous	Total **2**		

5	0.12 ± 0.01	1.71 ± 0.07	1.83	0.06 ± 0.00	0.11 ± 0.03*	0.17	2.00	0.17
10	0.34 ± 0.05	2.66 ± 0.16	3.00	0.98 ± 0.10	0.07 ± 0.07*	1.05	4.05	0.34
15	1.02 ± 0.11	1.66 ± 0.44	2.68	4.45 ± 0.13	0.51 ± 0.22*	4.95	7.64	0.64
20	1.56 ± 0.09	3.10 ± 0.11	4.66	4.37 ± 0.34	0.98 ± 0.27	5.35	10.01	0.83
25	1.19 ± 0.10	2.73 ± 0.36	3.92	3.66 ± 0.03	0.55 ± 0.14*	4.22	8.14	0.68
30	2.32 ± 0.28	6.14 ± 0.41	8.46	2.84 ± 0.51	1.36 ± 0.10	4.20	12.67	1.1

MSX92917

Temperature (ºC)	**39** (mg)[a]			**40** (mg)[a]			Combined Total (mg)[b]	Concentration for Commercial Production (mg/g)[d]
	n-Butanol	Aqueous	Total **1**	*n*-Butanol	Aqueous	Total **2**		
25	2.09 ± 0.14	4.83 ± 0.87	6.92	3.69 ± 0.02	3.52 ± 0.72	7.21	14.13	1.2
30	2.83 ± 0.17	5.69 ± 0.32	8.52	4.74 ± 0.31	4.07 ± 0.36	8.81	17.33	1.4
35	0.08 ± 0.00	1.49 ± 0.04	1.58	0.01 ± 0.00*	0.22 ± 0.04*	0.23	1.81	0.15

***** Indicates that concentrations were above limit of detection but below limit of quantitation

[a] [conc of mevalocidin] × total volume of extract = mass of mevalocidin in extract

µg/mL×mL×mg/100 µg = mg/extract

[b] Combined Total is to account for any potential shift in equilibrium between compounds **39** and **40** during the processing steps.

[c] Based on large scale 2.8-l Fernbach cultures (150 g of rice)

[d] Based on small scale screener cultures (12 g of rice)

Probing biosynthetic queries

It was originally unknown whether the fungi were producing both mevalocidin (**39**) and its lactone form or if the lactone was formed due to the use of acid through the extraction/isolation process. To address this, a droplet–LMJ–SSP coupled to a UPLC-HRMS system[81-83] was utilized to sample a solid-state rice culture of MSX92917. This system has recently been shown to be a viable tool for sampling the chemistry of fungal culture *in situ*.[120] When sampling fungal cultures MSX56446 and MSX92917, compounds **39** and **40** were detected readily off the surface; the HRMS and retention times were confirmed by comparison with standards of **39** and **40** (Figure S28). Furthermore, if any of the mevalocidin was being converted during the UPLC method, it would have been observed in the analysis of the standard as well. This confirmed that the fungus naturally produces both compounds.

Additionally, many questions regarding the biosynthesis of a fungal metabolite with herbicidal properties abound, particularly in fungi that are presumed to be saprobes. For instance, does the fungus interact with its environment, perhaps using the herbicidal compound to kill plant materials, giving the next generation a source of nutrients? If so, where does the fungus store the compound and how does it release it into its surroundings? To explore these questions, both mevalocidin producing cultures were grown on agar. Interestingly, it was observed that guttates (Figure 32) were produced by both fungal isolates when grown in this manner. Guttates are liquid droplets that are produced by the fungi and are exuded out via the mycelium to the surface[136,174] Previously, it has been observed that bioactive secondary metabolites concentrate in such

structures.[55,120,138] We hypothesized that they are a means for the fungus to interact with its surrounding habitat, as these are typically found upon the surface of the culture.

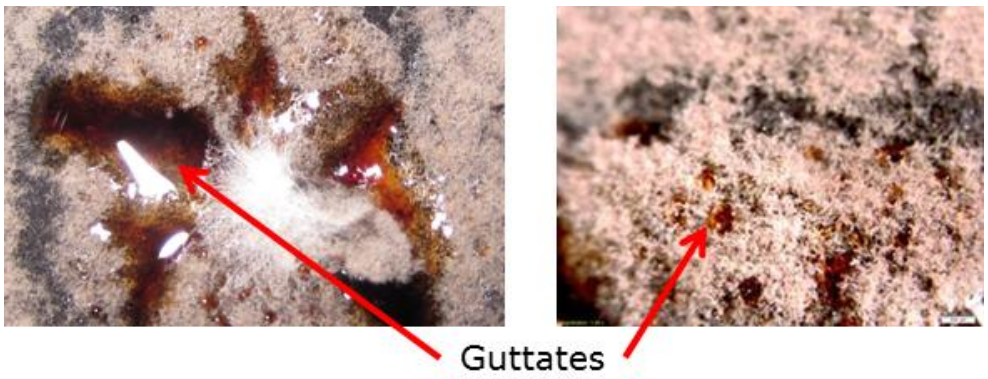

Figure 32. Guttates (Liquid Droplets) Residing on the Surface of Fungal Culture MSX56446.

To gain a better understanding of the biological and ecological purpose of these guttates, the cultures were analyzed by the droplet–LMJ–SSP coupled to an UPLC–HRMS. For both fungal cultures grown on agar, the mycelium, the guttates, and the surrounding agar were all explored in search for the molecular ion of mevalocidin (*m/z* 161.0808 ± 5 ppm). It was observed in both cultures that the guttates contained the highest concentrations of mevalocidin relative to the surrounding mycelium, as noted by the size of the blue circles in the heat map (Figure 33). Likewise, more mevalocidin was detected in the surrounding agar than directly on the surface of the mycelium. This indicated that mevalocidin was actively exuded out of the fungi into its surroundings. This supports the postulate that guttates are concentrated droplets of secondary metabolites and that the fungi are using the herbicidal compound to potentially kill plants in its environment. Importantly, the use of the droplet–LMJ–SSP allowed us to probe the

chemistry of the guttates, a feat that would have been impossible with traditional natural product protocols.[120]

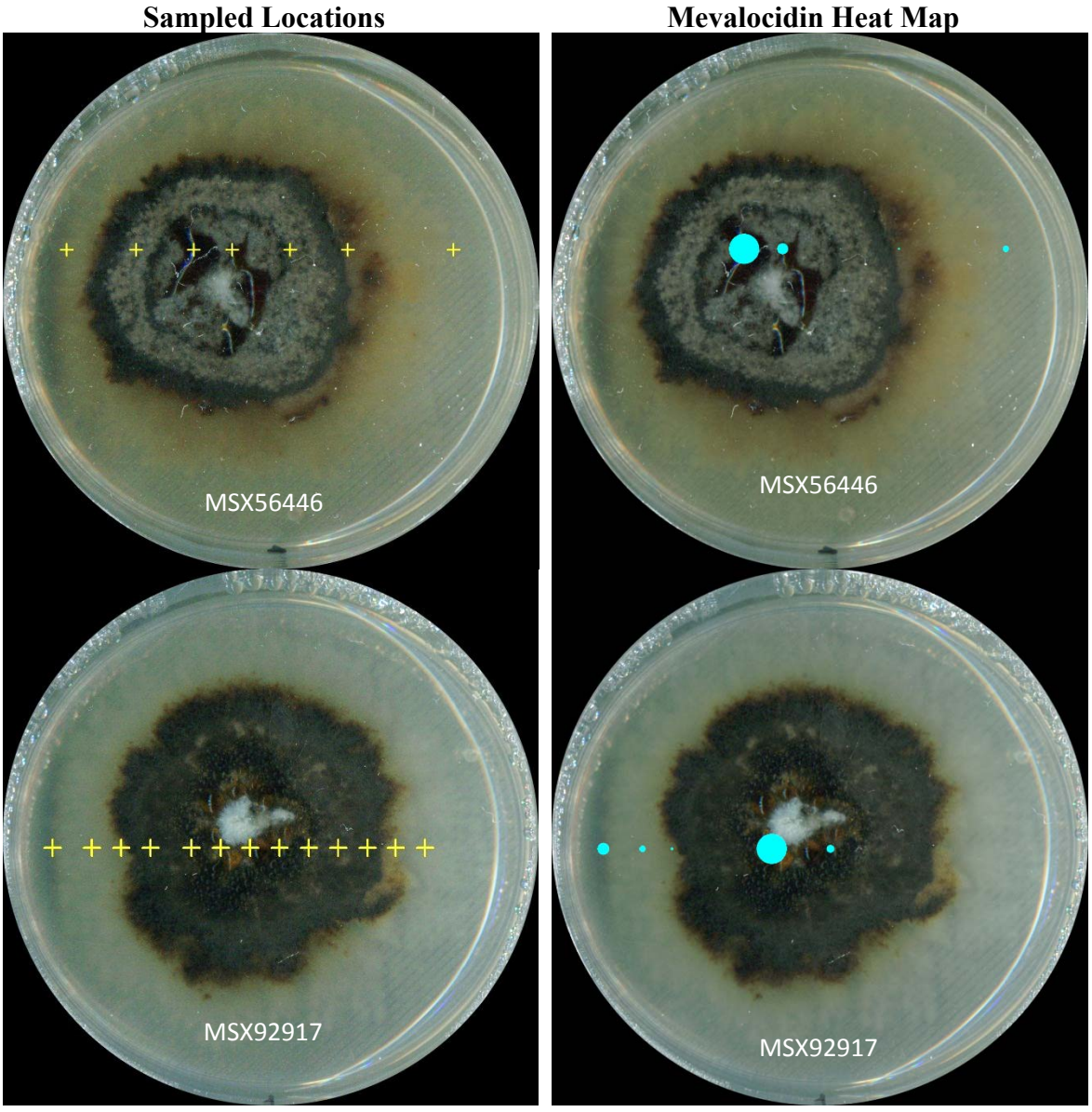

Figure 33. Heat Map Displaying the Presence of Mevalocidin (39) at Various Locations. The two images on the left indicate the locations that were sampled with the droplet–LMJ–SSP. The two images on the right show the heat map. Larger circles indicate higher concentrations of mevalocidin at that location.

In conclusion, mevalocidin had previously displayed promise as an organic herbicide.[160] These experiments were pursued to optimize conditions for mevalocidin production in fungal strains MSX92917 and MSX56446. Initial optimization studies argues that the best results could be realized on YESD agar medium containing 2.5% dextrose, incubated at 30 ºC for at least 20 days; ongoing studies are probing this further, with an aim towards commercial scale production. The conversions between **39** and **40** are prime examples of applying basic chemistry to solve isolation challenges. These results are currently being utilized to generate **39** for field trials as an organic bioherbicide. Furthermore, the data obtained from the droplet–LMJ–SSP demonstrates that the fungi are biosynthesizing both compounds **39** and **40**. The spatial distribution mapping experiments displayed valuable information about the production of mevalocidin, where the concentration of **39** in the guttates indicates an ecological use. Extruding this compound from the body of the fungus into the environment supports the hypothesis that the fungus is using mevalocidin to kill plants, which it can then decompose in its role as a saprobe.

Acknowledgments

This research was supported in part by a grant from the United States Department of Agriculture (NIFA 2012-33610-19523). The authors thank T. N. Graf of UNCG for assistance in isolation method development and Drs. Vilmos Kertesz and Gary J. Van Berkel (Mass Spectrometry and Laser Spectroscopy Group, Chemical Sciences Division, Oak Ridge National Laboratory) for inspiration and guidance with the droplet-LMJ-SSP.

CHAPTER VI

IN SITU ANALYSIS OF ASMINA TRILOBA (PAW PAW) PLANT TISSUES FOR ACETOGENINS

This chapter is intended for submission to the journal *Analytical Methods* and is presented in that style. Coauthors include Tamam El-Elimat and Nicholas H. Oberlies.

Introduction

Asimina triloba (L.) Dunal, Annonaceae, commonly known as paw paw (Figure 1A), has been studied for decades, notably by McLaughlin and colleagues,[175-177] due to the presence of Annonaceous acetogenins, which are polyketide-derived fatty acid derivatives. These compounds contain at least one tetrahydrofuran (THF) ring, a methylated γ-lactone, and a number of hydroxy groups along the hydrocarbon chain (Figure 1B). Over 400 acetogenins have been isolated from various plants in the Annonaceae family [176-178] with more discovered every year.[179-181] *A. triloba* is of particular interest because out of the roughly 120 genera and 2100 species from Annonaceae, it is the prominent temperate species; the rest are predominantly tropical or subtropical.[176,182,183]

Annonaceous acetogenins have shown activity for a number of assays, including antimalarial, anthelmintic, pesticidal,[184] piscicidal, antimicrobial, antiviral and antitumor.[185,186] Currently, they are used in commercial products as pesticidal

shampoos[187] and sprays, ointment for oral herpes (HSV-1), an anthelmintic pill, and as a botanical supplement for certain cancer patients.[176,181]

Annonaceous acetogenins can be subdivided into three structural classes: mono-THF, adjacent bis-THF, and nonadjacent bis-THF.[175-177] Full characterization of each acetogenin typically involves a compilation of techniques, including LC, NMR, MS, and CD.[188-190] However, a majority of the structure can be determined solely by HRMS/MS, specifically the positions of the THF ring(s) and the hydroxy groups along the hydrocarbon backbone. This is important because by identifying the structural class, number of hydroxy groups, and the distance between the lactone and the THF ring(s), one can infer the relative bioactivity of an acetogenin.[185,191] However, to utilize HRMS/MS, chromatography is vital due to the numerous isomers that exist in the plant.[192-195] Thus, while ambient ionization techniques have provided *in situ* MS screening protocols for many classes of secondary metabolites,[26,196,197] none currently exist for acetogenins. Moreover, only a few ambient ionization studies have been performed on entire plant m32aterials.[34,35,41,198] For this reason, *A. triloba* provided a great test case to explore ambient ionization techniques *in situ* for plants that contain a complex mixture of isomers.

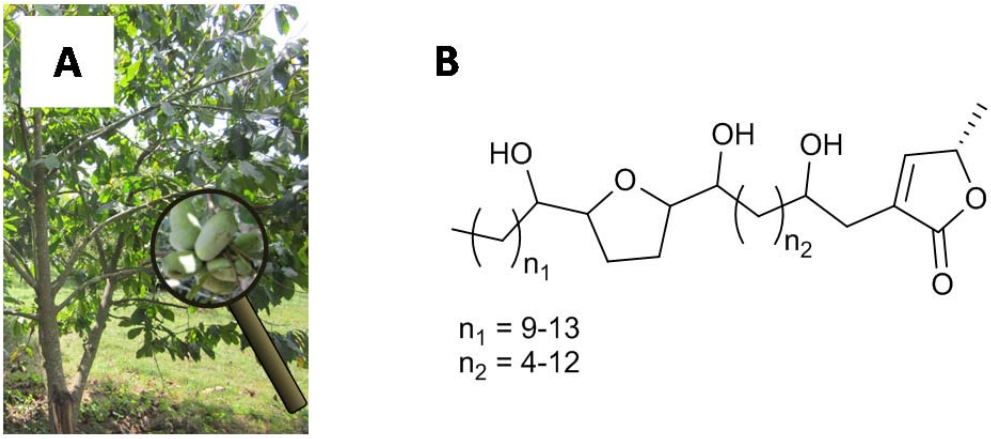

Figure 34. (A) Photograph of *Asimina triloba* and Magnification of the Fruit. (B) General backbone for the mono-tetrahydrofuran structural class of Annonaceous acetogenins.

Ambient ionization mass spectrometry techniques, such as desorption electrospray ionization (DESI) and nanoDESI, have shown to be efficient at detecting trace amounts of secondary metabolites directly on an organism,[35,41,54,77,199] but would struggle with the determination of isomers due to the lack of chromatographic separation.[120] Detecting the presence of acetogenins using accurate mass without the ability to differentiate between isomers is insufficient when trying to rapidly screen for particular constituents.

The recently developed droplet–liquid microjunction–surface sampling probe (droplet–LMJ–SSP) has the ability to perform microextractions directly on a sample while affording chromatographic separation.[81,82,120] This technique reintroduced this key element to ambient ionization mass spectrometry techniques, thus making the differentiation of isomers possible.[120] Here, we demonstrate the application of droplet–LMJ–SSP to elucidating the structures of the acetogenins observed in the seeds and pulp of the fruit, twigs and leaves of the branches, and the petals and ovaries from the flowers

of *A. triloba*. Interestingly, the flowers of plants are rarely studied, especially from the Annonaceae family,[200] therefore this was the first comparison of the acetogenins in the flower tissues to that of the rest of the well-studied tissues (i.e. seeds and twigs) for any plant in the Annonaceae family.[201]

Historically, electron impact (EI) and fast atom bombardment (FAB) ionization techniques were used to acquire MS/MS data to elucidate the structures of acetogenins.[192,202] However, when using the more modern approach of electrospray ionization (ESI), acetogenins do not form prominent product ions, confounding the use of MS/MS for structure elucidation. Thus, a clever development for gaining discernible fragmentation patterns from acetogenins using ESI was the post-column infusion of lithium.[188] Lithium addition greatly increased the sensitivity for HRMS/MS by forming prominent lithiated adducts ($[M + Li]^+$) to both the precursor and product ions.[188] Structures of acetogenins were then elucidated by obtaining the molecular formula from HRMS, and then determining the placement of the THF ring(s) and the hydroxy groups by deciphering the MS/MS fragmentation patterns.[188]

Finally, mass defect filtering (MDF) was applied to deconvolute the chromatograms afforded by the analysis of these complex mixtures.[203] MDF capitalized on the fact that related analogues will be similar in nominal mass (i.e. ±100 Da), but perhaps more importantly, similar in mass defect (i.e. ±25 mDa).[203] Additions (and inversely losses) of carbons, hydrogens, and/or oxygens to an acetogenin only adds 0.00 mDa, 7.82 mDa, or -5.09 mDa, respectively, to the overall mass.[203] This process rapidly generates a list of possible analogues to be explored further. This project aimed to

combine LC-MS surface sampling with MDF to quickly profile the acetogenins observed in *A. triloba*.

Results and Discussion

Identification of acetogenins from complex mixtures

Annonaceous acetogenins are produced in abundance from *Asimina triloba*.[184,192,195,204-214] Not only are a variety of analogues present, but each analogue is coupled with multiple isomers, resulting in a complex mixture of acetogenins (Figure 35A). Therefore, the identification of acetogenins was impossible by ambient ionization techniques without some form of separation. The droplet–LMJ–SSP provided *in situ* analysis of *A. triloba*, and by coupling it to UPLC–HRMS/MS, the separation of isomers was achieved. Furthermore, post-column lithium infusion increased the sensitivity for the tandem mass spectrometry, thus providing discernible fragmentation patterns (Figure 35B).

When sampling the various tissues from *A. triloba* (seeds, pulp, twigs, leaves and flowers), acetogenins were readily identified by their characteristic MS/MS spectra. This allowed for the rapid characterization of the acetogenins present in the each of the *A. triloba* tissues. For instance, a prominent accurate mass (*m/z* 603.4807) that was detected corresponded to an acetogenin with the formula of $C_{35}H_{64}O_7$. When searching the Dictionary of Natural Products,[215] there were 46 matches to that formula. Pairing the results with the MS/MS fragmentation patterns, three matches remained, all of which only differed by chirality: asitrilobin B,[192] annonacin,[216] and *cis*-annonacin.[217] Using an alternate way to search the data, a Dictionary of Natural Products[215] search for *A. triloba*

yielded 36 matches that were acetogenins. Narrowing this search by adding a filter for the formula of the prominently detected mass ($C_{35}H_{64}O_7$), resulted in 6 matches. Based on the MS/MS fragmentation pattern, only asitrilobin B remained a match for the mass.

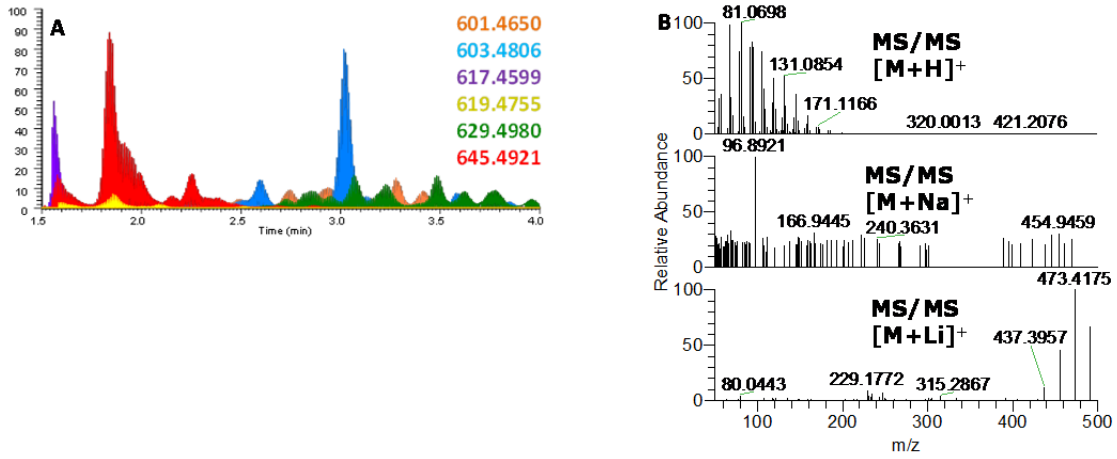

Figure 35. (A) Overlay of the Exact Mass Chromatograms for Various Acetogenin Analogues and Isomers Detected in the Pulp of a Paw Paw Fruit by the Droplet–LMJ–SSP–UPLC-HRMS System. (B) Comparison of the MS/MS fragmentation patterns with ESI after an HCD of 60 was applied to the molecular ions of $[M + H]^+$, $[M + Na]^+$, and $[M + Li]^+$ for annonacin (*m/z* 603.4807).

Screening *A. triloba* for acetogenins *in situ* with a more direct ambient ionization technique, DESI-MS, had less conclusive results. Reactive DESI[43,218,219] was performed to increase the detection of acetogenins by having a solvent spray system with lithium fluoride in it. While the HRMS signals for the acetogenins were observed, the MS/MS signals were indiscernible due to the complexity of the mixture (data not shown). This did nothing to alleviate the overwhelming issue of differentiating between isomers. Those same searches in the Dictionary of Natural Products[215] resulted in 46 matches for the formula $C_{35}H_{64}O_7$, but the lack of chromatography made differentiating between them

difficult. Even when the search was further limited to *A. triloba*, it was difficult to rule out any of the remaining 6 matches.

While the droplet–LMJ–SSP system provided the differentiation of isomers, it was not without its challenges. The chromatograms obtained by the droplet microextraction were difficult to navigate due to the complexity of the mixture and the small extraction volume (5 μL) of the droplet. With such a complex mixture and low extraction volume, the chromatographic peaks for the acetogenins were very low in intensity (Figure 36A), especially considering the amount of sugars extracted from the fruit, further suppressing the signal.

Consequently, scan filters were applied to make the data easier to navigate. By setting a *m/z* filter to 550-700, some minor peaks associated with acetogenins became observable, but were still insignificant (Figure 36B). Furthermore, narrowing the retention time range to 1.0 – 8.0 min, where the acetogenins typically eluted (Figure 36C), gave rise to several discernible peaks that were attributed to acetogenins. Alternatively, rather than filtering the existing data, a new microextraction was performed with a narrow mass window (550-700) and with the first 90 sec diverted from the mass spectrometer (Figure 36D). This too resulted in the rise of several peaks identified as acetogenins. However, while these methods helped generate lists of the acetogenins present, the lists were subjective and not comprehensive. The questions of *how many* and *which* acetogenins were present were left inconclusive and imprecise.

To obtain a more objective list when answering *how many* and *which* acetogenins were present, mass defect filtering (MDF) was incorporated.[203] The most prominent

acetogenin in most of the samples was attributed to annonacin based on the HRMS and MS/MS data. This assignment was confirmed by isolation and structure elucidation (Figure S29).[194,216] A mass range of ±100 Da with a mass defect of ±25 mDa was applied around the accurate mass of annonacin (*m/z* 603.4807 $[M + Li]^+$), and the newly created chromatogram (Figure 36E) displayed an abundance of prominent peaks that were acetogenins.

Although the mass defect filtered chromatogram was relatively similar to the manually filtered chromatograms, the more important information obtained was the population of an objective list of acetogenin peaks (Table S4 and Figure S30). This provided a comprehensive target set to perform data dependent fragmentation on subsequent samples. Furthermore, MDF did not limit the amount of data collected (i.e. *m/z* ranges, diverted flows, etc.), therefore the data could always be re-examined in search for other substituents that may become of interest in the future.

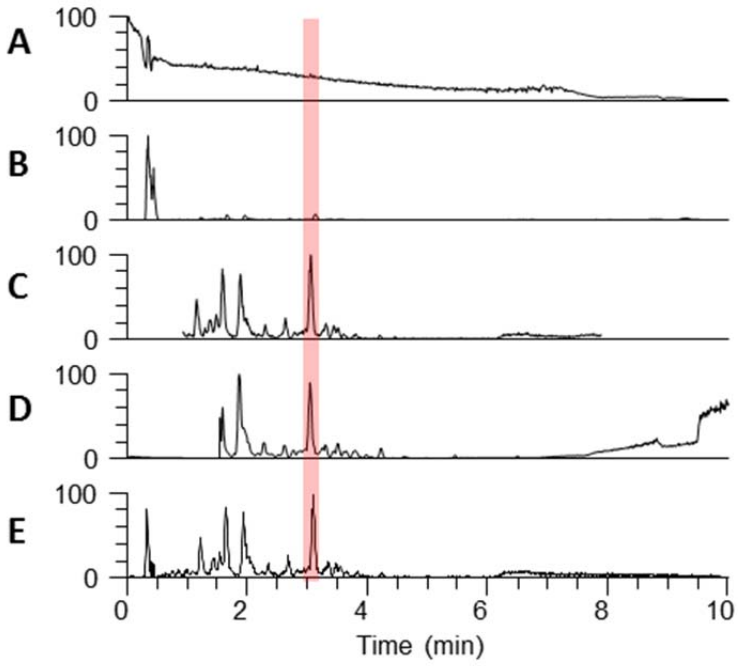

Figure 36. (A) The Unfiltered Base Peak, (B) the Mass Range Filtered Data (*m/z* 550-700), and (C) the Retention Time Filtered Data (1.0 – 8.0 min) Chromatograms for the Direct Analysis of a Paw Paw Flower Petal. (D) A subsequent injection only collecting *m/z* 550-700 and 1.0-8.0 min. (E) The original sample (Figure 3A) after applying a mass defect filter of ± 25mDa to 603.4807 ±100 Da. The highlighted region (red) indications the location of annonacin (*m/z* 603.4807).

Elucidation of acetogenins

Like peptides, acetogenins fragment in predictable patterns. Acetogenins fragment around the hydroxy groups, which help determine the placement of the THF ring(s), the length of hydrocarbon chains, and the positions of each hydroxy group (Figure 37).[175-177] The loss of *m/z* 112 Da (red) indicated the removal of the lactone moiety. The subsequent losses of water (18 Da) denoted the number of hydroxy groups throughout the molecule (red).

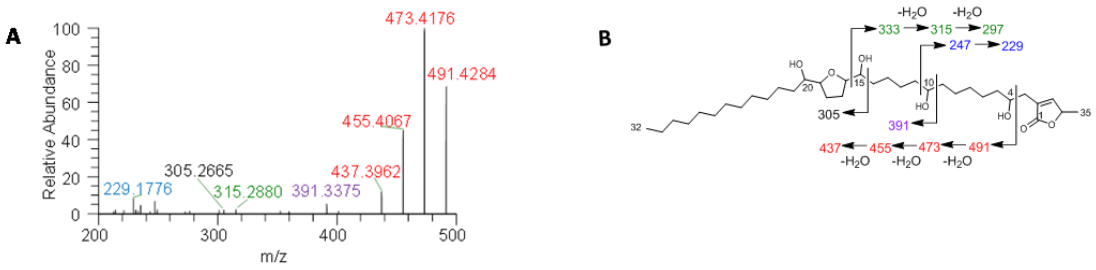

Figure 37. (A) Fragmentation Pattern of Annonacin from Direct Analysis of a Paw Paw Seed. (B) Elucidation of annonacin. The accuracy of annonacin between the observed and calculated was 0.8 ppm (603.4802 observed vs. 603.4807 calculated for $[C_{35}H_{64}O_7 + Li]^+$).

The remaining fragmentations indicated breaks at each hydroxy group, including those that flank the THF rings. In the case of annonacin, the fragments on both sides of C-10 were observed by *m/z* 247 & 229 (blue) and *m/z* 391 (purple) and similarly with C-15 at *m/z* 333 & 315 (green) and *m/z* 305 (black). These fragments complete the portion of the molecule to the right of the THF ring (Figure 37). The only remaining pieces must be the THF ring, its flanking hydroxy group, and the other hydrocarbon chain, which finalized the structure to the left of the THF ring. The ability to separate the acetogenins and then elucidate the structures via MS/MS reopens the possibility of high-throughput screening for particular acetogenins of interest.

Spatial distribution of acetogenins

Annonaceous acetogenins from *A. triloba* have been primarily isolated from the seeds[192,209] and twigs.[204,214] While there is some research investigating the leaves,[201] the flowers have not yet been explored for the presence of acetogenins, even for other members of the Annonaceae family. A comparison of the fruits (seed and pulp), twigs, leaves, and flowers (petal and ovary) was performed using the droplet–LMJ–SSP coupled to a UPLC–HRMS/MS system with post-column lithium infusion (Figure 38). The

samples were analyzed using MDF to build chromatograms of the acetogenins that were present in each sample (Figure 38B). Ultimately, the secondary metabolite profiles of each plant tissue were similar, with some shifts in the relative abundances of distinct isomers (Figure 38B). Interestingly, MDF revealed that the ovaries contained the most extensive list of Annonaceous acetogenin analogues (Table S4 and Figure S30), however, they are an underexplored organ from *A. triloba* due to the short life cycle, thus low availability. This data suggested that the flowers may be an untapped resource when searching for new acetogenins. Furthermore, this technique may prove beneficial for other plant species, where the flowers are underexplored for bioactive secondary metabolites.

The seeds, pulp, and twigs were all directly sampled with the droplet–LMJ–SSP, and signals for the lithiated acetogenin adducts were readily detected via the mass spectrometer. The droplet–LMJ–SSP protocol on a suite of plant parts provided a detailed profile of secondary metabolites *in situ*, including the ability to differentiate between isomers. However, when the leaves and flowers were sampled directly, the metabolites were not detected. This is a common issue when performing ambient mass spectrometry experiments on leaves due to their waxy, hydrophobic surfaces. There are three common remedies to overcome this challenge: imprint the metabolites on Teflon,[42] remove the waxy surface with chloroform,[198] or create cross-sections using a cryotome.[220]

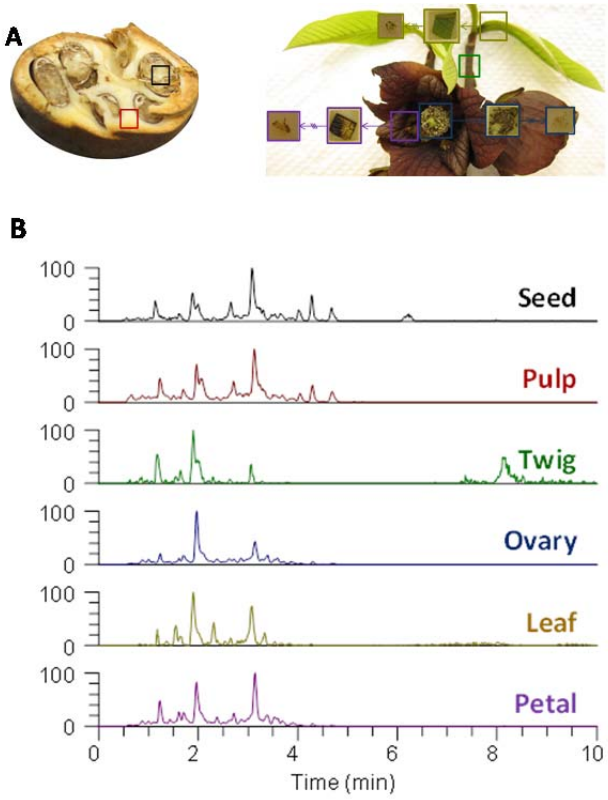

Figure 38. (A) Locations of Paw Paw Where the Droplet–LMJ–SSP Directly Sampled Seed (Black), Pulp (Red), and Twig (Green) and the Portions That Were Cross-Sectioned: Ovary (Blue), Leaf (Yellow), and Petal (Purple). (B) The mass defect filtered chromatograms around annonacin; 603.4807 ± 100 Da with a mass defect of ±25 mDa.

Initially, chloroform was used to remove the waxy, hydrophobic surface of the leaves and flower petals (Figure 39A-B). This procedure worked for the leaves, albeit with low signal (Figure 39C), but acetogenins were still not detected on the petals (Figure 39D). Instead, the leaves, petals, and ovaries were subjected to cross-sectioning using a cryotome (Figure 39E-F). After sectioning, the sliced plant materials were subjected to surface analysis, and acetogenins were readily detected on all three plant tissues (leaves, petals, and ovaries). Since this project aimed to perform direct sample surface analysis, the imprint methodology was not examined.

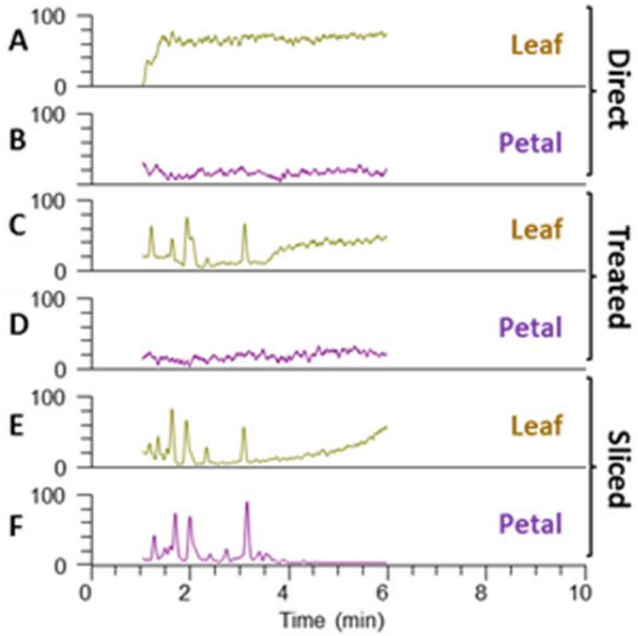

Figure 39. The Droplet–LMJ–SSP Directly Sampled a (A) Leaf (Yellow) and a (B) Petal (Purple). $CHCl_3$ was used to remove the waxy surface and the (C) leaf and (D) petal were resampled with only minimal success on the leaf. Finally, the cryotome sliced tissues of the (E) leaf and (F) petal were sampled with the droplet–LMJ–SSP. All chromatograms were filtered with an *m/z* range of 550-700 and retention time of 1.0-6.0 min.

Experimental

Instrumentation methods

The data were collected on a QExactive Plus mass spectrometer (ThermoFisher, San Jose, CA) with a spray voltage of 3.7 kV, a nitrogen sheath gas set to 25 arb, and an auxiliary gas set to 5 arb. The HCD fragmentation used a normalized collision energy of 60 for all compounds. An Acquity ultra–performance liquid chromatography (UPLC) system (Waters Corp., Milford, MA) was used with a flow rate set to 300 µL/min using a BEH C_{18} (2.1 × 50 mm × 1.7 µm) equilibrated at 40 °C with a 2 mM solution of LiF in MeOH infused post-column at a rate of 5 µL/min. The mobile phase consisted of Fisher optima LC–MS grade CH_3CN—H_2O (acidified with 0.1% formic acid), starting at 70%

CH_3CN and increasing linearly to 100% CH_3CN over 8 min. It was held at 100% CH_3CN for 1.5 min before returning to starting conditions for re–equilibration. Microextractions of 5 μL were performed using a CTC/LEAP HTC PAL auto–sampler (LEAP Technologies Inc., Carrboro, NC) converted into an automated droplet–LMJ–SSP system by using the dropletProbe Premium software.[81,82,120] The 5 μL droplet was composed of 50:50 MeOH–H_2O. Compound Discoverer (ThermoFisher, San Jose, CA) was used to perform the mass defect filtering. The filter was set to ±100 Da and ±25mDa around *m/z* 603.4807.

Preparation of leaves and flowers

A voucher specimen of the plant material was deposited in the Herbarium of the University of North Carolina at Chapel Hill (NCU602030). The leaves and flowers from a paw paw tree were removed and cut into small (0.5 × 0.5 cm) pieces (Figure S31). A customized tray (Figure S31) was designed using SketchUp Make (Trimble Navigation Limited), sliced using Simplify3D (Simplify3D LLC), and printed out of poly(lactic acid) using an F306 3D printer (Fusion3 Design LLC). The design contained four removable cells, and a piece of each material was placed in an individual cell. Each cell was filled with Tissue-Tek optimum cutting temperature (O.C.T.) embedding medium and the tray was placed in a -80 ˚C freezer. Once frozen, the material was removed from the cell and cut to 15 μm cross-sections using the Leica CM1100 cryostat (Leica Biosystems Inc., Buffalo Grove, IL). The cross-sections were thaw mounted to a microscope slide.

Conclusion

The droplet–LMJ–SSP overcame the challenge of exploring a suite of plant parts from *A. triloba* directly with little to no sample preparation. While other direct ionization technique, such as DESI, nanoDESI, and MALDI, can profile some of the plant's substituents, the lack of chromatographic separation greatly limits their abilities to discern isomers. By coupling the droplet–LMJ–SSP with LC-MS and applying it towards *A. triloba* analysis *in situ*, the power of chromatographic separation in conjunction with mass spectrometry fragmentation was revealed. Acetogenins were rapidly screened, characterized, and compared directly from the various organ tissues. The use of post-column lithium infusion and MDF provided increased sensitivity and objective data analysis, respectively. Furthermore, the flowers from *A. triloba* were analyzed for acetogenins for the first time, revealing an abundance of analogues that warrant further exploration. In particular, ovaries were a rich source of acetogenins and their analysis via traditional natural products protocols would be nearly impossible.

Acknowledgments

The authors thank Drs. Vilmos Kertesz and Gary J. Van Berkel (Mass Spectrometry and Laser Spectroscopy Group, Chemical Sciences Division, Oak Ridge National Laboratory) for acquisition of the droplet–LMJ–SSP and for helpful discussions related to the technique. Furthermore, we thank Drs. Norman H. Chiu and Adam R. Brown (UNCG) for use of the cryostat and for assistance with the acquisition of *A. triloba*, respectively.

CHAPTER VII

CONCLUDING REMARKS

The studies presented here explored the applications of surface sampling mass spectrometry techniques towards natural products research. Chapter II highlighted the initial venture into ambient ionization via desorption electrospray ionization (DESI). While this technique provided some initial details about fungal-fungal interactions, it faced many obstacles such as overcoming fungal topography and the loss of mutually supportive data. Chapter III addresses these issues by turning to the droplet–liquid microjunction–surface sampling probe (droplet–LMJ–SSP) for fungal surface analysis. This technique was more robust and amenable to sampling a fungal culture and provided a new high-throughput screening protocol. Additionally, it showcased mass spectrometry mapping experiments as a compliment to mass spectrometry imaging experiments. While the maps created only a superficial analysis, it created a template for future experiments.

Chapter IV took the mapping concept and applied it for a more in depth analysis of fungal-fungal interactions. By mapping the spatial and temporal distributions of an antifungal agent, the ecology between the two fungal cultures became better understood. Similarly, Chapter V applied the mass spectrometry mapping procedures towards two fungi that produced an herbicidal agent. This study explored the ecological role that this herbicide played while using it to kill plants, thus providing material to fulfill its

decomposing lifestyle. Finally, Chapter VI showcased the droplet–LMJ–SSP as a powerful tool, capable of elucidating structures in situ, even when encountering complex mixtures. Additionally, the versatility of the technique was highlighted as it utilized a suite of analytical techniques to accomplish its goals.

Moving forward, this new instrumentation will be used in a variety of ways, all stemming from these original projects. Additional mass spectrometry mapping experiments will be performed to better understand the chemical ecology. The *in situ* elucidation will be applied towards other structure classes, such as peptides, for the rapid characterization of compounds. Finally, the screening protocol will be utilized to increase the output of new chemical entities as well as optimize their production, thus improving our process of natural products drug discovery.

REFERENCES

(1) Newman, D. J.; Cragg, G. M., *J. Nat. Prod.* **2012,** *75*, 311-335.
(2) Kell, D. B., *FEBS J* **2013,** *280*, 5957-5980.
(3) Kola, I.; Landis, J., *Nat. Rev. Drug Discov.* **2004,** *3*, 711-715.
(4) Kwong, E.; Higgins, J.; Templeton, A. C., *Int. J. Pharm.* **2011,** *412*, 1-7.
(5) Newman, D. J.; Cragg, G. M., *Curr. Drug Targets* **2006,** *7*, 279-304.
(6) Cannon, P. F., *Biodivers. Conserv.* **1997,** *6*, 669-680.
(7) Hawksworth, D. L., *Mycol. Res.* **2001,** *105*, 1422-1432.
(8) Keating, G.; Figgitt, D., *Drugs* **2003,** *63*, 2235-2263.
(9) Strader, C. R.; Pearce, C. J.; Oberlies, N. H., *J. Nat. Prod.* **2011,** *74*, 900-907.
(10) Ondeyka, J. G.; Byrne, K.; Vesey, D.; Zink, D. L.; Shoop, W. L.; Goetz, M. A.; Singh, S. B., *J. Nat. Prod.* **2003,** *66*, 121-124.
(11) Brady, S. F.; Bondi, S. M.; Clardy, J., *J. Am. Chem. Soc.* **2001,** *123*, 9900-9901.
(12) Kirk, P. M.; Stalpers, J. A.; Minter, D. W.; Cannon, P. F., *Dictionary of the Fungi*. CABI Publishing: 2011.
(13) Cole, R. J.; Schweikert, M. A.; Jarvis, B. B., *Handbook of secondary fungal metabolites*. Academic: Amsterdam; Boston, 2003.
(14) Wisecaver, J. H.; Slot, J. C.; Rokas, A., *PLoS Genetics* **2014,** *10*.
(15) Higginbotham, S. J.; Arnold, A. E.; Ibanez, A.; Spadafora, C.; Coley, P. D.; Kursar, T. A., *PloS one* **2013,** *8*, e73192.
(16) Berdy, J., *J. Antibiot.* **2005,** *58*, C1-C1.
(17) Marschner, P.; Marhan, S.; Kandeler, E., *Soil. Biol. Biochem.* **2012,** *49*, 174-183.
(18) Kusari, P.; Kusari, S.; Spiteller, M.; Kayser, O., *Fungal. Divers.* **2013,** *60*, 137-151.
(19) Zhang, L.; Demain, A. L., *Natural Products: Drug Discovery and Therapeutic Medicine*. Springer: 2005.
(20) Andersen, B.; Smedsgaard, J.; Frisvad, J. C., *J. Agr. Food Chem.* **2004,** *52*, 2421-2428.
(21) Cooks, R. G.; Ouyang, Z.; Takats, Z.; Wiseman, J. M., *Science* **2006,** *311*, 1566-1570.
(22) Wu, C.; Dill, A. L.; Eberlin, L. S.; Cooks, R. G.; Ifa, D. R., *Mass. Spectrom. Rev.* **2013,** *32*, 218-243.
(23) Venter, A.; Sojka, P. E.; Cooks, R. G., *Anal. Chem.* **2006,** *78*, 8549-8555.
(24) Cotte-Rodriguez, I.; Mulligan, C. C.; Cooks, R. G., *Anal. Chem.* **2007,** *79*, 7069-7077.
(25) Chen, H.; Talaty, N. N.; Takats, Z.; Cooks, R. G., *Anal. Chem.* **2005,** *77*, 6915-6927. (26) Li, L. P.; Feng, B. S.; Yang, J. W.; Chang, C. L.; Bai, Y.; Liu, H. W., *Analyst* **2013,** *138*, 3097-3103.

(27) Campbell, I. S.; Ton, A. T.; Mulligan, C. C., *J. Am. Soc. Mass Spectrom.* **2011,** *22*, 1285-1293.
(28) Garcia-Reyes, J. F.; Jackson, A. U.; Molina-Diaz, A.; Cooks, R. G., *Anal. Chem.* **2009,** *81*, 820-829.
(29) Takats, Z.; Wiseman, J. M.; Cooks, R. G., *J. Mass. Spectrom.* **2005,** *40*, 1261-1275.
(30) Huang, G.; Chen, H.; Zhang, X.; Cooks, R. G.; Ouyang, Z., *Anal. Chem.* **2007,** *79*, 8327-8332.
(31) Cotte-Rodriguez, I.; Hernandez-Soto, H.; Chen, H.; Cooks, R. G., *Anal. Chem.* **2008,** *80*, 1512-1519.
(32) Eberlin, L. S.; Ferreira, C. R.; Dill, A. L.; Ifa, D. R.; Cheng, L.; Cooks, R. G., *Chembiochem* **2011,** *12*, 2129-2132.
(33) Eberlin, L. S.; Ferreira, C. R.; Dill, A. L.; Ifa, D. R.; Cooks, R. G., *Biochim. Biophys. Acta* **2011,** *1811*, 946-960.
(34) Jarmusch, A. K.; Cooks, R. G., *Nat. Prod. Rep.* **2014,** *31*, 730-738.
(35) Srimany, A.; Ifa, D. R.; Naik, H. R.; Bhat, V.; Cooks, R. G.; Pradeep, T., *Analyst* **2011,** *136*, 3066-3068.
(36) Esquenazi, E.; Yang, Y. L.; Watrous, J.; Gerwick, W. H.; Dorrestein, P. C., *Nat. Prod. Rep.* **2009,** *26*, 1521-1534.
(37) Grassl, J.; Taylor, N. L.; Millar, A. H., *Plant Methods* **2011,** *7*.
(38) Esquenazi, E.; Coates, C.; Simmons, L.; Gonzalez, D.; Gerwick, W. H.; Dorrestein, P. C., *Mol. Biosyst.* **2008,** *4*, 562-570.
(39) Yarnold, J. E.; Hamilton, B. R.; Welsh, D. T.; Pool, G. F.; Venter, D. J.; Carroll, A. R., *Mol. Biosyst.* **2012,** *8*, 2249-2259.
(40) Jaeger, R. J. R.; Lamshoft, M.; Gottfried, S.; Spiteller, M.; Spiteller, P., *J. Nat. Prod.* **2013,** *76*, 127-134.
(41) Li, B.; Bjarnholt, N.; Hansen, S. H.; Janfelt, C., *J. Mass. Spectrom.* **2011,** *46*, 1241-1246.
(42) Thunig, J.; Hansen, S. H.; Janfelt, C., *Anal. Chem.* **2011,** *83*, 3256-3259.
(43) Nyadong, L.; Hohenstein, E. G.; Galhena, A.; Lane, A. L.; Kubanek, J.; Sherrill, C. D.; Fernandez, F. M., *Anal. Bioanal. Chem.* **2009,** *394*, 245-254.
(44) Lane, A. L.; Nyadong, L.; Galhena, A. S.; Shearer, T. L.; Stout, E. P.; Parry, R. M.; Kwasnik, M.; Wang, M. D.; Hay, M. E.; Fernandez, F. M.; Kubanek, J., *Proc. Natl. Acad. Sci. U.S.A.* **2009,** *106*, 7314-7319.
(45) Rath, C. M.; Alexandrov, T.; Higginbottom, S. K.; Song, J.; Milla, M. E.; Fischbach, M. A.; Sonnenburg, J. L.; Dorrestein, P. C., *Anal. Chem.* **2012,** *84*, 9259-9267.
(46) Watrous, J.; Hendricks, N.; Meehan, M.; Dorrestein, P. C., *Anal. Chem.* **2010,** *82*, 1598-1600.
(47) Watrous, J.; Roach, P.; Heath, B.; Alexandrov, T.; Laskin, J.; Dorrestein, P. C., *Anal. Chem.* **2013,** *85*, 10385-10391.

(48) Figueroa, M.; Jarmusch, A. K.; Raja, H. A.; El-Elimat, T.; Kavanaugh, J. S.; Horswill, A. R.; Cooks, R. G.; Cech, N. B.; Oberlies, N. H., *J. Nat. Prod.* **2014,** *77*, 1351-1358.

(49) Moree, W. J.; Yang, J. Y.; Zhao, X. L.; Liu, W. T.; Aparicio, M.; Atencio, L.; Ballesteros, J.; Sanchez, J.; Gavilan, R. G.; Gutierrez, M.; Dorrestein, P. C., *J. Chem. Ecol.* **2013,** *39*, 1045-1054.

(50) Watrous, J. D.; Dorrestein, P. C., *Nat. Rev. Microbiol.* **2011,** *9*, 683-694.

(51) McDonnell, L. A.; Heeren, R. M. A., *Mass. Spectrom. Rev.* **2007,** *26*, 606-643.

(52) Monge, M. E.; Harris, G. A.; Dwivedi, P.; Fernandez, F. M., *Chem. Rev.* **2013,** *113*, 2269-2308.

(53) Jarmusch, A. K.; Cooks, R. G., *Nat. Prod. Rep.* **2014,** *31*, 730-738.

(54) Hsu, C. C.; Elnaggar, M. S.; Peng, Y.; Fang, J.; Sanchez, L. M.; Mascuch, S. J.; Moller, K. A.; Alazzeh, E. K.; Pikula, J.; Quinn, R. A.; Zeng, Y.; Wolfe, B. E.; Dutton, R. J.; Gerwick, L.; Zhang, L.; Liu, X.; Mansson, M.; Dorrestein, P. C., *Anal. Chem.* **2013,** *85*, 7014-7018.

(55) Figueroa, M.; Jarmusch, A. K.; Raja, H. A.; El-Elimat, T.; Kavanaugh, J. S.; Horswill, A. R.; Cooks, R. G.; Cech, N. B.; Oberlies, N. H., *J. Nat. Prod.* **2014,** *77*, 1351-1358.

(56) Hsu, C. C.; Dorrestein, P. C., *Curr. Opin. Biotechnol.* **2014,** *31C*, 24-34.

(57) Watrous, J.; Roach, P.; Alexandrov, T.; Heath, B. S.; Yang, J. Y.; Kersten, R. D.; van der Voort, M.; Pogliano, K.; Gross, H.; Raaijmakers, J. M.; Moore, B. S.; Laskin, J.; Bandeira, N.; Dorrestein, P. C., *Proc. Natl. Acad. Sci. U.S.A.* **2012,** *109*, E1743-1752.

(58) White, T. J., Bruns, T., Lee, S.B., Taylor, J.W., Amplification and direct sequencing of fungal ribosomal RNA genes for phylogenetics. In *PCR protocols: a guide to methods and application.* , Innis, M. A., Gefland, D.H., Sninsky, J.J., White, T.J., Ed. Academic Press: San Diego, 1990; pp 315-322.

(59) Hussain, H.; Krohn, K.; Ahmed, I.; Draeger, S.; Schulz, B.; Pietro, S.; Pescitelli, G., *Eur. J. Org. Chem.* **2012,** *2012*, 1783-1789.

(60) Meyer, B. N.; Ferrigni, N. R.; Putnam, J. E.; Jacobsen, L. B.; Nichols, D. E.; McLaughlin, J. L., *Planta Med.* **1982,** *45*, 31-34.

(61) Li, Y.; Wang, Z.; Beier, R. C.; Shen, J.; De Smet, D.; De Saeger, S.; Zhang, S., *J. Agr. Food Chem.* **2011,** *59*, 3441-3453.

(62) Strakowska, J.; Blaszczyk, L.; Chelkowski, J., *J. Basic Microbiol.* **2014**.

(63) Raja, H. A.; Oberlies, N. H.; Figueroa, M.; Tanaka, K.; Hirayama, K.; Hashimoto, A.; Miller, A. N.; Zelski, S. E.; Shearer, C. A., *Mycologia* **2013,** *105*, 959-976.

(64) Holker, U.; Lenz, J., *Curr. Opin. Microbiol.* **2005,** *8*, 301-306.

(65) Rodrigues, A. A.; Menezes, M., *Mycopathologia* **2005,** *159*, 79-85.

(66) El-Elimat, T.; Raja, H. A.; Graf, T. N.; Faeth, S. H.; Cech, N. B.; Oberlies, N. H., *J. Nat. Prod.* **2014,** *77*, 193-199.

(67) Zech, K.; Huber, R.; Elgass, H., *J. Chromatogr. A* **1983,** *282*, 161-167.

(68) Wolf, D.; Siems, K., *Chimia* **2007,** *61*, 339-345.

(69) Jaroszewski, J. W., *Planta Med.* **2005,** *71*, 691-700.

(70) Nielsen, K. F.; Smedsgaard, J., *J. Chromatogr. A* **2003,** *1002*, 111-136.
(71) Bérdy, J., *CRC Handbook of Antibiotic Compounds: Microbial Metabolites*. CRC Press: 1987.
(72) Lang, G.; Mayhudin, N. A.; Mitova, M. I.; Sun, L.; Van Der Sar, S.; Blunt, J. W.; Cole, A. L. J.; Ellis, G.; Laatsch, H.; Munro, M. H. G., *J. Nat. Prod.* **2008,** *71*, 1595-1599.
(73) El-Elimat, T.; Figueroa, M.; Ehrmann, B. M.; Cech, N. B.; Pearce, C. J.; Oberlies, N. H., *J. Nat. Prod.* **2013,** *76*, 1709-1716.
(74) Sy-Cordero, A. A.; Graf, T. N.; Wani, M. C.; Kroll, D. J.; Pearce, C. J.; Oberlies, N. H., *J. Antibiot.* **2010,** *63*, 539-544.
(75) Kai, M.; González, I.; Genilloud, O.; Singh, S. B.; Svatoš, A., *Rapid Commun. Mass Spectrom.* **2012,** *26*, 2477-2482.
(76) Yang, J. Y.; Sanchez, L. M.; Rath, C. M.; Liu, X.; Boudreau, P. D.; Bruns, N.; Glukhov, E.; Wodtke, A.; de Felicio, R.; Fenner, A.; Wong, W. R.; Linington, R. G.; Zhang, L.; Debonsi, H. M.; Gerwick, W. H.; Dorrestein, P. C., *J. Nat. Prod.* **2013,** *76*, 1686-1699.
(77) Sica, V. P.; Raja, H. A.; El-Elimat, T.; Oberlies, N. H., *RSC Adv.* **2014,** *4*, 63221-63227.
(78) Hsu, C. C.; Dorrestein, P. C., *Curr. Opin. Biotechnol.* **2015,** *31C*, 24-34.
(79) Wiseman, J. M.; Ifa, D. R.; Zhu, Y.; Kissinger, C. B.; Manicke, N. E.; Kissinger, P. T.; Cooks, R. G., *Proc. Natl. Acad. Sci. U.S.A.* **2008,** *105*, 18120-18125.
(80) Nielsen, K. F.; Larsen, T. O., *Front. Microbiol.* **2015,** *6*, 71.
(81) Kertesz, V.; Van Berkel, G. J., *Anal. Chem.* **2010,** *82*, 5917-5921.
(82) Kertesz, V.; Van Berkel, G. J., *Bioanalysis* **2013,** *5*, 819-826.
(83) Kertesz, V.; Van Berkel, G. J., *Rapid Commun. Mass Spectrom.* **2014,** *28*, 1553-1560.
(84) Kertesz, V.; Paranthaman, N.; Moench, P.; Catoire, A.; Flarakos, J.; Van Berkel, G. J., *Bioanalysis* **2014,** *6*, 2599-2606.
(85) Kertesz, V.; Weiskittel, T. M.; Van Berkel, G. J., *Anal. Bioanal. Chem.* **2015,** *407*, 2117-2125.
(86) Takats, Z.; Wiseman, J. M.; Gologan, B.; Cooks, R. G., *Science* **2004,** *306*, 471-473.
(87) Roach, P. J.; Laskin, J.; Laskin, A., *Analyst* **2010,** *135*, 2233-2236.
(88) Cornett, D. S.; Reyzer, M. L.; Chaurand, P.; Caprioli, R. M., *Nature Methods* **2007,** *4*, 828-833.
(89) Nemes, P.; Vertes, A., *Anal. Chem.* **2007,** *79*, 8098-8106.
(90) Kertesz, V.; Van Berkel, G. J., *J. Mass. Spectrom.* **2010,** *45*, 252-260.
(91) El-Elimat, T.; Zhang, X. L.; Jarjoura, D.; Moy, F. J.; Orjala, J.; Kinghorn, A. D.; Pearce, C. J.; Oberlies, N. H., *ACS Med. Chem. Lett.* **2012,** *3*, 645-649.
(92) El-Elimat, T.; Raja, H. A.; Day, C. S.; Chen, W. L.; Swanson, S. M.; Oberlies, N. H., *J. Nat. Prod.* **2014,** *77*, 2088-2098.
(93) Kaur, A.; Raja, H. A.; Darveaux, B. A.; Chen, W. L.; Swanson, S. M.; Pearce, C. J.; Oberlies, N. H., *Magn. Reson. Chem.* **2015,** *(In Press: DOI: 10.1002/mrc.4254)*.

(94) Vandermolen, K. M.; Raja, H. A.; El-Elimat, T.; Oberlies, N. H., *AMB Express* **2013,** *3*, 71.
(95) Figueroa, M.; Graf, T. N.; Ayers, S.; Adcock, A. F.; Kroll, D. J.; Yang, J.; Swanson, S. M.; Munoz-Acuna, U.; de Blanco, E. J. C.; Agrawal, R.; Wani, M. C.; Darveaux, B. A.; Pearce, C. J.; Oberlies, N. H., *J. Antibiot.* **2012,** *65*, 559-564.
(96) Ayers, S.; Ehrmann, B. M.; Adcock, A. F.; Kroll, D. J.; de Blanco, E. J. C.; Shen, Q.; Swanson, S. M.; Falkinham, J. O.; Wani, M. C.; Mitchell, S. M.; Pearce, C. J.; Oberlies, N. H., *J. Pept. Sci.* **2012,** *18*, 500-510.
(97) Kiss, A.; Heeren, R. M. A., *Anal. Bioanal. Chem.* **2011,** *399*, 2623-2634.
(98) Angel, T. E.; Aryal, U. K.; Hengel, S. M.; Baker, E. S.; Kelly, R. T.; Robinson, E. W.; Smith, R. D., *Chem. Soc. Rev.* **2012,** *41*, 3912-3928.
(99) White, T. J.; Bruns, T.; Lee, S.; Taylor, J., *PCR protocols: a guide to methods and applications* **1990,** *18*, 315-322.
(100) Bayry, J.; Aimanianda, V.; Guijarro, J. I.; Sunde, M.; Latge, J. P., *PLoS Pathog.* **2012,** *8*, e1002700.
(101) Smedsgaard, J., *J. Chromatogr. A* **1997,** *760*, 264-270.
(102) Larsen, T. O.; Smedsgaard, J.; Nielsen, K. F.; Hansen, M. E.; Frisvad, J. C., *Nat. Prod. Rep.* **2005,** *22*, 672-695.
(103) Raja, H. A.; Kaur, A.; El-Elimat, T.; Figueroa, M.; Kumar, R.; Deep, G.; Agarwal, R.; Faeth, S. H.; Cech, N. B.; Oberlies, N. H., *Mycology* **2015,** *6*, 8-27.
(104) Petersen, A. B.; Ronnest, M. H.; Larsen, T. O.; Clausen, M. H., *Chem. Rev.* **2014,** *114*, 12088-107.
(105) Oxford, A. E.; Raistrick, H.; Simonart, P., *Biochem. J.* **1939,** *33*, 240-248.
(106) Brian, P., *Trans. Brit. Mycol. Soc.* **1946,** *29*, 173-187.
(107) McGowan, J. C., *Trans. Brit. Mycol. Soc.* **1946,** *29*, 188-0.
(108) Grove, J. F.; McGowan, J. C., *Nature* **1947,** *160*, 574.
(109) Grove, J. F.; MacMillan, J.; Mulholland, T. P. C.; Rogers, M. A. T., *J. Chem. Soc.* **1952**, 3949-3958.
(110) Levine, S. G.; Hicks, R. E., *Tetrahedron Lett.* **1971,** *12*, 311-314.
(111) Malmros, G.; Wägner, A.; Maron, L., *Cryst. Struct. Commun.* **1977,** *6*, 463.
(112) Gentles, J. C., *Nature* **1958,** *182*, 476-477.
(113) Williams, D. I.; Marten, R. H.; Sarkany, I., *Lancet* **1958,** *2*, 1212-1213.
(114) Ho, Y.-S.; Duh, J.-S.; Jeng, J.-H.; Wang, Y.-J.; Liang, Y.-C.; Lin, C.-H.; Tseng, C.-J.; Yu, C.-F.; Chen, R.-J.; Lin, J.-K., *Int. J. Cancer* **2001,** *91*, 393-401.
(115) Kim, Y.; Alpmann, P.; Blaum-Feder, S.; Kramer, S.; Endo, T.; Lu, D.; Carson, D.; Schmidt-Wolf, I. G., *Leuk. Res.* **2011,** *35*, 1070-3.
(116) Liéby-Muller, F.; Heudré Le Baliner, Q.; Grisoni, S.; Fournier, E.; Guilbaud, N.; Marion, F., *Bioorg. Med. Chem. Lett.* **2015,** *25*, 2078-2081.
(117) Robinson, R. C. V., *Southern Med. J.* **1960,** *53*, 73-76.
(118) Corvis, Y.; Barzyk, W.; Brezesinski, G.; Mrabet, N.; Badis, M.; Hecht, S.; Rogalska, E., *Langmuir* **2006,** *22*, 7701-7711.
(119) Nweze, E. I.; Mukherjee, P. K.; Ghannoum, M. A., *J. Clin. Microbiol.* **2010,** *48*, 3750-2.

(120) Sica, V. P.; Raja, H. A.; El-Elimat, T.; Kertesz, V.; Van Berkel, G. J.; Pearce, C. J.; Oberlies, N. H., *J. Nat. Prod.* **2015,** *78*, 1926-1936.
(121) Tata, A.; Perez, C. J.; Ore, M. O.; Lostun, D.; Passas, A.; Morin, S.; Ifa, D. R., *RSC Adv.* **2015,** *5*, 75458-75464.
(122) Park, J. H.; Choi, G. J.; Lee, H. B.; Kim, K. M.; Jung, H. S.; Lee, S. W.; Jang, K. S.; Cho, K. Y.; Kim, J. C., *J. Microbiol. Biotechnol.* **2005,** *15*, 112-117.
(123) Richardson, S. N.; Walker, A. K.; Nsiama, T. K.; McFarlane, J.; Sumarah, M. W.; Ibrahim, A.; Miller, J. D., *Fungal Ecol.* **2014,** *11*, 107-113.
(124) Bills, G. F.; González-Menéndez, V.; Martín, J.; Platas, G.; Fournier, J.; Peršoh, D.; Stadler, M., *PloS one* **2012,** *7*.
(125) Pažoutová, S.; Follert, S.; Bitzer, J.; Keck, M.; Surup, F.; Šrůtka, P.; Holuša, J.; Stadler, M., *Fungal. Divers.* **2013,** *60*, 107-123.
(126) Stadler, M.; Quang, D. N.; Tomita, A.; Hashimoto, T.; Asakawa, Y., *Mycol. Res.* **2006,** *110*, 811-20.
(127) Liu, Y. J.; Whelen, S.; Hall, B. D., *Mol. Biol. Evol.* **1999,** *16*, 1799-808.
(128) Malkus, A.; Chang, P. F.; Zuzga, S. M.; Chung, K. R.; Shao, J.; Cunfer, B. M.; Arseniuk, E.; Ueng, P. P., *Mycol. Res.* **2006,** *110*, 1152-64.
(129) Hsieh, H. M.; Lin, C. R.; Fang, M. J.; Rogers, J. D.; Fournier, J.; Lechat, C.; Ju, Y. M., *Mol. Phylogenet. Evol.* **2010,** *54*, 957-69.
(130) Raja, H. A.; El-Elimat, T.; Oberlies, N. H.; Shearer, C. A.; Miller, A. N.; Tanaka, K.; Hashimoto, A.; Fournier, J., *Mycologia* **2015,** *107*, 845-62.
(131) Gardes, M.; Bruns, T. D., *Mol. Ecol.* **1993,** *2*, 113-118.
(132) U'Ren, J. M.; Lutzoni, F.; Miadlikowska, J.; Laetsch, A. D.; Elizabeth Arnold, A., *Am. J. Bot.* **2012,** *99*, 898-914.
(133) Ayers, S.; Graf, T. N.; Adcock, A. F.; Kroll, D. J.; Matthew, S.; Carcache de Blanco, E. J.; Shen, Q.; Swanson, S. M.; Wani, M. C.; Pearce, C. J.; Oberlies, N. H., *J. Nat. Prod.* **2011,** *74*, 1126-31.
(134) Figueroa, M.; Graf, T. N.; Ayers, S.; Adcock, A. F.; Kroll, D. J.; Yang, J.; Swanson, S. M.; Munoz-Acuna, U.; Carcache De Blanco, E. J.; Agrawal, R.; Wani, M. C.; Darveaux, B. A.; Pearce, C. J.; Oberlies, N. H., *J. Antibiot.* **2012,** *65*, 559-564.
(135) Simpson, T. J.; Holker, J. S. E., *Phytochemistry* **1977,** *16*, 229-233.
(136) Singh, S., Guttation: Quantification, microbiology and implications for phytopathology. In *Prog. Bot.*, Lüttge, U.; Beyschlag, W.; Cushman, J., Eds. Springer Berlin Heidelberg: 2014; Vol. 75, pp 187-214.
(137) Daly, S. M.; Elmore, B. O.; Kavanaugh, J. S.; Triplett, K. D.; Figueroa, M.; Raja, H. A.; El-Elimat, T.; Crosby, H. A.; Femling, J. K.; Cech, N. B.; Horswill, A. R.; Oberlies, N. H.; Hall, P. R., *Antimicrob. Agents Chemother.* **2015,** *59*, 2223-35.
(138) Wang, X.; Sena Filho, J. G.; Hoover, A. R.; King, J. B.; Ellis, T. K.; Powell, D. R.; Cichewicz, R. H., *J. Nat. Prod.* **2010,** *73*, 942-948.
(139) Paguigan, N. D.; Raja, H. A.; Day, C. S.; Oberlies, N. H., *Phytochemistry* **2016**, (In Press).
(140) Klich, M. A.; Arthur, K. S.; Lax, A. R.; Bland, J. M., *Mycopathologia* **1994,** *127*, 123-127.

(141) Rogers, J. D., *Mycologia* **1984,** *76*, 23-33.
(142) Whalley, A. J. S.; Suwannasai, N.; Ruchikachorn, N.; Sangvichien, E.; Sihanonth, P., *Suan Sunandha Journal of Science and Technology* **2015,** *2*, 11-17.
(143) Rodrigues, K. F., *Mycologia* **1994,** *86*, 376-385.
(144) Frohlich, J.; Hyde, K. D.; Petrini, O., *Mycol. Res.* **2000,** *104*, 1202-1212.
(145) Davis, E. C.; Franklin, J. B.; Shaw, A. J.; Vilgalys, R., *Am. J. Bot.* **2003,** *90*, 1661-7.
(146) Okane, I.; Srikitikulchai, P.; Toyama, K.; Læssøe, T.; Sivichai, S.; Hywel-Jones, N.; Nakagiri, A.; Potacharoen, W.; Suzuki, K. I., *Mycoscience* **2008,** *49*, 359-372.
(147) Okane, I.; Srikitikulchai, P.; Tabuchi, Y.; Sivichai, S.; Nakagiri, A., *Mycoscience* **2012,** *53*, 122-132.
(148) Carroll, G., *Ecology* **1988,** *69*, 2-9.
(149) Petrini, O.; Petrini, L.; Rodrigues, K., *Fitopatol. Bras.* **1995,** *20*, 531-539.
(150) Whalley, A. J. S., *Mycol. Res.* **1996,** *100*, 897-922.
(151) Oberholtzer, L.; Dunutru, C., *EIB* **2009,** *58*.
(152) Willer, H.; Kilcher, L., The World of Organic Agriculture. Statistics and Emerging Trends 2011. In 2011 ed.; IFOAM, Bonn, & FiBL: 2011.
(153) Cantrell, C. L.; Dayan, F. E.; Duke, S. O., *J. Nat. Prod.* **2012,** *75*, 1231-1242.
(154) Hoagland, R. E., *Weed. Technol.* **2001,** *15*, 835-857.
(155) Copping, L. G.; Duke, S. O., *Pest. Manag. Sci.* **2007,** *63*, 524-554.
(156) Young, S. L., *Weed. Technol.* **2004,** *18*, 580-587.
(157) Dayan, F. E.; Cantrell, C. L.; Duke, S. O., *Bioorg. Med. Chem.* **2009,** *17*, 4022-34.
(158) Johnson, W. C.; Boudreau, M. A.; Davis, J. W., *Weed. Technol.* **2013,** *27*, 417-421.
(159) Shrestha, A.; Moretti, M.; Mourad, N., *Weed. Technol.* **2012,** *26*, 110-116.
(160) Gerwick, B. C.; Brewster, W. K.; deBoer, G. J.; Fields, S. C.; Graupner, P. R.; Hahn, D. R.; Pearce, C. J.; Schmitzer, P. R.; Webster, J. D., *J. Chem. Ecol.* **2013,** *39*, 253-261.
(161) Gerwick, B. C.; Graupner, P. R.; Fields, S. C.; Schmitzer, P. R.; Brewster, W. K. Methylidene mevalonates and their use as herbicides. US 7,393,812 B2, 2008.
(162) Raja, H. A.; Oberlies, N. H.; Figueroa, M.; Tanaka, K.; Hirayama, K.; Hashimoto, A.; Miller, A. N.; Zelski, S. E.; Shearer, C. A., *Mycologia* **2013,** *105*, 959-76.
(163) Schoch, C. L.; Seifert, K. A.; Huhndorf, S.; Robert, V.; Spouge, J. L.; Levesque, C. A.; Chen, W.; Bolchacova, E.; Voigt, K.; Crous, P. W.; Miller, A. N.; Wingfield, M. J.; Aime, M. C.; An, K. D.; Bai, F. Y.; Barreto, R. W.; Begerow, D.; Bergeron, M. J.; Blackwell, M.; Boekhout, T.; Bogale, M.; Boonyuen, N.; Burgaz, A. R.; Buyck, B.; Cai, L.; Cai, Q.; Cardinali, G.; Chaverri, P.; Coppins, B. J.; Crespo, A.; Cubas, P.; Cummings, C.; Damm, U.; de Beer, Z. W.; de Hoog, G. S.; Del-Prado, R.; B, D.; Dieguez-Uribeondo, J.; Divakar, P. K.; Douglas, B.; Duenas, M.; Duong, T. A.; Eberhardt, U.; Edwards, J. E.; Elshahed, M. S.; Fliegerova, K.; Furtado, M.; Garcia, M. A.; Ge, Z. W.; Griffith, G. W.; Griffiths, K.; Groenewald, J. Z.; Groenewald, M.; Grube, M.; Gryzenhout, M.; Guo, L. D.; Hagen, F.; Hambleton, S.; Hamelin, R. C.; Hansen, K.; Harrold, P.; Heller, G.;

Herrera, G.; Hirayama, K.; Hirooka, Y.; Ho, H. M.; Hoffmann, K.; Hofstetter, V.; Hognabba, F.; Hollingsworth, P. M.; Hong, S. B.; Hosaka, K.; Houbraken, J.; Hughes, K.; Huhtinen, S.; Hyde, K. D.; James, T.; Johnson, E. M.; Johnson, J. E.; Johnston, P. R.; Jones, E. B.; Kelly, L. J.; Kirk, P. M.; Knapp, D. G.; Koljalg, U.; GM, K.; Kurtzman, C. P.; Landvik, S.; Leavitt, S. D.; Liggenstoffer, A. S.; Liimatainen, K.; Lombard, L.; Luangsa-Ard, J. J.; Lumbsch, H. T.; Maganti, H.; Maharachchikumbura, S. S.; Martin, M. P.; May, T. W.; McTaggart, A. R.; Methven, A. S.; Meyer, W.; Moncalvo, J. M.; Mongkolsamrit, S.; Nagy, L. G.; Nilsson, R. H.; Niskanen, T.; Nyilasi, I.; Okada, G.; Okane, I.; Olariaga, I.; Otte, J.; Papp, T.; Park, D.; Petkovits, T.; Pino-Bodas, R.; Quaedvlieg, W.; Raja, H. A.; Redecker, D.; T, R.; Ruibal, C.; Sarmiento-Ramirez, J. M.; Schmitt, I.; Schussler, A.; Shearer, C.; Sotome, K.; Stefani, F. O.; Stenroos, S.; Stielow, B.; Stockinger, H.; Suetrong, S.; Suh, S. O.; Sung, G. H.; Suzuki, M.; Tanaka, K.; Tedersoo, L.; Telleria, M. T.; Tretter, E.; Untereiner, W. A.; Urbina, H.; Vagvolgyi, C.; Vialle, A.; Vu, T. D.; Walther, G.; Wang, Q. M.; Wang, Y.; Weir, B. S.; Weiss, M.; White, M. M.; Xu, J.; Yahr, R.; Yang, Z. L.; Yurkov, A.; Zamora, J. C.; Zhang, N.; Zhuang, W. Y.; Schindel, D.; Consortium, F. B., *Proc. Natl. Acad. Sci. U.S.A.* **2012,** *109*, 6241-6.

(164) Gouy, M.; Guindon, S.; Gascuel, O., *Mol. Biol. Evol.* **2010,** *27*, 221-4.

(165) Swofford, D. L. *PAUP*: Phylogenetic Analysis Using Parsimony (* and other methods). Version 4*, Sinauer Associates, : Sunderland, Massachusetts 2002.

(166) Guindon, S.; Delsuc, F.; Dufayard, J. F.; Gascuel, O., *Methods Mol. Biol.* **2009,** *537*, 113-37.

(167) Schoch, C. L.; Robbertse, B.; Robert, V.; Vu, D.; Cardinali, G.; Irinyi, L.; Meyer, W.; Nilsson, R. H.; Hughes, K.; Miller, A. N.; Kirk, P. M.; Abarenkov, K.; Aime, M. C.; Ariyawansa, H. A.; Bidartondo, M.; Boekhout, T.; Buyck, B.; Cai, Q.; Chen, J.; Crespo, A.; Crous, P. W.; Damm, U.; De Beer, Z. W.; Dentinger, B. T.; Divakar, P. K.; Duenas, M.; Feau, N.; Fliegerova, K.; Garcia, M. A.; Ge, Z. W.; Griffith, G. W.; Groenewald, J. Z.; Groenewald, M.; Grube, M.; Gryzenhout, M.; Gueidan, C.; Guo, L.; Hambleton, S.; Hamelin, R.; Hansen, K.; Hofstetter, V.; Hong, S. B.; Houbraken, J.; Hyde, K. D.; Inderbitzin, P.; Johnston, P. R.; Karunarathna, S. C.; Koljalg, U.; Kovacs, G. M.; Kraichak, E.; Krizsan, K.; Kurtzman, C. P.; Larsson, K. H.; Leavitt, S.; Letcher, P. M.; Liimatainen, K.; Liu, J. K.; Lodge, D. J.; Luangsa-ard, J. J.; Lumbsch, H. T.; Maharachchikumbura, S. S.; Manamgoda, D.; Martin, M. P.; Minnis, A. M.; Moncalvo, J. M.; Mule, G.; Nakasone, K. K.; Niskanen, T.; Olariaga, I.; Papp, T.; Petkovits, T.; Pino-Bodas, R.; Powell, M. J.; Raja, H. A.; Redecker, D.; Sarmiento-Ramirez, J. M.; Seifert, K. A.; Shrestha, B.; Stenroos, S.; Stielow, B.; Suh, S. O.; Tanaka, K.; Tedersoo, L.; Telleria, M. T.; Udayanga, D.; Untereiner, W. A.; Dieguez Uribeondo, J.; Subbarao, K. V.; Vagvolgyi, C.; Visagie, C.; Voigt, K.; Walker, D. M.; Weir, B. S.; Weiss, M.; Wijayawardene, N. N.; Wingfield, M. J.; Xu, J. P.; Yang, Z. L.; Zhang, N.; Zhuang, W. Y.; Federhen, S., *Database (Oxford)* **2014,** *2014*.

(168) Rehner, S. A.; Samuels, G. J., *Can. J. Bot.* **1995,** *73*, 816-823.

(169) Checa, J.; Arenal, F.; Blanco, N.; Rogers, J. D., *Mycol. Res.* **2008,** *112*, 795-801.

(170) Sy-Cordero, A. A.; Graf, T. N.; Adcock, A. F.; Kroll, D. J.; Shen, Q.; Swanson, S. M.; Wani, M. C.; Pearce, C. J.; Oberlies, N. H., *J. Nat. Prod.* **2011,** *74*, 2137-42.
(171) Garcia, D.; Stchigel, A. M.; Cano, J.; Calduch, M.; Hawksworth, D. L.; Guarro, J., *Mycol. Res.* **2006,** *110*, 1271-89.
(172) Zare, R.; Asgari, B.; Gams, W., *Mycologia* **2010,** *102*, 1383-1388.
(173) Bills, G. F.; Dombrowski, A. W.; Goetz, M. A., *Methods Mol. Biol.* **2012,** *944*, 79-96.
(174) Hutwimmer, S.; Wang, H.; Strasser, H.; Burgstaller, W., *Mycologia* **2010,** *102*, 1-10.
(175) Rupprecht, J. K.; Hui, Y. H.; McLaughlin, J. L., *J. Nat. Prod.* **1990,** *53*, 237-78.
(176) McLaughlin, J. L., *J. Nat. Prod.* **2008,** *71*, 1311-21.
(177) Alali, F. Q.; Liu, X. X.; McLaughlin, J. L., *J. Nat. Prod.* **1999,** *62*, 504-40.
(178) Gupta, A.; Pandey, S.; Shah, D. R.; Yadav, J. S.; Seth, N. R., *Sys. Rev. Pharm.* **2011,** *2*, 104-109.
(179) Lima, L. A. R. D.; Pimenta, L. P. S.; Boaventura, M. A. D., *Planta Med.* **2009,** *75*, 80-83.
(180) Chen, Y.; Chen, J. W.; Wang, Y.; Xu, S. S.; Li, X., *Food Chem.* **2012,** *135*, 960-966.
(181) Smith, R. E.; Tran, K.; Richards, K. M., *Stud. Nat. Prod. Chem.* **2014,** *41*, 95-117.
(182) Donno, D.; Beccaro, G. L.; Mellano, M. G.; Cerutti, A. K.; Bounous, G., *J. Food. Nutr. Res.* **2014,** *53*, 81-95.
(183) Brannan, R. G.; Peters, T.; Talcott, S. T., *Food Chem.* **2015,** *168*, 656-661.
(184) Rupprecht, J. K.; Chang, C. J.; Cassady, J. M.; Mclaughlin, J. L.; Mikolajczak, K. L.; Weisleder, D., *Heterocycles* **1986,** *24*, 1197-1201.
(185) Oberlies, N. H.; Chang, C. J.; McLaughlin, J. L., *J. Med. Chem.* **1997,** *40*, 2102-6.
(186) Deep, G.; Kumar, R.; Jain, A. K.; Dhar, D.; Panigrahi, G. K.; Hussain, A.; Agarwal, C.; El-Elimat, T.; Sica, V. P.; Oberlies, N. H.; Agarwal, R., *Sci. Rep.* **2016,** *6*, 23135.
(187) McCage, C. M.; Ward, S. M.; Paling, C. A.; Fisher, D. A.; Flynn, P. J.; McLaughlin, J. L., *Phytomedicine* **2002,** *9*, 743-748.
(188) Le Ven, J.; Schmitz-Afonso, I.; Lewin, G.; Laprevote, O.; Brunelle, A.; Touboul, D.; Champy, P., *J. Mass. Spectrom.* **2012,** *47*, 1500-9.
(189) Allegrand, J.; Touboul, D.; Schmitz-Afonso, I.; Guerineau, V.; Giuliani, A.; Le Ven, J.; Champy, P.; Laprevote, O., *Rapid Commun. Mass Spectrom.* **2010,** *24*, 3602-8.
(190) Gawronski, J.; Wu, Y. C., *Pol. J. Chem.* **1999,** *73*, 241-243.
(191) Mangal, M.; Khan, M. I.; Agarwal, S. M., *Anticancer Agents Med. Chem.* **2016,** *16*, 138-159.
(192) Woo, M. H.; Kim, D. H.; McLaughlin, J. L., *Phytochemistry* **1999,** *50*, 1033-1040.
(193) Liu, X. X.; Alali, F. Q.; Pilarinou, E.; McLaughlin, J. L., *J. Nat. Prod.* **1998,** *61*, 620-624.

(194) Rieser, M. J.; Gu, Z. M.; Fang, X. P.; Zeng, L.; Wood, K. V.; McLaughlin, J. L., *J. Nat. Prod.* **1996,** *59*, 100-108.
(195) Woo, M. H.; Zeng, L.; Ye, Q.; Gu, Z. M.; Zhao, G. X.; Mclaughlin, J. L., *Bioorg. Med. Chem. Lett.* **1995,** *5*, 1135-1140.
(196) Talaty, N.; Takats, Z.; Cooks, R. G., *Analyst* **2005,** *130*, 1624-33.
(197) Jackson, A. U.; Tata, A.; Wu, C.; Perry, R. H.; Haas, G.; West, L.; Cooks, R. G., *Analyst* **2009,** *134*, 867-874.
(198) Muller, T.; Oradu, S.; Ifa, D. R.; Cooks, R. G.; Krautler, B., *Anal. Chem.* **2011,** *83*, 5754-61.
(199) Bjarnholt, N.; Li, B.; D'Alvise, J.; Janfelt, C., *Nat. Prod. Rep.* **2014,** *31*, 818-37.
(200) Goodrich, K. R.; Zjhra, M. L.; Ley, C. A.; Raguso, R. A., *Int. J. Plant Sci.* **2006,** *167*, 33-46.
(201) Ratnayake, S.; Rupprecht, J. K.; Potter, W. M.; McLaughlin, J. L., *J. Econ. Entomol.* **1992,** *85*, 2353-6.
(202) Woo, M. H.; Chung, S. O.; Kim, D. H., *Bioorg. Med. Chem* **2000,** *8*, 285-290.
(203) Sleno, L., *J. Mass. Spectrom.* **2012,** *47*, 226-236.
(204) He, K.; Zhao, G. X.; Shi, G.; Zeng, L.; Chao, J. F.; McLaughlin, J. L., *Bioorg. Med. Chem.* **1997,** *5*, 501-6.
(205) Kim, E. J.; Suh, K. M.; Kim, D. H.; Jung, E. J.; Seo, C. S.; Son, J. K.; Woo, M. H.; McLaughlin, J. L., *J. Nat. Prod.* **2005,** *68*, 194-197.
(206) He, K.; Shi, G.; Zhao, G. X.; Zeng, L.; Ye, Q.; Schwedler, J. T.; Wood, K. V.; McLaughlin, J. L., *J. Nat. Prod.* **1996,** *59*, 1029-1034.
(207) Zhao, G. X.; Chao, J. F.; Zeng, L.; McLaughlin, J. L., *Nat. Toxins* **1996,** *4*, 128-134.
(208) Zhao, G. X.; Chao, J. F.; Zeng, L.; Rieser, M. J.; McLaughlin, J. L., *Bioorg. Med. Chem* **1996,** *4*, 25-32.
(209) Woo, M. H.; Cho, K. Y.; Zhang, Y.; Zeng, L.; Gu, Z. M.; McLaughlin, J. L., *J. Nat. Prod.* **1995,** *58*, 1533-42.
(210) Woo, M. H.; Zeng, L.; Mclaughlin, J. L., *Heterocycles* **1995,** *41*, 1731-1742.
(211) Zhao, G. X.; Gu, Z. M.; Zeng, L.; Chao, J. F.; Kozlowski, J. F.; Wood, K. V.; Mclaughlin, J. L., *Tetrahedron* **1995,** *51*, 7149-7160.
(212) Zhao, G. X.; Miesbauer, L. R.; Smith, D. L.; McLaughlin, J. L., *J. Med. Chem.* **1994,** *37*, 1971-1976.
(213) Zhao, G. x.; Ng, J. H.; Kozlowzki, J. F.; Smith, D. L.; McLaughlin, J. L., *Heterocycles* **1994,** *38*, 1897-1908.
(214) Zhao, G. X.; Rieser, M. J.; Hui, Y. H.; Miesbauer, L. R.; Smith, D. L.; McLaughlin, J. L., *Phytochemistry* **1993,** *33*, 1065-73.
(215) Dictionary of Natural Products 24.2. In Taylor & Francis Group: London, 2013.
(216) Potts, L. F.; Luzzio, F. A.; Smith, S. C.; Hetman, M.; Champy, P.; Litvan, I., *Neurotoxicology* **2012,** *33*, 53-58.
(217) Zeng, L.; Wu, F.-E.; Oberlies, N. H.; McLaughlin, J. L.; Sastrodihadjo, S., *J. Nat. Prod.* **1996,** *59*, 1035-1042.

(218) Wu, C.; Ifa, D. R.; Manicke, N. E.; Cooks, R. G., *Anal. Chem.* **2009,** *81*, 7618-24.
(219) Lostun, D.; Perez, C. J.; Licence, P.; Barrett, D. A.; Ifa, D. R., *Anal. Chem.* **2015,** *87*, 3286-3293.
(220) Li, B.; Knudsen, C.; Hansen, N. K.; Jorgensen, K.; Kannangara, R.; Bak, S.; Takos, A.; Rook, F.; Hansen, S. H.; Moller, B. L.; Janfelt, C.; Bjarnholt, N., *Plant J.* **2013,** *74*, 1059-71.

APPENDIX A

SUPPLEMENTARY TABLES

Table S1. Fungal Metabolites That Were Detected by the Droplet-LMJ-SSP, Recording the Retention Time (Rt), UV Data, HRMS, and MS/MS

Table S2. ^{1}H (400 MHz) and ^{13}C NMR (100 MHz) Data for Griseofulvin in $CDCl_3$

Table S3. The Lengths and Weights for the Three Groups of Stroma Used for the Spatial Distribution of Griseofulvin Along the Stroma

Table S4. The Populated List Using Mass Defect Filtering for ±100 Da With a Mass Defect of ±25 mDa Around *m/z* 603.4807 for a Seed, Pulp, Twig, Ovary, Leaf, and Petal from an *Asimina triloba* Tree.

Table S1. Fungal Metabolites That Were Identified by the Droplet-LMJ-SSP, Recording the Retention Time (Rt), UV Data, HRMS, and MS/MS.

G100[13]
Clohesyomyces aquaticus
GenBank # KM589854
Freshwater fungus isolated from submerged wood

#	Chemical Structure and Chemical formula	Rt (min)	UV (nm)	Positive Ionization Mode	
				$[M+H]^+$	MS/MS
3	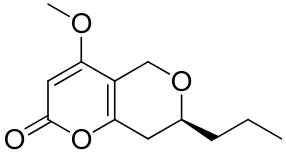 **Phomopsinone A** $C_{12}H_{16}O_4$	4.36	205 221 284	225.1120 (-0.6)	153.0546 111.0440, 135.0440 125.0597, 97.0646 79.0178, 121.0283
4	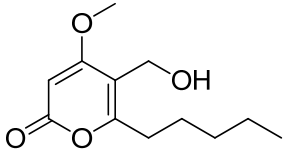 **Pyrenocine M** $C_{12}H_{18}O_4$	3.62	208 221 283	227.1278 (+0.1)	209.1171 167.0703, 131.0854 93.0699, 79.0541 197.1172, 139.0390

5	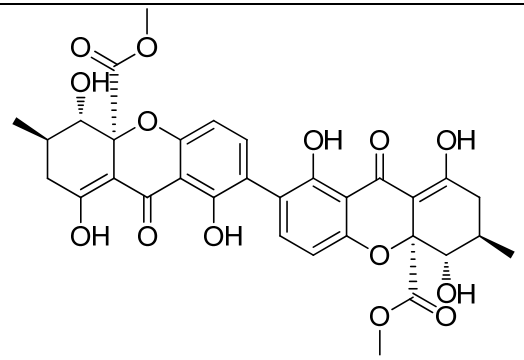 **Secalonic acid A** $C_{32}H_{30}O_{14}$	5.50	193 222 264 337	639.1713 (+0.7)	183.0651, 561.1390 193.0495, 501.1177 579.1493, 483.1071 589.1340, 377.0652 169.0495, 455.0979 543.1285, 151.0390
6	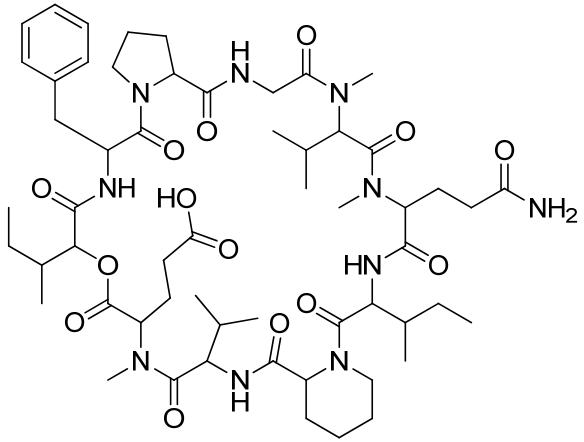 **Sch 217048** $C_{57}H_{88}N_{10}O_{14}$	4.98	192 216	1137.6570 (+1.4)	86.0963, 268.1651 256.1653, 228.1704 350.2066, 39.1958 377.2065, 405.2017 211.1438, 286.1754 484.2432, 155.0813 654.3506, 559.2763

G87[31]
Halenospora* aff. *varia
GenBank # KJ803850
Fungus isolated from submerged wood in fresh water

#	Chemical Structure and Chemical formula	Rt (min)	UV (nm)	Positive Ionization Mode	
				$[M+H]^+$	MS/MS
7	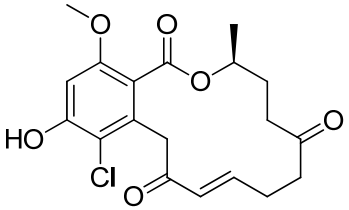 **Greensporone A** $C_{19}H_{21}O_6Cl$	4.03	222 294	381.1099 (0.0)	265.0259, 237.0310 241.0261, 123.0804 145.0648, 215.0102 253.0260, 263.0466 209.0364, 345.0883 363.0987, 281.0574 303.0415, 289.0260
8	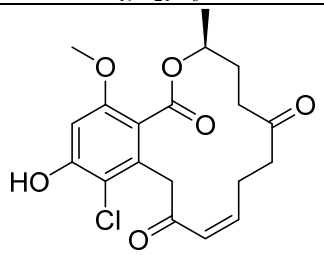 **Greensporone B** $C_{19}H_{21}O_6Cl$	4.20	238 291	381.1099 (0.0)	265.0262, 237.0312 241.0261, 253.0261 145.0648, 209.0362 123.0805, 215.0104 289.0265, 345.0886 363.0995, 303.0793

9	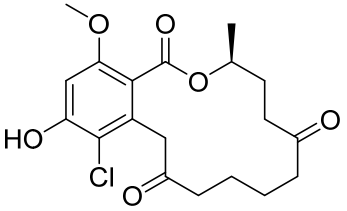 **8,9-Dihydrogreensporone A** $C_{19}H_{23}O_6Cl$	4.45	218 291	383.1256 (0.0)	265.0619, 263.0472 215.0104, 125.0961 83.0491, 171.0209 224.9948, 243.0054 253.0261, 237.0673 227.0624, 293.0577 305.0581, 329.0937 347.1045, 365.1153
10	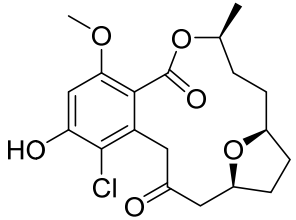 **Greensporone F** $C_{19}H_{23}O_6Cl$	4.70	217 290	383.1255 (-0.2)	241.0252, 107.0857 79.0543, 97.1014 125.0958, 211.0159 224.9953, 253.0249 265.0253, 293.0578 309.0531, 347.1031 365.1136, 329.0913
		**MSX19583**[32] ***Aspergillus sydowii*** **GenBank # ITS: KP702233; RPB1: KP702234; RPB2: KP702231, KP702232** **Fungus from MSX library**			
#	**Chemical Structure and Chemical formula**	**Rt (min)**	**UV (nm)**	**Positive Ionization Mode**	
				$[M+H]^+$	**MS/MS**

11	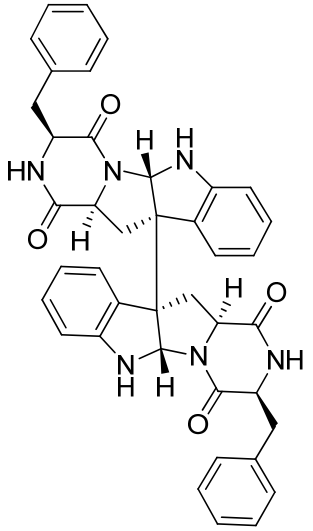 **Diketopiperazine dimer** $C_{40}H_{36}N_6O_4$	4.48	192 208 300	665.2877 (+0.9)	157.0763, 304.1448 332.1401, 130.0652 120.0811, 185.0715 241.0845, 433.1996 259.1226, 286.1351
12	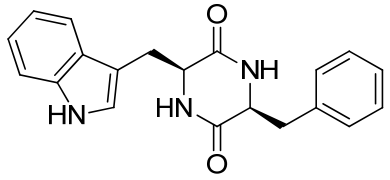 **Cyclo-(L-phenylalaninyl-L-tryptophanyl)** $C_{20}H_{19}N_3O_2$	3.46	191 218 279 289 364	334.1549 (-0.3)	130.0652, 170.0596 120.0810, 159.0914 175.0863, 234.1275 205.0968, 289.1338 261.1387, 91.0543
13	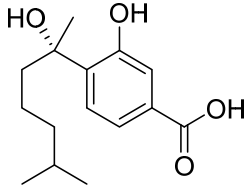 ***S*-sydonic acid** $C_{15}H_{22}O_4$	5.07	212 240 300	[M+H-H_2O]$^+$ 249.1486 (+0.3)	165.0549, 151.0386 69.0699, 107.0490 121.0646, 179.0704 193.0865, 231.1387 85.1010, 213.1267

14	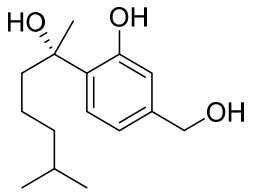 **S-sydonol** $C_{15}H_{24}O_3$	4.96	198 221 278	[M+H-H_2O]$^+$ 235.1694 (+0.6)	151.0755, 137.0601 121.0647, 161.0956 217.1589, 107.0490 175.1121, 147.0808 205.1593, 69.0700
		**G77[33]** ***Aspergillus iizukae*** **GenBank # AB859956** **Endophytic fungus isolated from surface sterilized leaves of *Silybum marianum***			
#	**Chemical Structure and Chemical formula**	**Rt (min)**	**UV (nm)**	**Positive Ionization Mode**	
				[M+H]$^+$	**MS/MS**
15	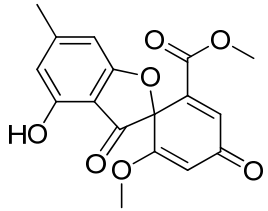 **Bisdechlorogeodin** $C_{17}H_{14}O_7$	4.06	218 284	331.0810 (-0.7)	272.0681, 299.0535 275.0446, 284.0308 287.0917, 255.0649 244.0726, 228.0408
16	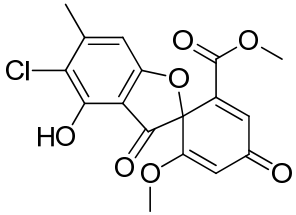	4.52	214 284	365.0423 (+0.1)	306.0286, 333.0149 291.0060, 317.9919 321.0529, 286.0828 263.0098, 277.0258 286.0844, 271.0587

	Antibiotic SS 19508D; SS 19508D $C_{17}H_{13}O_7Cl$				
17	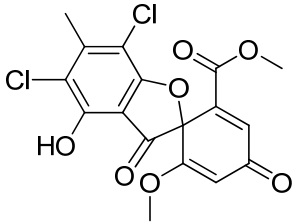 **Geodin** $C_{17}H_{12}O_7Cl_2$	5.15	220 284 352	399.0034 (+0.3)	339.9913, 324.9667 366.9775, 351.9529 296.9696, 310.9878 268.9758, 295.9627 355.0136, 320.0448
18	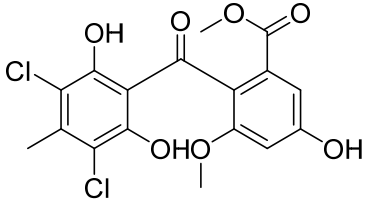 **Dihydrogeodin** $C_{17}H_{14}O_7Cl_2$	5.26	220 281 347	401.0190 (+0.2)	209.0444, 237.0391 277.0262, 341.9870 219.0286, 151.0389 326.9632, 368.9863 179.0337, 86.9995 305.0213, 297.9612
				**G324** ***Penicillium* sp.** **GenBank # KM215636** **Endophytic fungus isolated from surface sterilized leaves of *Silybum marianum***	
#	**Chemical Structure and Chemical formula**	**Rt (min)**	**UV (nm)**	**Positive Ionization Mode**	
				$[M+H]^+$	**MS/MS**

19	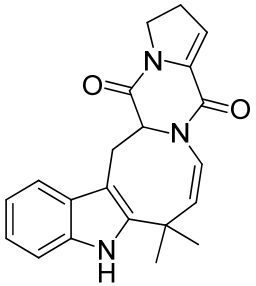 **10, 20-dehydro[12,13-dehydroprolyl-2-(1,1-dimethylallyl) tryptophyl] diketopiperazine]** $C_{21}H_{21}N_3O_2$	3.56	222 270	348.1708 (+0.4)	196.1120, 292.1077 182.0964, 264.1128 237.1020, 306.1232 331.1448, 280.1080 169.0759, 130.0652
20	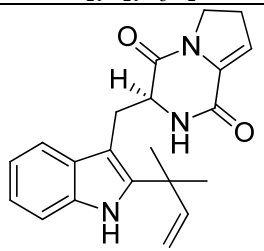 **12,13-Dehydroprolyl-2-(1,1-dimethyl-allyltryptophyl)diketopiperazine** $C_{21}H_{23}N_3O_2$	4.09	217 288 437	350.1864 (+0.3)	130.0651, 198.1276 153.0657, 69.0700 238.1338, 294.1234 282.1232, 144.0807 221.1075, 183.1042 170.0598, 151.0500

G142[34]
***Fusicolla* sp.**
GenBank # AB858346
Fungus isolated from submerged wood in fresh water

#	Chemical Structure and Chemical formula	Rt (min)	UV (nm)	Positive Ionization Mode	
				$[M+H]^+$	MS/MS

21	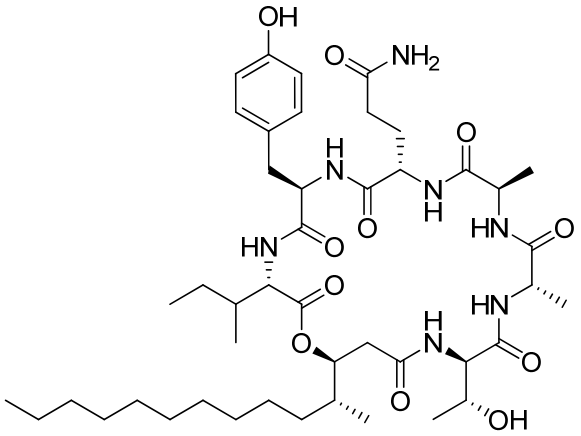 **Acuminatum B** $C_{45}H_{73}N_7O_{11}$	6.57	193 224 277	888.5443 (+0.2)	306.2430, 324.2522 377.2790, 101.0708 136.0760, 86.0964 395.2893, 349.2832 143.0818, 296.2573 448.3170, 466.3271 576.3774, 778.0210

	**G121** ***Cylindrocarpon* sp.** **GenBank # KM816764** **Endophytic fungus isolated from surface sterilized roots of *Yerba mansa***

#	Chemical Structure and Chemical formula	Rt (min)	UV (nm)	Positive Ionization Mode	
				$[M+H]^+$	MS/MS

22	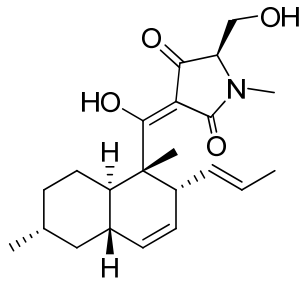 **Equisetin** $C_{22}H_{31}NO_4$	7.08	224 295	374.2328 (+0.6)	175.1475, 71.0700 119.0853, 188.0562 105.0701, 83.0855 133.1012, 147.1166 170.0806, 200.0913 302.1758, 356.2210
		**G168** ***Fusarium* sp.** **GenBank # KP897159** **Endophytic fungus isolated from surface sterilized stems of *Hedera helix***			
#	**Chemical Structure and Chemical formula**	**Rt (min)**	**UV (nm)**	**Positive Ionization Mode**	
				$[M+H]^+$	**MS/MS**
23	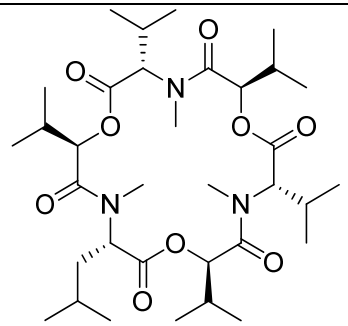 **Enniatin D (Analogue)** $C_{34}H_{59}N_3O_9$	7.87	210	654.4301 (-3.5)	196.1325, 214.1431 86.0962, 100.1117 186.1486, 314.1964 210.1487, 228.1586 328.2092, 414.2442

24	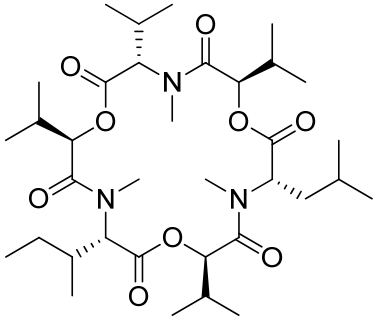 **Enniatin E (Analogue)** $C_{35}H_{61}N_3O_9$	8.24	210	668.4458 (-3.4)	210.1489, 100.1117 228.1586, 196.1325 86.0962, 328.2093 200.1639, 217.1433 186.1487, 314.1956 441.2947, 598.7202
25	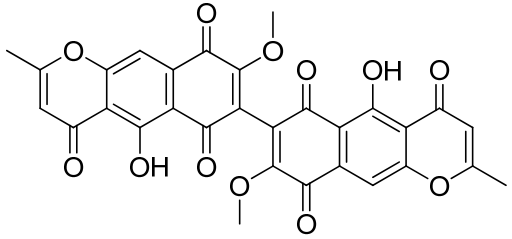 **Aurofusarin** $C_{30}H_{18}O_{12}$	5.05	223	571.0860 (-2.6)	485.0493, 556.0576 541.0351, 528.0696 496.0432, 456.0803 441.0589, 571.0832 513.0442, 511.0640 231.0291, 297.0352
				**MSX59553**[35] **Hypocreales sp.** **GenBank # JQ749725** **Fungus from MSX library**	
#	**Chemical Structure and Chemical formula**	**Rt (min)**	**UV (nm)**	**Positive Ionization Mode**	
				$[M+H]^+$	**MS/MS**

26	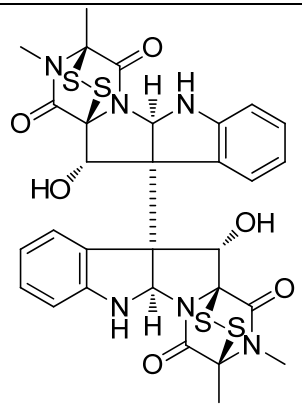 **Verticillin A** $C_{30}H_{28}N_6O_6S_4$	5.63	212 303	697.1026 (0.0)	169.0603, 383.1494 232.0990, 615.1462 284.1017, 551.2020 401.1592, 266.0911 465.1022, 348.0461
27	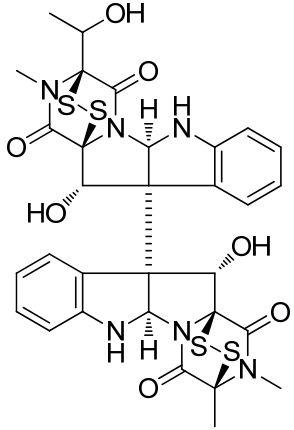 **Sch 52900** $C_{31}H_{30}N_6O_7S_4$	5.44	210 300	727.11334 (0.3)	169.0671, 199.0712 232.0991, 284.1025 268.1075, 296.1021 314.1130, 383.1498 413.1608, 266.0918

MSX70741[36]
Hypocreales sp.
GenBank # JN377382
Fungus from MSX library

#	Chemical Structure and Chemical formula	Rt (min)	UV (nm)	Positive Ionization Mode	
				$[M+H]^+$	MS/MS
28	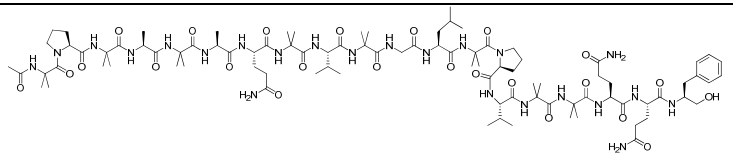 **Alamethicin F50** $C_{92}H_{151}N_{23}O_{24}$	6.38	217	1963.1342 8 (-1.6)	931.5340, 750.4118 849.4814, 466.2643 537.3010, 1189.6916 991.5539, 623.3485 381.2119, 744.4483

MSX57715[36]
Hypocreales sp.
GenBank # JN377381
Fungus from MSX library

#	Chemical Structure and Chemical formula	Rt (min)	UV (nm)	Positive Ionization Mode	
				$[M+H]^+$	MS/MS
29	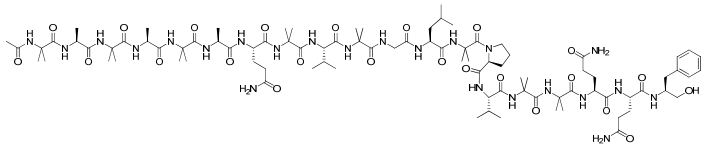	6.09	222	1937.1214 6 (-0.2)	908.5174, 724.3960 823.4647, 440.2488 511.2867, 774.4476 1163.6768, 335.1964 639.3439, 965.5388

	Trichokonin VI $C_{90}H_{149}N_{23}O_{24}$				1078.6225, 284.1588

G169
***Alternaria* sp.**
GenBank # KP897160
Endophytic fungus isolated from surface sterilized stems of *Hedera helix*

#	Chemical Structure and Chemical formula	Rt (min)	UV (nm)	Negative Ionization Mode	
				[M-H]$^-$	MS/MS
30	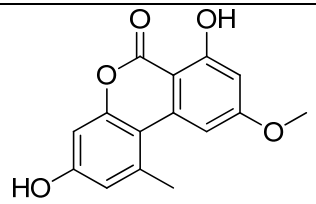 **Alternariol monomethyl ether** $C_{15}H_{12}O_5$	5.03	222 255 287 298 332 341	271.06070	256.0372, 250.9916 210.9987, 190.9926 231.0053, 204.9888 59.0135, 154.9923
31	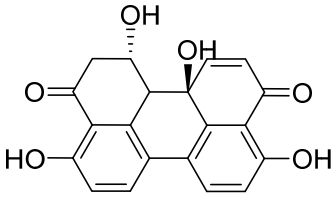 **Alterperylenol** $C_{20}H_{14}O_6$	3.89	216 257 285 356	349.0708 (+0.4)	303.0653, 261.0557 331.0616, 285.0551 313.0494, 275.0694 287.0371, 317.0466 301.0532, 338.3737

32	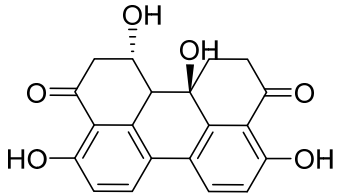 **Dihydroalterperylenol** $C_{20}H_{16}O_6$	3.81	218 258 283 356	351.0863 (0.0)	315.0647, 333.0765 305.0819, 263.0714 301.0494, 289.0500 285.0555, 298.0639 297.0555, 287.0700

Table S2. ^{1}H (400 MHz) and ^{13}C NMR (100 MHz) Data for Griseofulvin in $CDCl_3$.

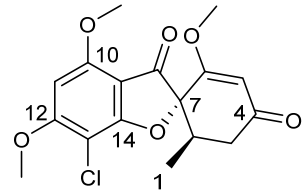

#	δ_H (mult., *J*)	δ_C
1	0.97 (d, 6.75)	14.3
2	2.85 (m, 4.72, 6.80, 13.66)	36.4
3	2.45 (dd, 4.64, 16.57) 3.04 (dd, 13.36, 16.57)	40.1
4		197.2
5	5.54 (s)	104.9
6		170.9
7		90.8
8		192.6
9		105.1
10		157.8
11	6.13 (s)	89.5
12		169.6
13		97.2
14		164.7
6-OMe	3.62 (s)	56.8
10-OMe	3.98 (s)	56.5
12-OMe	4.03 (s)	57.1

Table S3. The Lengths and Weights for the Three Groups of Stroma Used for the Spatial Distribution of Griseofulvin Along the Stroma. Each segment (i.e. Group 1A, Group 1B, etc.) was extracted and subjected to LC-MS. The area under the curve (AUC) for griseofulvin (*m/z* 353.0792 ± 5 ppm) was compared for each segment.

Group 1					
	Thin (mm)	Medium (mm)	Thick (mm)	Combined weight (mg)	AUC
A (top)	9.5	9.5	11.9	26.79	4.84×10^4
B (mid)	15.6	18.5	19.5	89.18	1.92×10^5
C (base)	15.1	18.1	20.0	99.21	1.04×10^8
Group 2					
	Thin (mm)	Medium (mm)	Thick (mm)	Combined weight (mg)	AUC
A (top)	9.2	10.3	11.0	6.55	7.77×10^4
B (mid)	15.0	17.8	18.0	42.25	6.49×10^5
C (base)	15.5	17.5	18.2	52.35	3.01×10^8
Group 3					
	Thin (mm)	Medium (mm)	Thick (mm)	Combined weight (mg)	AUC
A (top)	10.0	16.5	10.2	5.10	2.50×10^5
B (mid)	15.5	16.5	18.3	36.48	2.21×10^8
C (base)	16.0	10.7	19.0	57.70	6.53×10^7

Table S4. The Populated List Using Mass Defect Filtering for ±100 Da With a Mass Defect of ±25 mDa Around *m/z* 603.4807 for a Seed, Pulp, Twig, Ovary, Leaf, and Petal from an *Asimina triloba* Tree.

Retention Time (min)	$[M + Li]^+$					
	Seed	Pulp	Twig	Ovary	Leaf	Petal
1.02		663.5031		663.5035		
1.12				661.4886		
1.15				647.5056		
1.20		621.4915				
1.23	645.4911	645.4913	645.4930			645.4927
1.25		697.5055				
1.30				661.4882		661.4875
1.37		647.5084		619.4775		
1.53		619.4758				
1.56						669.4760
1.61				619.4770	619.4779	619.4775
1.63				659.4738		
1.70				639.4852		
1.71		603.4822		603.4823		603.4822
1.83		647.5071		661.4876		
1.96	645.4911				645.4932	
1.97		671.5073				671.5078
1.97				651.4984		651.5001
1.98				697.5064		
1.99		645.4913	645.4925	619.4774	619.4778	619.4775
2.02				687.5037		
2.08	645.4911	645.4913				
2.09		647.5008				
2.17		661.4863		661.4871		
2.19	647.5079	647.5071		647.5084		647.5084
2.22						603.4827
2.25				627.4820		
2.27		643.4758		643.4770		643.4774
2.36		603.4810				
2.38					645.4932	
2.63						619.4789
2.68				627.4820		
2.72	603.4811	603.4810		603.4822	603.4838	603.4827
2.73		655.4949				
2.87				653.4797		
2.89				627.4820		
2.96		631.5076		631.5119		
2.98				645.4932		
3.13						655.4960
3.14	603.4810	603.4810	603.4837	603.4822	603.4825	603.4824
3.15	655.4946			655.4958		
3.18		681.5083				
3.19		629.4965		629.4979		629.4981
3.34						629.4981
3.59				629.4979		629.4981
3.64	689.5172	689.5174		689.5189		
3.67		631.5122		631.5106		
3.70	603.4829			603.4823		603.4825
3.82		631.5126		631.5107		
3.95				603.4826		603.4819

4.08	**629.4961**	**629.4965**				
4.17	**631.5119**	**631.5121**		**631.5137**		
4.22				**643.4773**		
4.31	**629.4961**	**629.4965**		**629.4979**		**629.4981**
4.32				**681.5095**		
4.62				**587.4877**		
4.70	**629.4961**	**629.4965**				**629.4981**
4.78				**611.4872**		
4.94		**629.4965**				
5.04				**611.4866**		
5.06				**587.4874**		**587.4880**
5.14		**645.4917**				
5.38	**677.4804**					
5.47		**587.4858**				
6.14	**689.5173**					
6.20	**645.4901**					
6.23	**629.5170**					
6.29				**569.4768**		
6.52		**613.5013**		**613.5026**		**613.5027**
6.54				**629.4770**		
6.64	**613.5018**					
7.31	**657.5126**					
7.57				**595.4928**		**595.4942**
7.68	**653.4917**					

APPENDIX B

SUPPLEMENTARY FIGURES

Figure S1. ^{1}H and ^{13}C NMR Spectra of Compound **1**

Figure S2. ^{1}H and ^{13}C NMR Spectra of Compound **2**

Figure S3. Growth Patterns After 3 Weeks of Fungi on Balsa Wood

Figure S4. An Insert Was Inoculated in Liquid Media, and then Placed on Agar in a Petri Dish.

Figure S5. (A) G100 (Left) on Agar Grown Against G3 (Right) on Agar.

Figure S6. (A) The Cardboard Inserts Used Were the Reinforcing Cardboard Bottom Inserts for the Pendaflex® Box-Bottom Hanging File Folders at Staples (item # 521401)

Figure S7. (**A**) The Guttate (Red Circle) and Mycelium (Blue Circle) of Fungal Code G100, *Clohesyomyces aquaticus*, Were Sampled Using the Droplet-LMJ-SSP

Figure S8. Comparison of the MS/MS Fragmentation for (**A**) Compound **7** with (**B**) Its Standard and (**C**) Compound **8** with its (**D**) Standard

Figure S9. The Extracted Ion Chromatogram (XIC) of *m/z* (**A**) 381.1099 ± 5 ppm and (**B**) 399.1204 ± 5 ppm

Figure S10. (**A**) Contaminated Fungal Culture Coded MSX19583 with the "Green" Fungus Indicated by the Green Circles and the "Purple" Fungus Indicated by the Purple Circles

Figure S11. Structure of a Diketopiperazine Dimer (**11**) Detected on the Green Fungal Culture Coded MSX19583

Figure S12. Structure of Cyclo-(L-phenylalaninyl-L-tryptophanyl) (**12**) Detected on the Green Fungal Culture Coded MSX19583

Figure S13. (**A**) Image of Pure Culture MSX15983 with Yellow Crosshairs Indicating Sampled Areas

Figure S14. 3D Model Created Using SketchUp Make of the Custom Tray Designed to Hold a Petri Dish and a Solvent Vial

Figure S15. ^{1}H (400 MHz; Top) and ^{13}C NMR (100 MHz; Middle) NMR Data (Both Acquired in $CDCl_3$) and the HRMS Data for Griseofulvin

Figure S16. The Three Groups of Stroma (1, 2, 3) and the Length of Their Respective Segments (A, B, C) in mm

Figure S17. Phylogram of the Most Likely Tree (-lnL = 29759.75) from a RAxML Analysis of 95 Sequences Based on Partial RPB2 Data (1236 bp)

Figure S18. Phylogram of the Most Likely Tree (-lnL = 1351.36) from a RAxML Analysis of 35 Sequences Based on ITS Data (568 bp)

Figure S19. The Base Peak Chromatograms for the Stromata of *X. cubensis* (G536) Displayed a Significant Increase in Detection of Griseofulvin (Boxed in Red) in the Base

Figure S20. Secondary Metabolites (**34**-**38**) of *P. restrictum* After 2.5 Weeks on the (**A**) Mycelium and (**B**) Agar

Figure S21. Secondary Metabolites (**34**-**38**) of *P. restrictum* After 5.5 Weeks on the (**A**) Mycelium and (**B**) Agar.

Figure S22. Detection of Griseofulvin (**33**) on the Surface of a Guttate, Mycelium, and Stromata (Base and Tip) for *X. cubensis*.

Figure S23. Phylogram of the Most Likely Tree (-lnL = 1766.4) from a PHYML Analysis of 18 Sequences Based on Complete ITS rDNA (467 bp)

Figure S24. Phylogram of the Most Likely Tree (-lnL = 1461.94) from a PHYML Analysis of 21 Sequences Based on a Portion of the D1/D2 Divergent Domains of the 28SrDNA (396 bp)

Figure S25. General Procedure for the Extraction, Fractionation, and Initial Chromatography Utilized for the Isolation of Mevalocidin and/or Methylidene Mevalonolactone

Figure S26. ^{1}H NMR Spectrum of Mevalocidin

Figure S27. The Base Peak Chromatograms (Top) of Both Mevalocidin (**39**) and Methylidene Mevalonolactone (**40**) for Their Accurate (±5 ppm) Molecular Ion Peaks of 161.0808 and 143.0703, Respectively

Figure S28. (A) The Extracted Ion Chromatogram (XIC) of *m/z* 161.0808 (±5 ppm) for the Mevalocidin (**39**) Standard

Figure S29. The Structure, the ^{1}H NMR (400 MHz, $CDCl_3$), ^{13}C NMR (100 MHz, $CDCl_3$), HRMS and MS/MS Spectra for Annonacin

Figure S30. The Generated Plots of Mass Defects for *m/z* 603.4807±100 Da with a Mass Defect of ±25 mDa

Figure S31. The Leaves and Flowers as They Were Prepared for Cryotome Cross-Sectioning

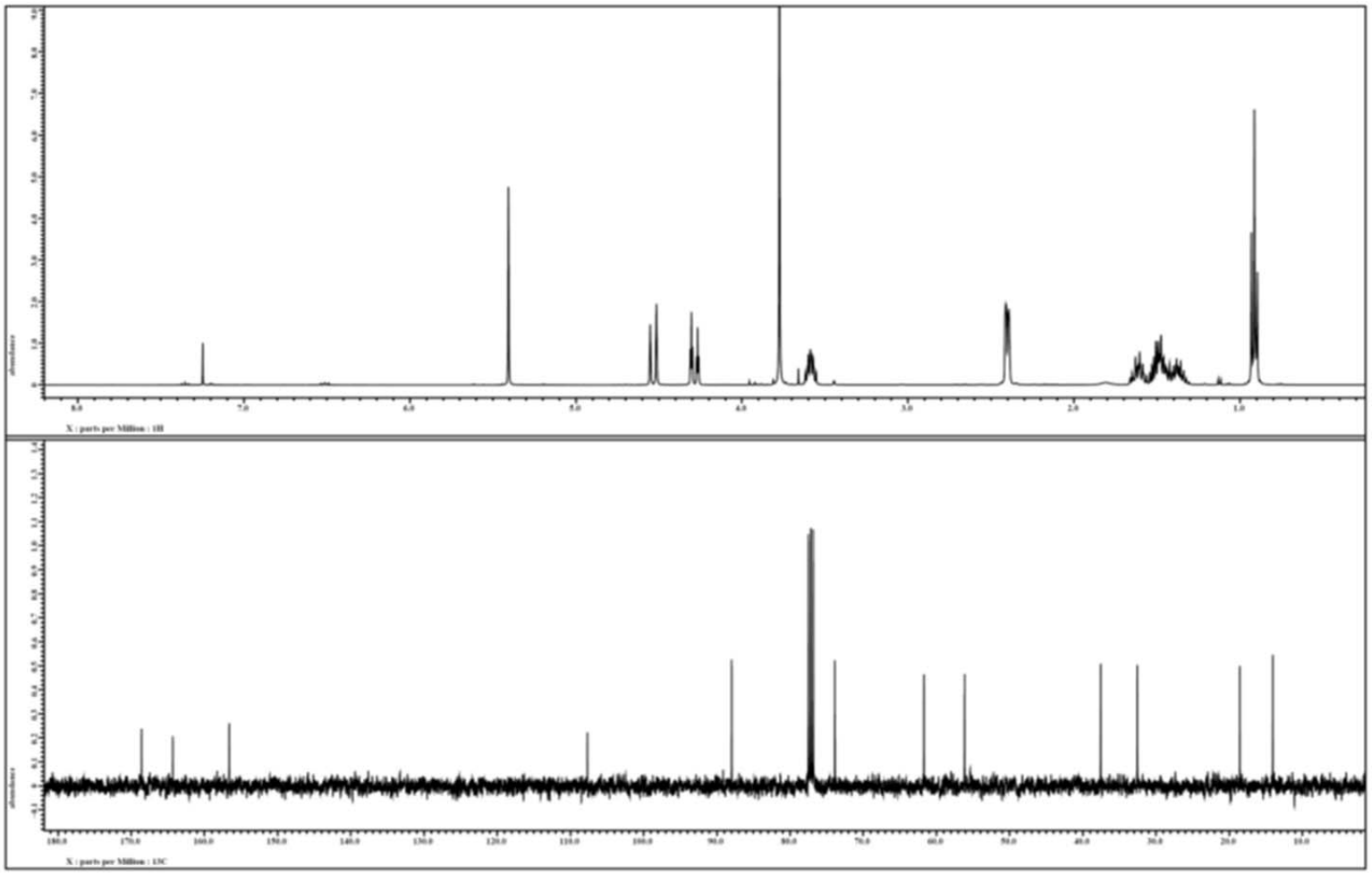

Figure S1. ^{1}H and ^{13}C NMR Spectra of Compound 1 [400 MHz for ^{1}H and 100 MHz for ^{13}C, $CDCl_3$].

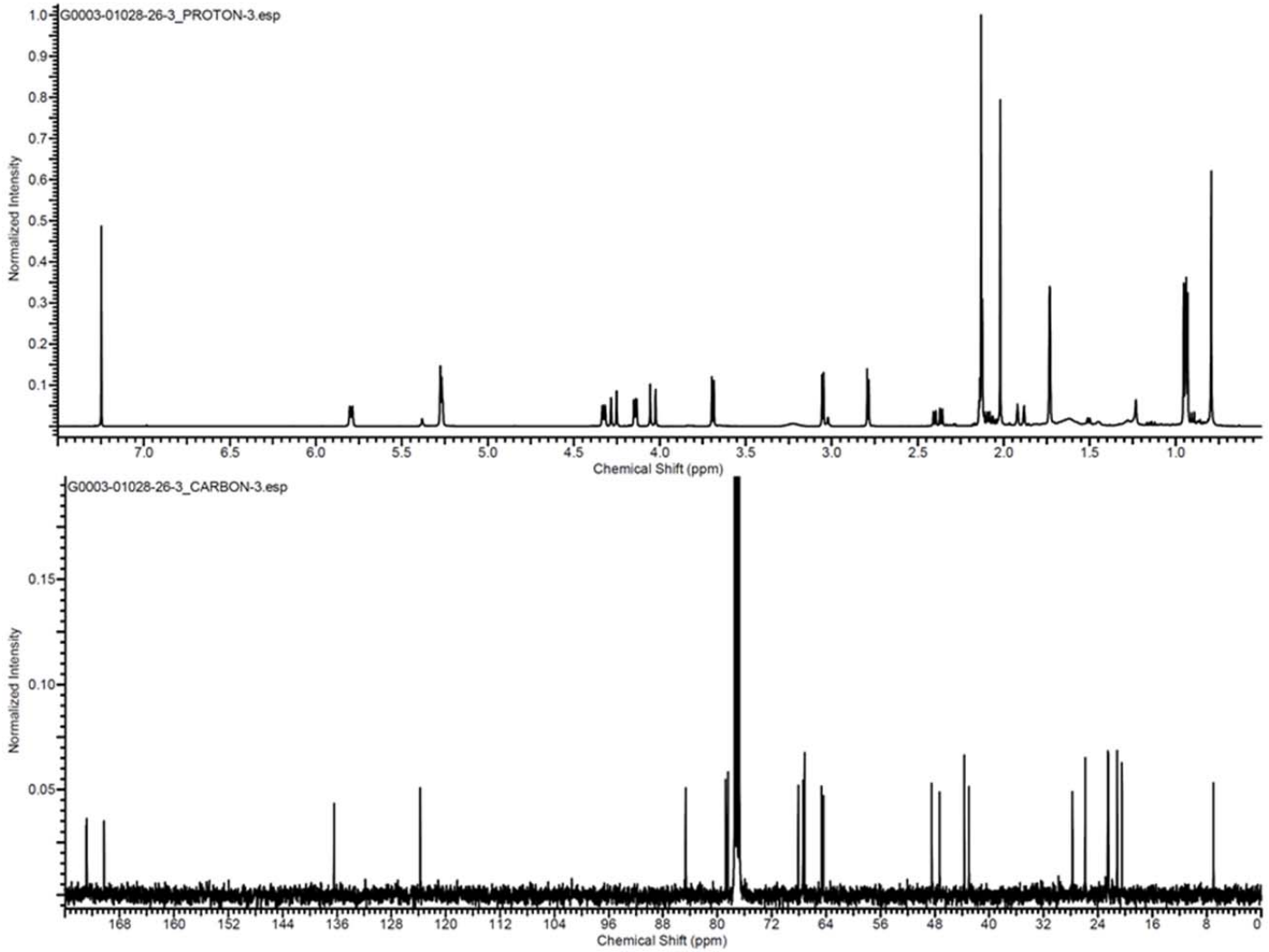

Figure S2. ^{1}H and ^{13}C NMR Spectra of Compound 2 [400 MHz for ^{1}H and 100 MHz for ^{13}C, $CDCl_3$].

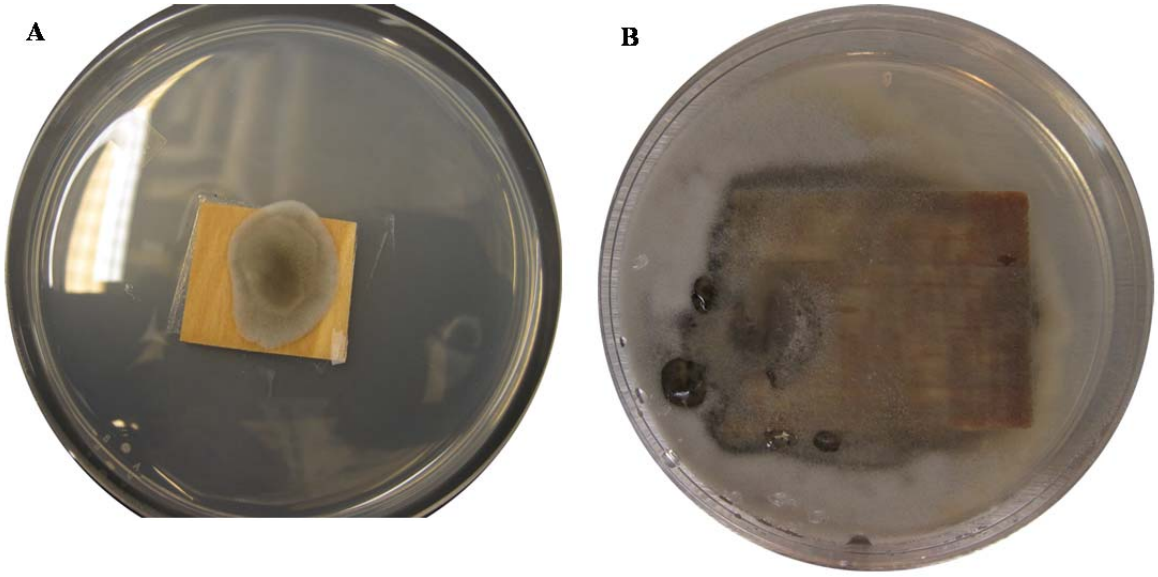

Figure S3. Examples of the Inconsistent Growth Patterns of G100 on Balsa Wood. (A) A Raised, Bulbous Fungal Growth and (B) a Thin, Transparent Fungal Growth.

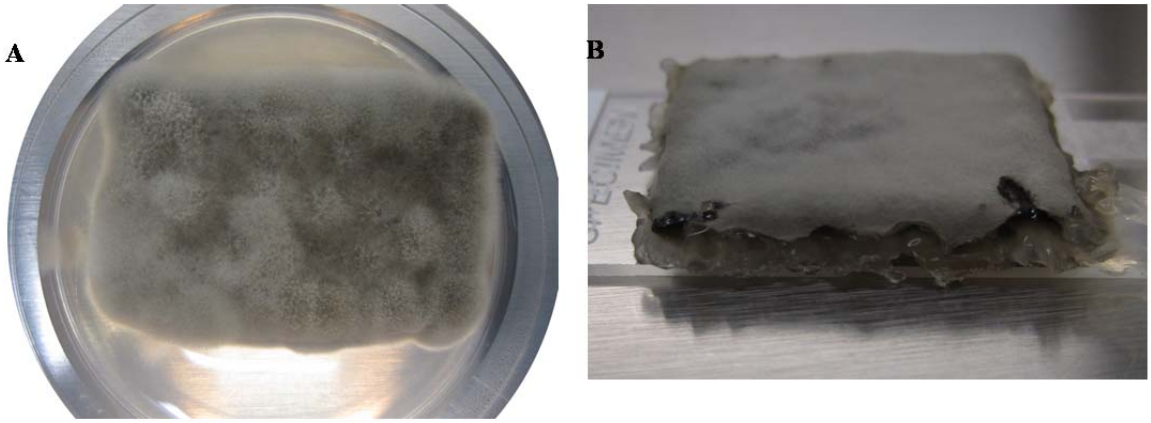

Figure S4. An Insert Was Inoculated in Liquid Media, and then Placed on Agar in a Petri Dish. After 3 weeks (A), the insert was removed from the Petri dish and placed on a microscope slide (B) in preparation for DESI-MS anaylsis.

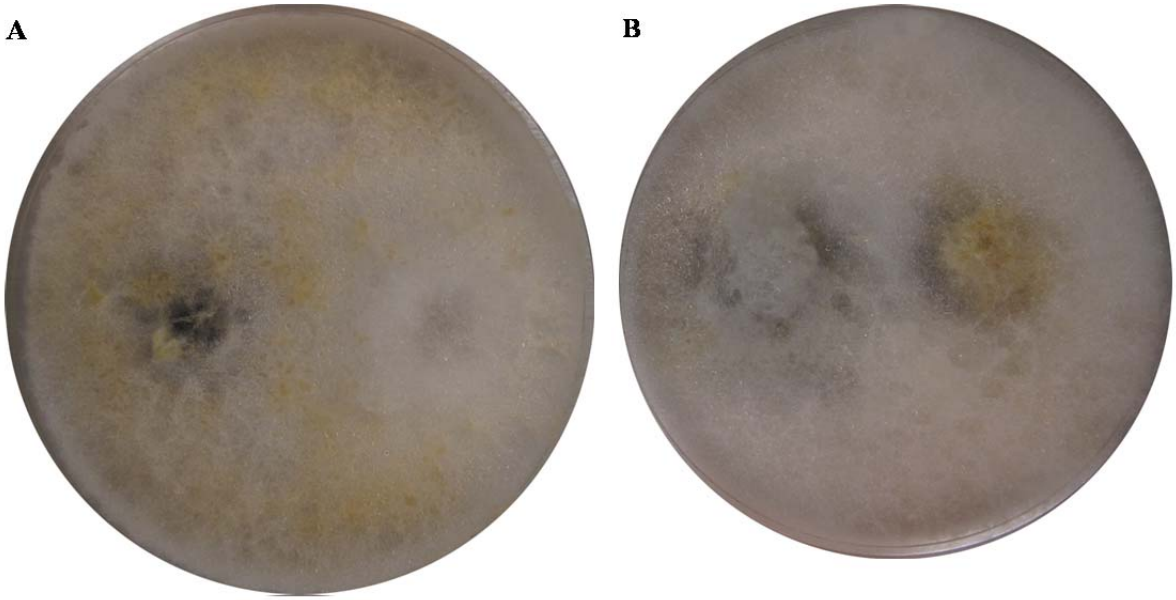

Figure S5. (A) G100 (Left) on Agar Grown Against G3 (Right) on Agar. (B) G100 (left) on cardboard against G3 (right) on agar. In both cases, when the two cultures were inoculated simultaneously, G3 (white/yellow mycelium) rapidly overgrew the plates.

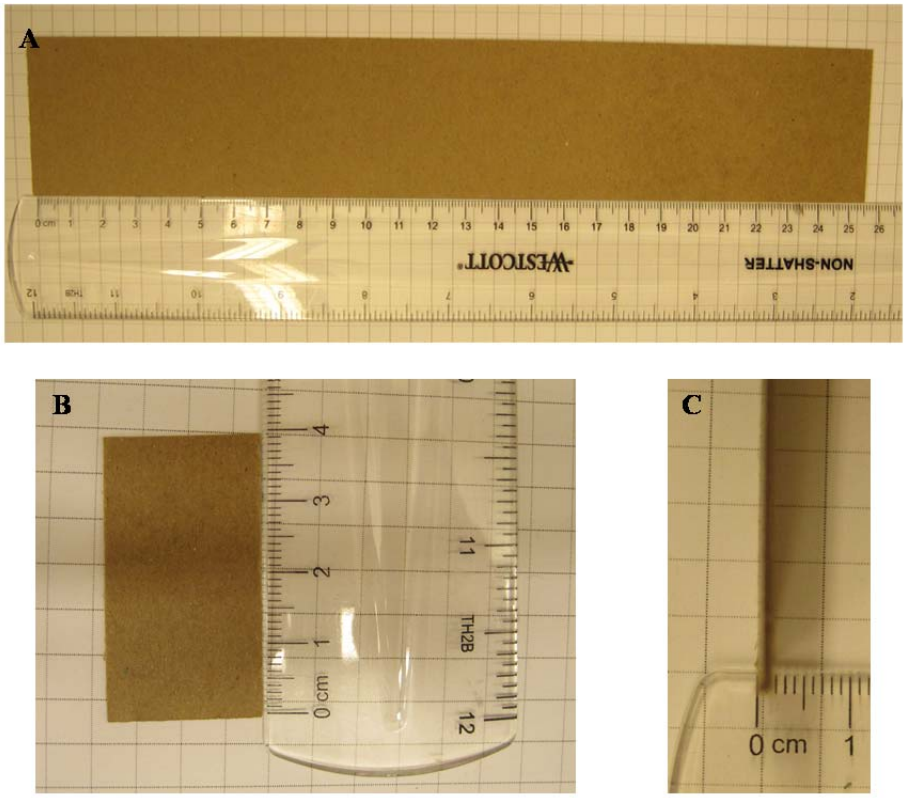

Figure S6. (A) The Cardboard Inserts Used Were the Reinforcing Cardboard Bottom Inserts for the Pendaflex® Box-Bottom Hanging File Folders at Staples (item # 521401). These strips were (B) cut to 40 mm × 20 mm pieces. The cardboard was 1 mm thick and non-corrugated.

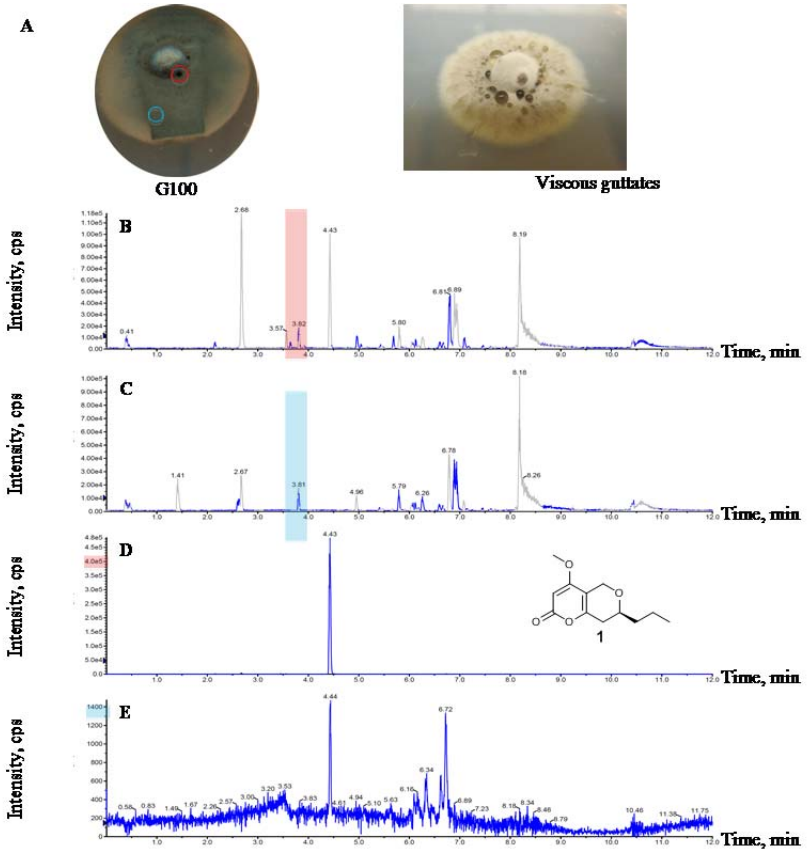

Figure S7. (A) The Guttate (Red Circle) and Mycelium (Blue Circle) of Fungal Code G100, *Clohesyomyces aquaticus*, Were Sampled Using the Droplet-LMJ-SSP. A clearer picture of the guttates from a different culture of G100 is shown on the right. (**B**) The base peak chromatogram displayed phomopsinone A in the guttate (red). (**C**) The same peak was not apparent in the mycelium (blue). The XIC for phomopsinone A (m/z 225.11 at 4.43 min) was over two orders of magnitude higher in counts per second (cps) for (**D**) the guttate ($4.8x10^5$ cps) over (**E**) the mycelium ($1.4x10^3$ cps).

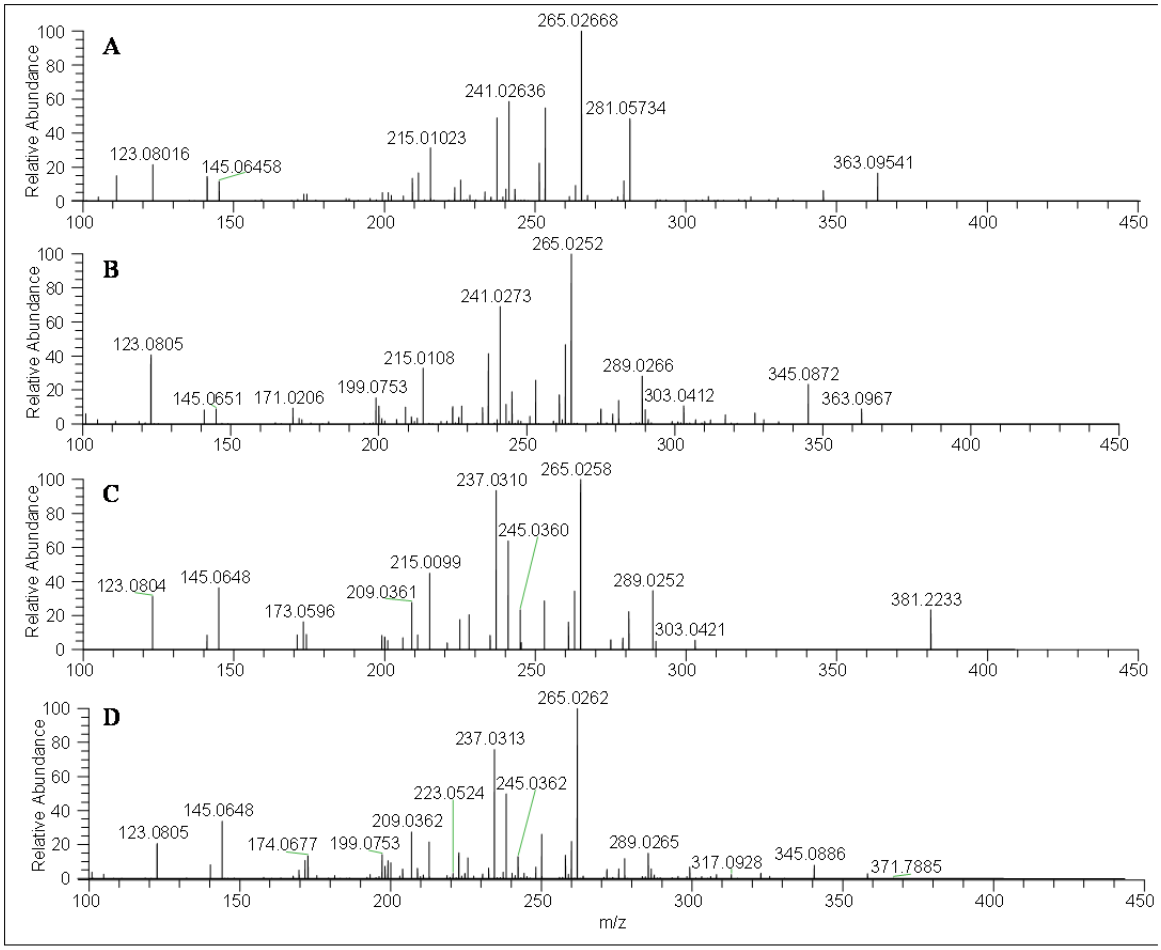

Figure S8. Comparison of the MS/MS Fragmentation for (A) Compound 7 with (B) Its Standard and (C) Compound 8 with its (D) Standard.

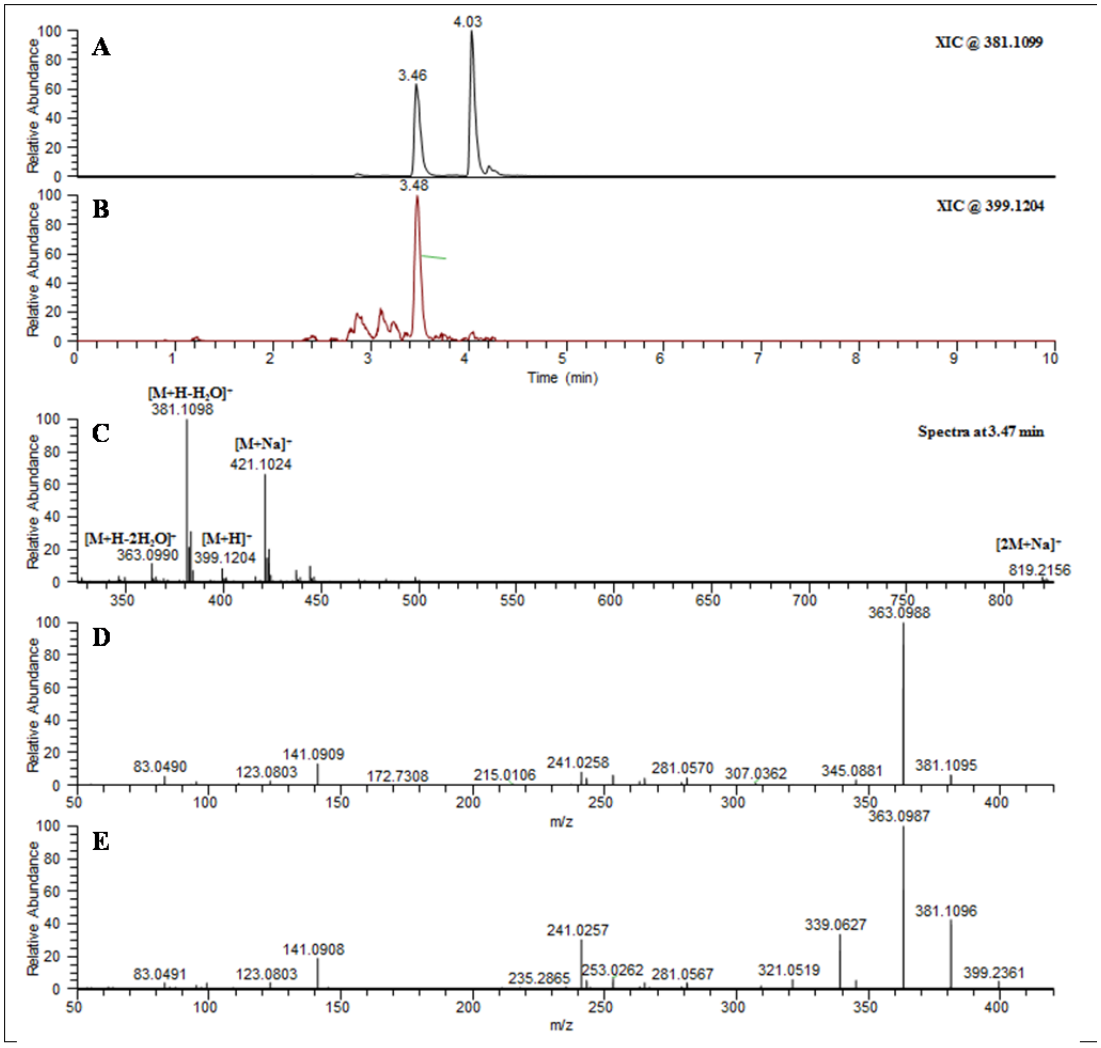

Figure S9. The Extracted Ion Chromatogram (XIC) of *m/z* (A) 381.1099 ± 5 ppm and (B) 399.1204 ± 5 ppm. (**C**) At 3.47 min, the accuracy for $[M + H]^+$ between the observed and calculated was 0.3 ppm (399.1204 observed vs. 399.1205 calculated for $[C_{19}H_{24}O_7Cl + H]^+$ with multiple indicators suggesting for the parent ion. The HCD fragmentation (NCE =23) of molecular ions with *m/z* (**D**) 381.11 and (**E**) 399.12 detected at 3.47 min. (**F**) The proposed structure based off of the presumed biosynthetic route, where the hydroxy group was placed at position 8 due to similar oxygenation patterns observed with related analogues.

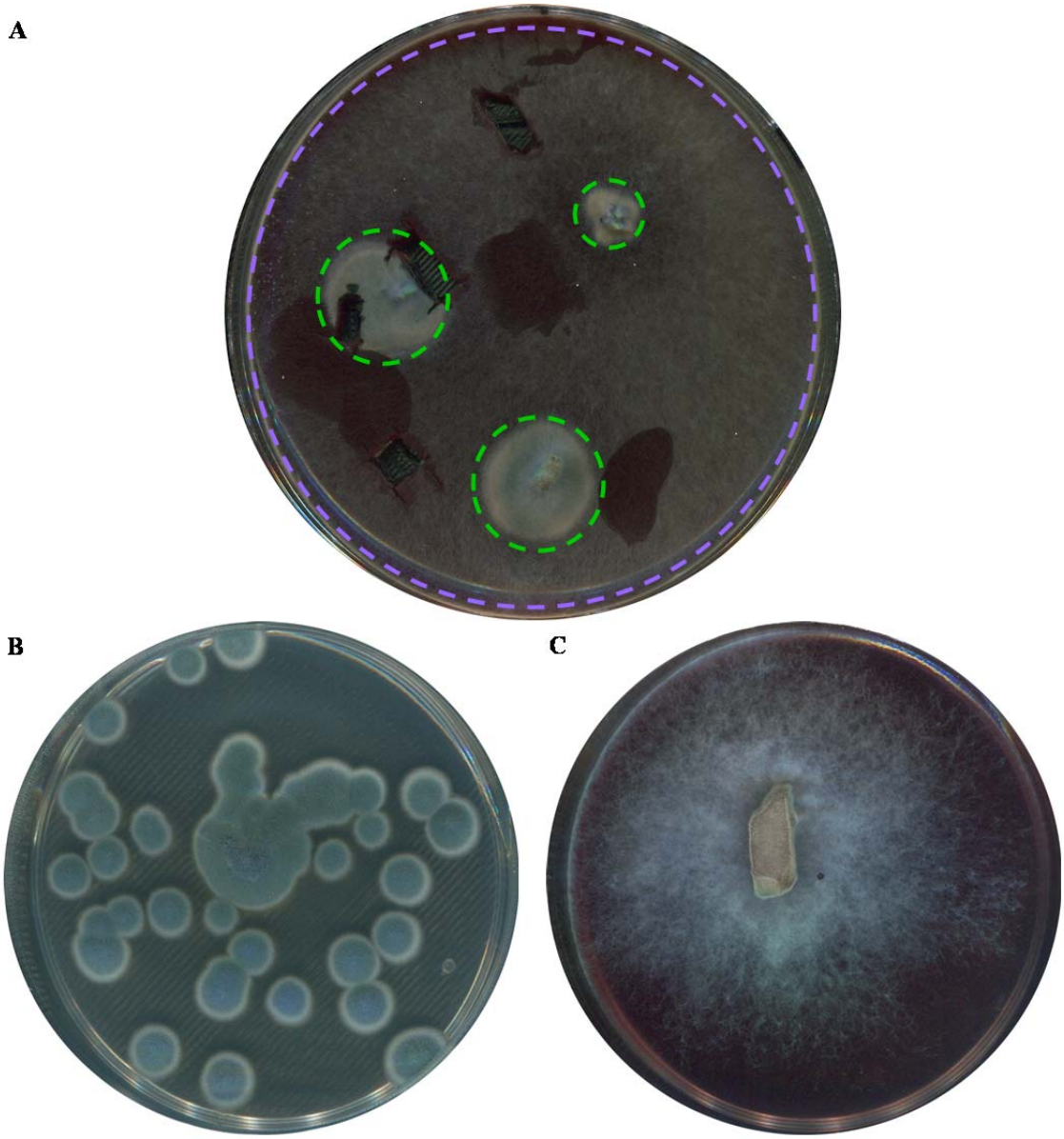

Figure S10. (A) Contaminated Fungal Culture Coded MSX19583 with the "Green" Fungus Indicated by the Green Circles and the "Purple" Fungus Indicated by the Purple Circle. (**B**) Isolated fungal cultures of MSX19583 (green), *Aspergillus sydowii*, (**B**) and the contaminant (purple), *Chaetomium* sp. (**C**).

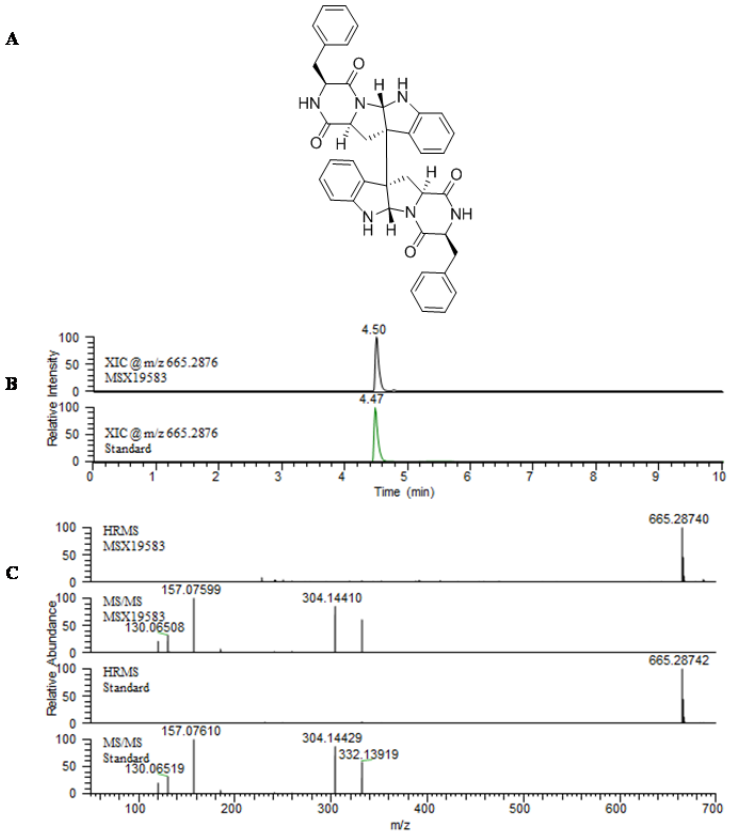

Figure S11. (A) Structure of a Diketopiperazine Dimer (11) Detected on the Green Fungal Culture Coded MSX19583. (**B**) A comparison of the extracted ion chromatograms (XIC) from the fungal culture (top) and the standard (bottom) for the accurate mass of compound **11.** (**C**) A comparison of the HRMS and the MS/MS for the fungal culture and the standard for compound **11**.

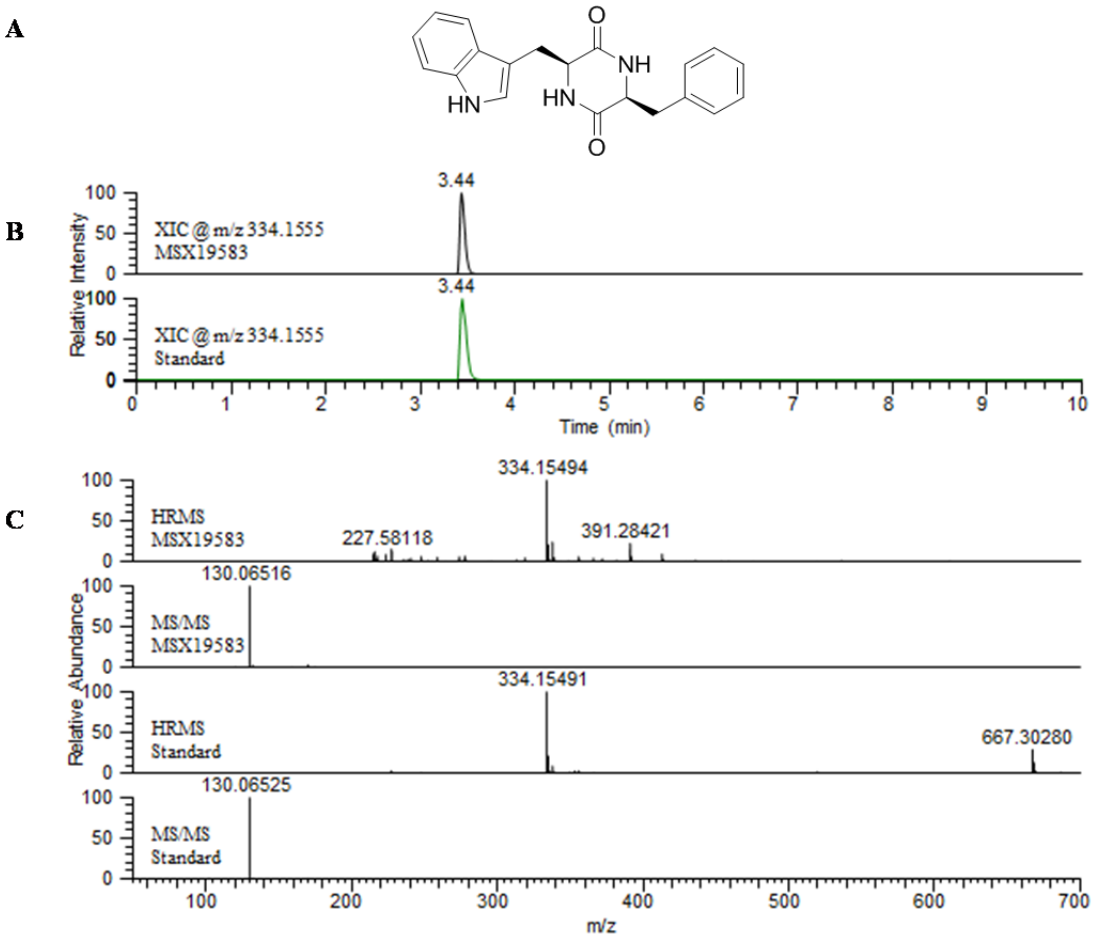

Figure S12. (A) Structure of Cyclo-(L-phenylalaninyl-L-tryptophanyl) (12) Detected on the Green Fungal Culture Coded MSX19583. (**B**) A comparison of the extracted ion chromatograms (XIC) from the fungal culture (top) and the standard (bottom) for the accurate mass of compound **12.** (**C**) A comparison of the HRMS and the MS/MS for the fungal culture and the standard for compound **12**.

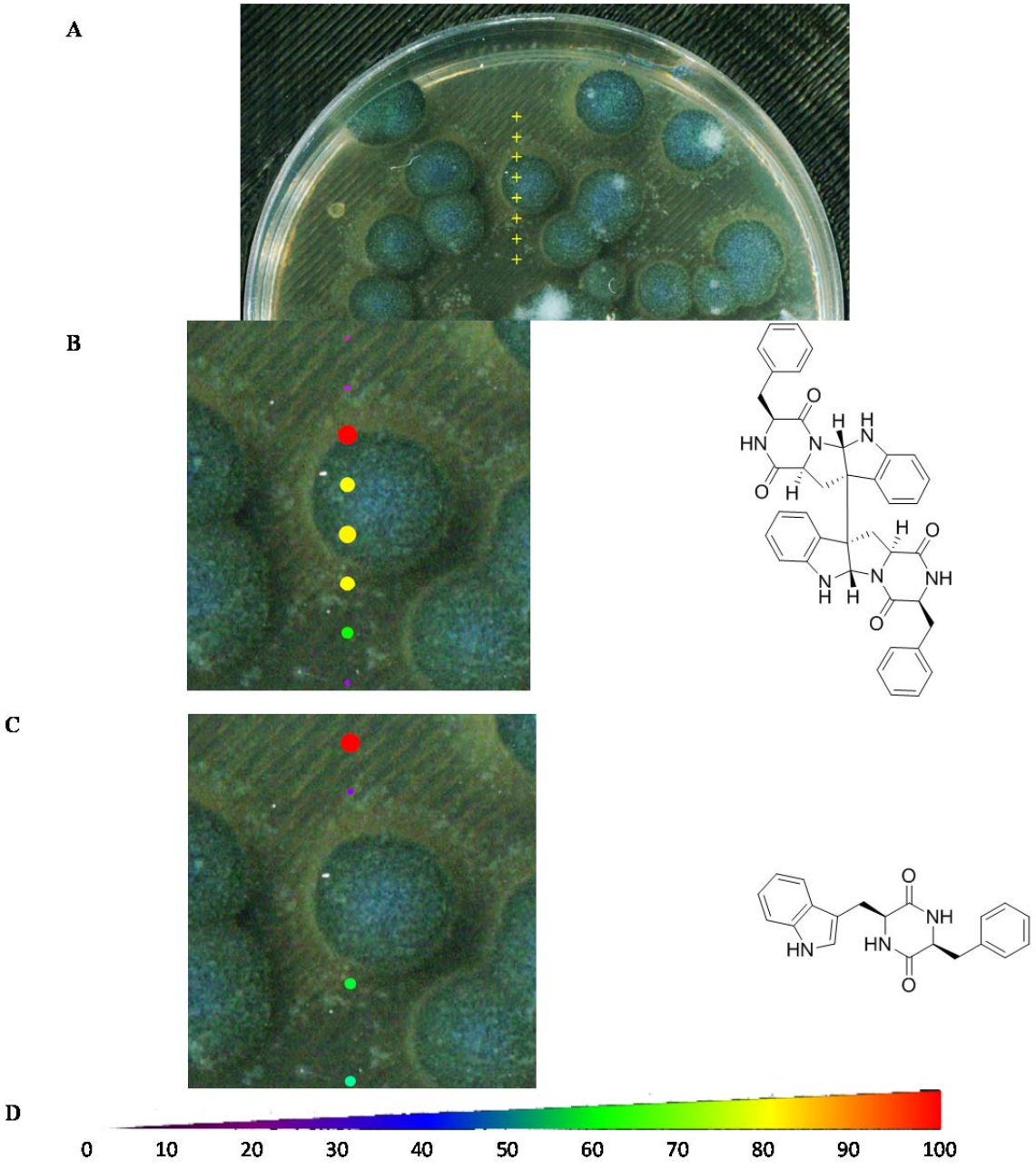

Figure S13. (A) Image of Pure Culture MSX15983 with Yellow Crosshairs Indicating Sampled Areas. (**B**) Heat map of compound **11** as sampling from the contaminant to the culture. (**C**) Heat map of compound **12** as sampling from the contaminant to the culture. (**D**) The color scale and diameter of spot indicate the relative amount of signal detected for the given analytes.

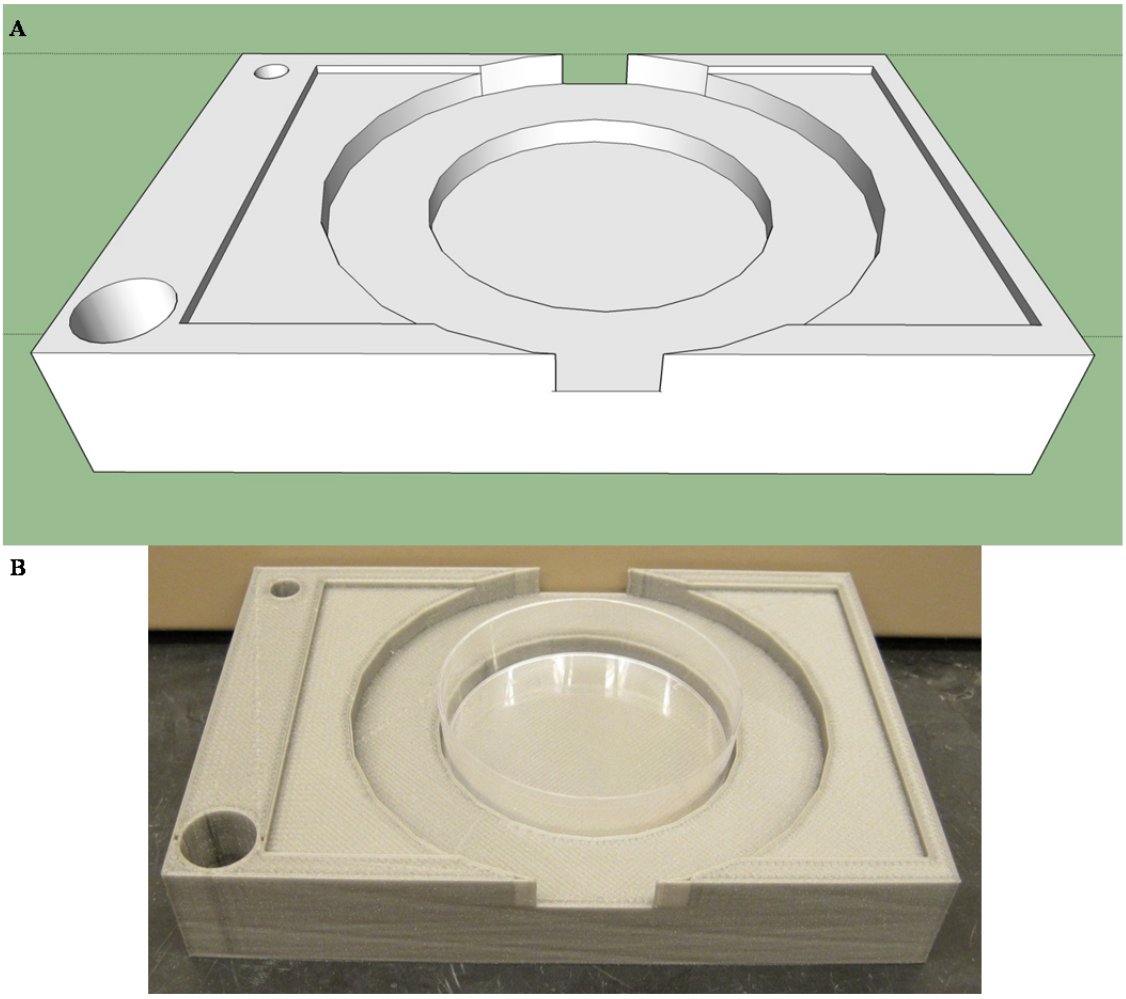

Figure S14. 3D Model Created Using SketchUp Make of the Custom Tray Designed to Hold a Petri Dish and a Solvent Vial (A). Photograph of the printed tray using the F306 3D printer (B).

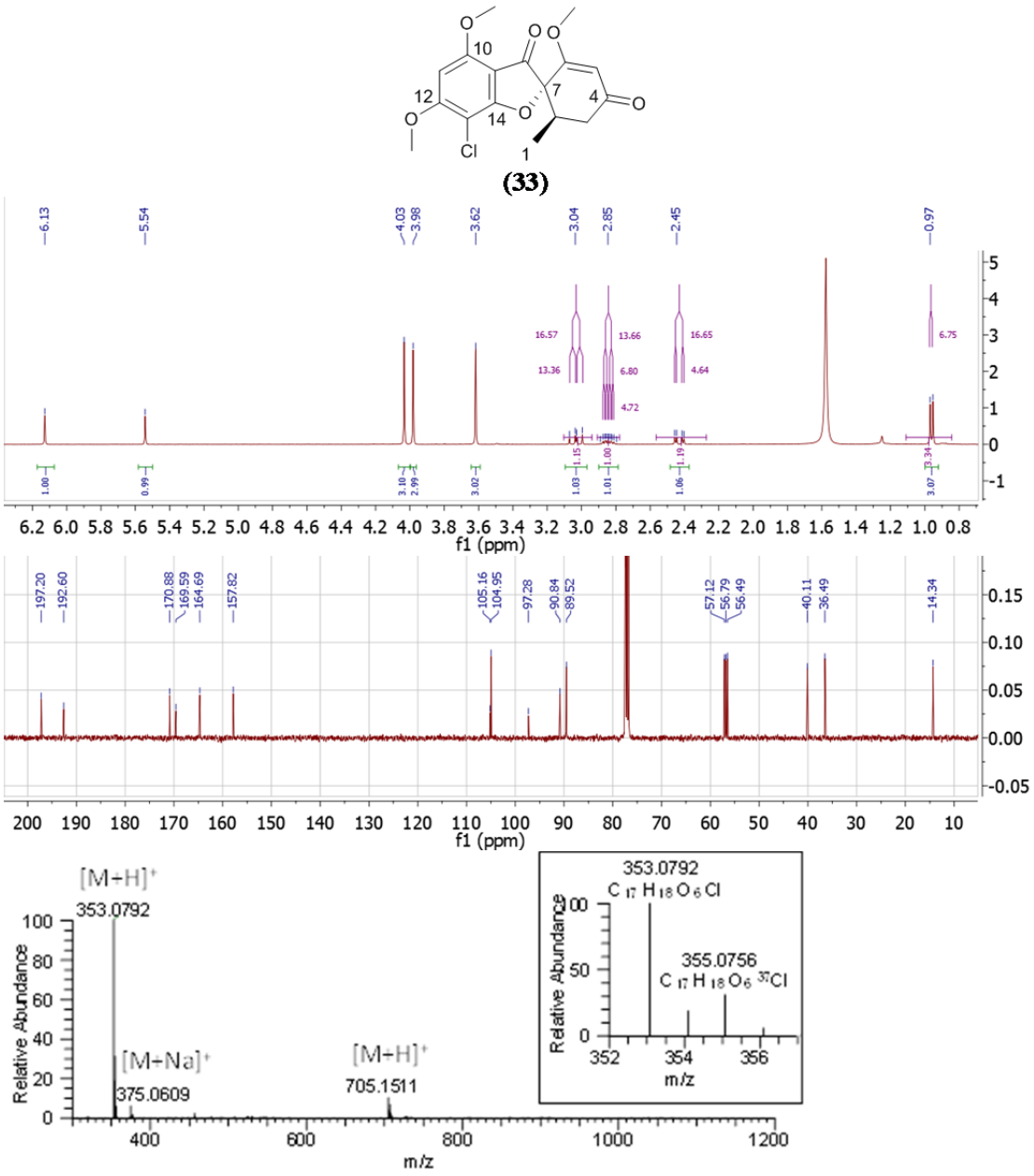

Figure S15. ^{1}H (400 MHz; Top) and ^{13}C NMR (100 MHz; Middle) NMR Data (Both Acquired in $CDCl_3$) and the HRMS Data for Griseofulvin. The HRMS data was 0.0 ppm for $C_{17}H_{18}O_6Cl$ ($[M+H]^+$ from calculated (*m/z* 353.0792).

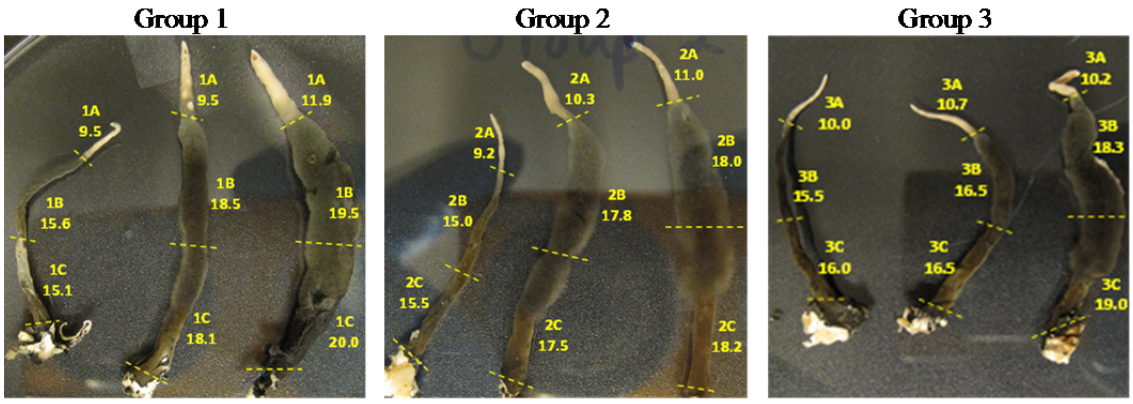

Figure S16. The Three Groups of Stroma (1, 2, 3) and the Length of Their Respective Segments (A, B, C) in mm.

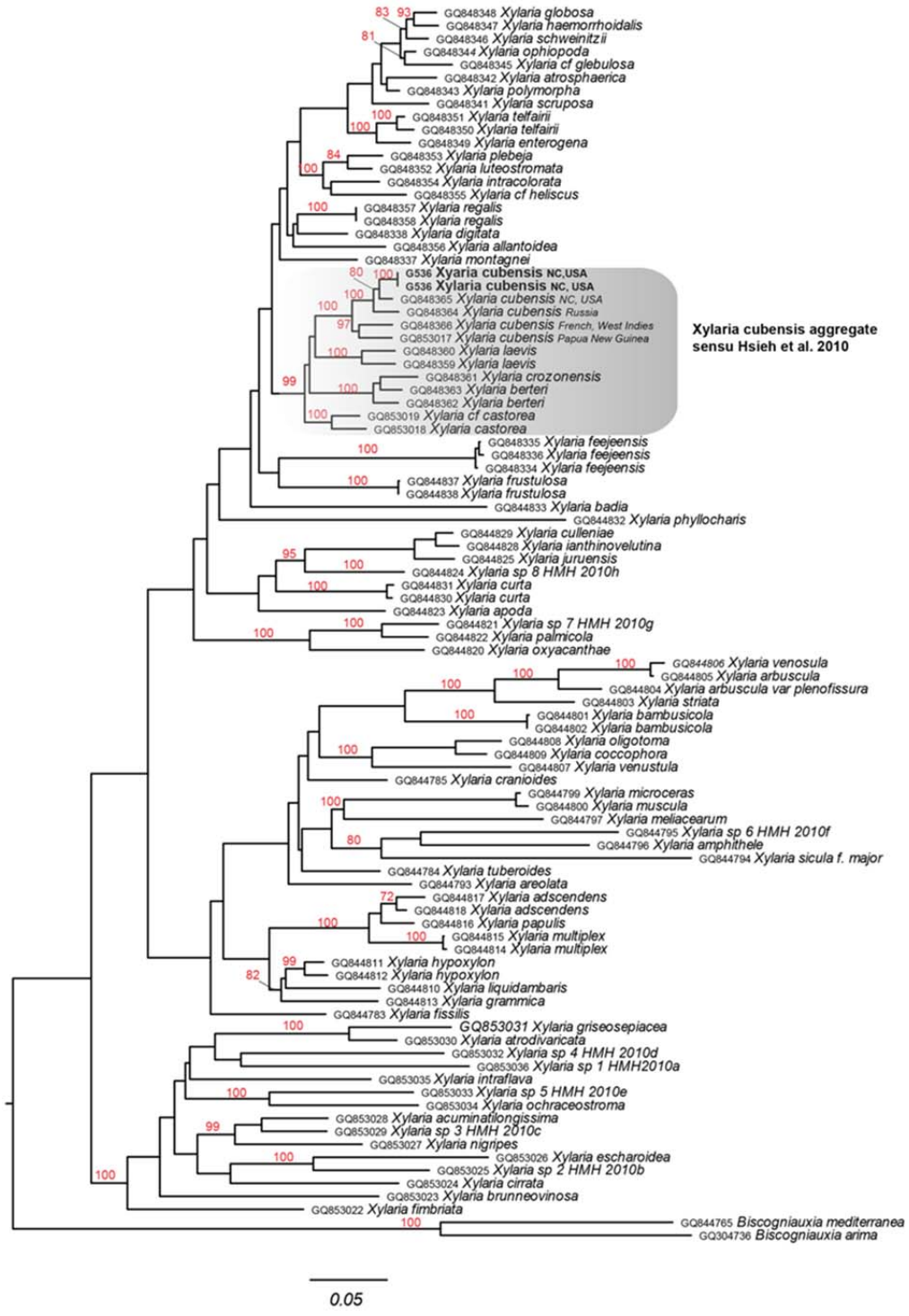

Figure S17. Phylogram of the Most Likely Tree (-lnL = 29759.75) from a RAxML Analysis of 95 Sequences Based on Partial RPB2 Data (1236 bp). Numbers refer to RAxML bootstrap support values ≥ 70% based on 1000 replicates. Bar indicates nucleotide substitutions per site. Strain G536 is identified as *Xylaria cubensis*, (bold, and highlighted in gray).

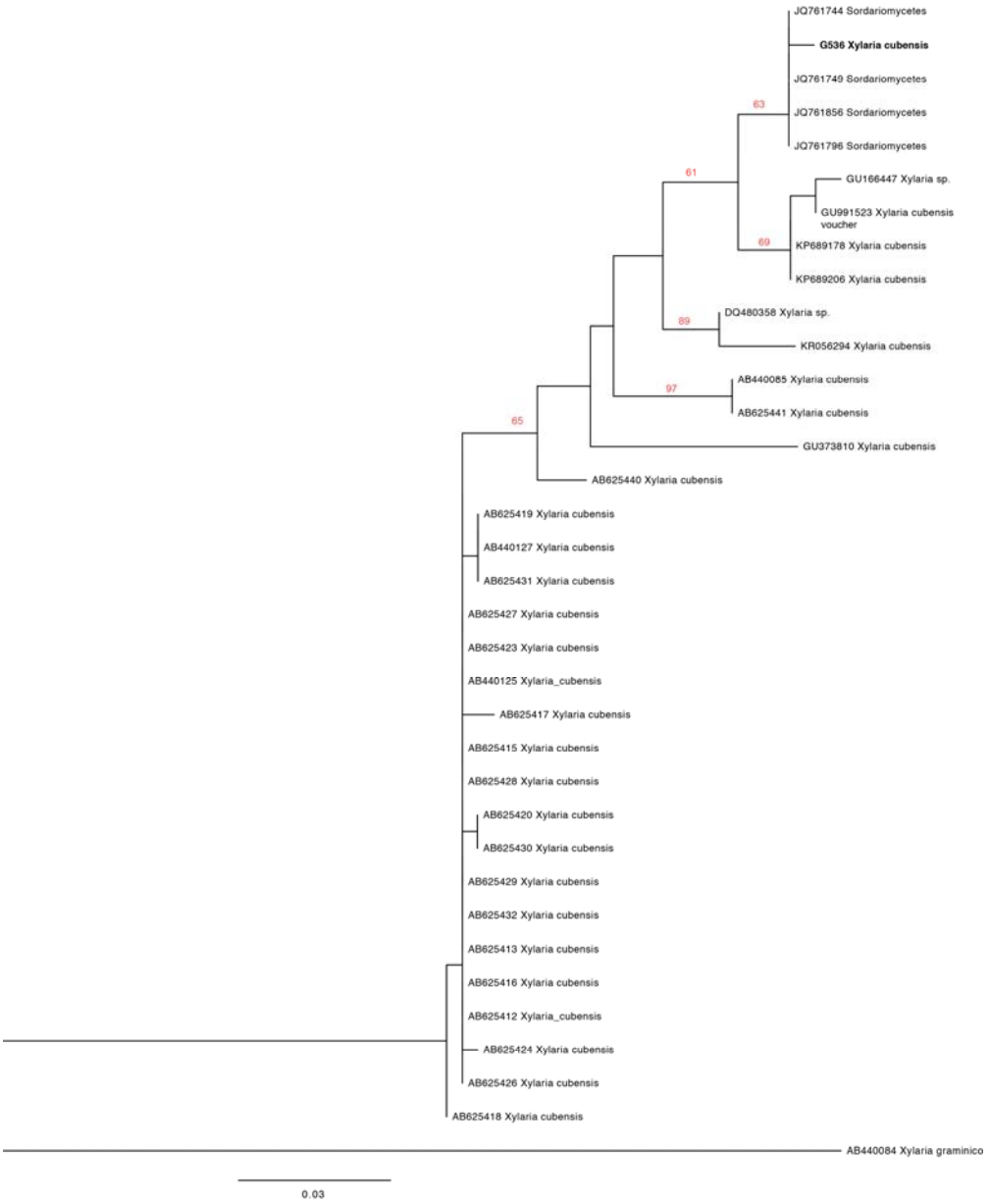

Figure S18. Phylogram of the Most Likely Tree (-lnL = 1351.36) from a RAxML Analysis of 35 Sequences Based on ITS Data (568 bp). Numbers refer to RAxML bootstrap support values ≥ 50% based on 1000 replicates. Bar indicates nucleotide substitutions per site. Strain G536 is identified as *Xylaria cubensis* (bold) as it is nested with an authenticate voucher collection (JDR 860, GU991523).

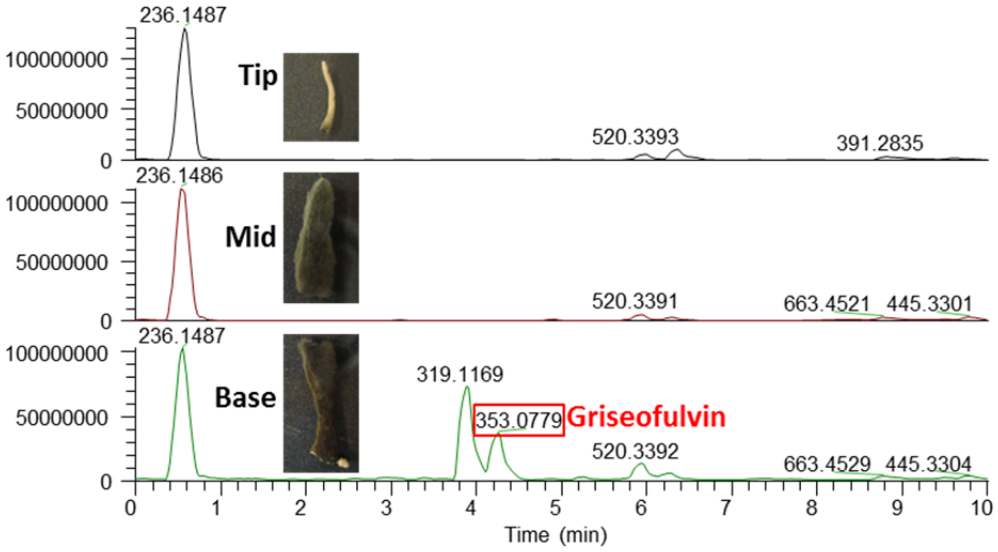

Figure S19. The Base Peak Chromatograms for the Stromata of *X. cubensis* (G536) Displayed a Significant Increase in Detection of Griseofulvin (Boxed in Red) in the Base.

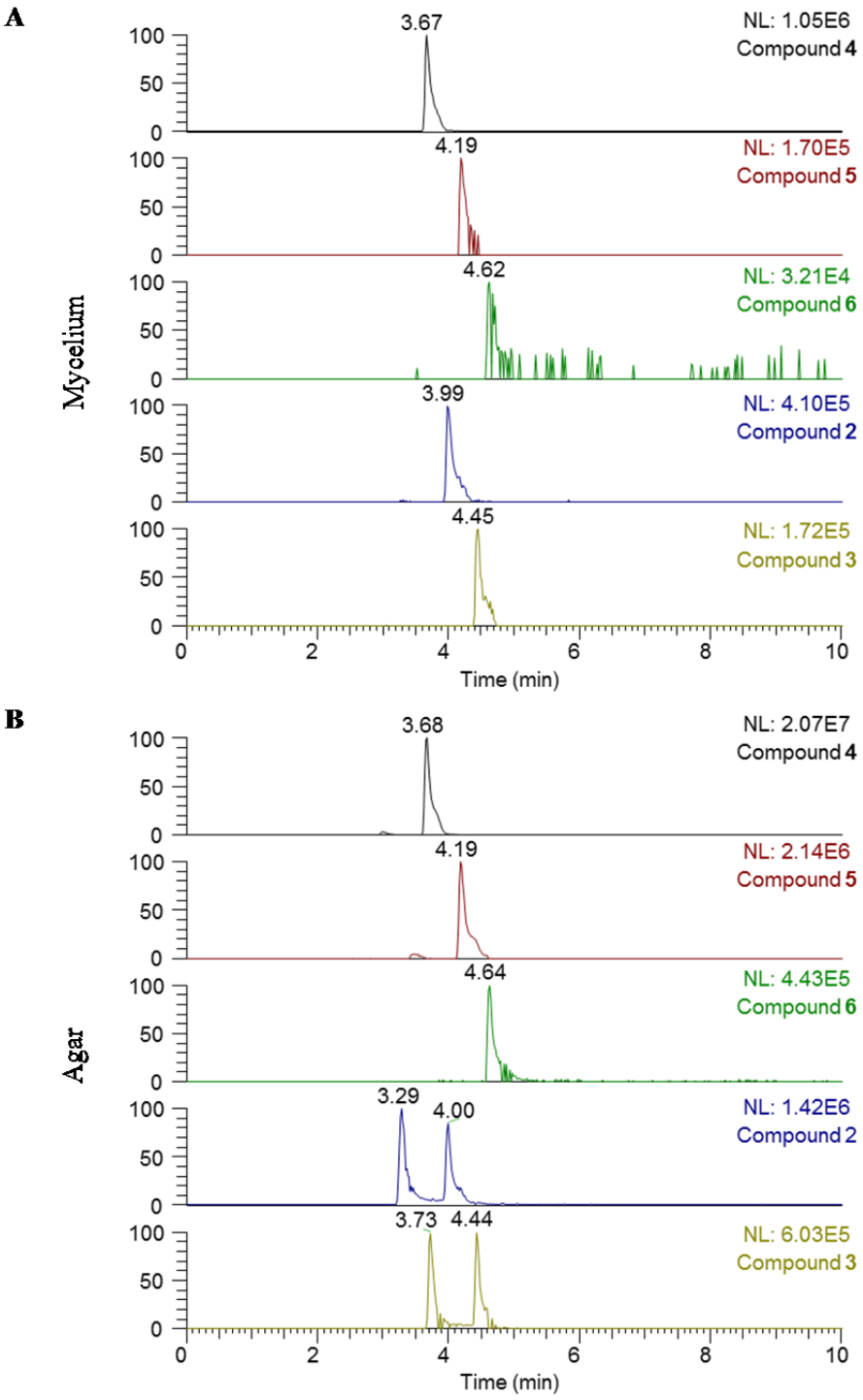

Figure S20. Secondary Metabolites (2-6) of *P. restrictum* After 2.5 Weeks on the (A) Mycelium and (B) Agar.

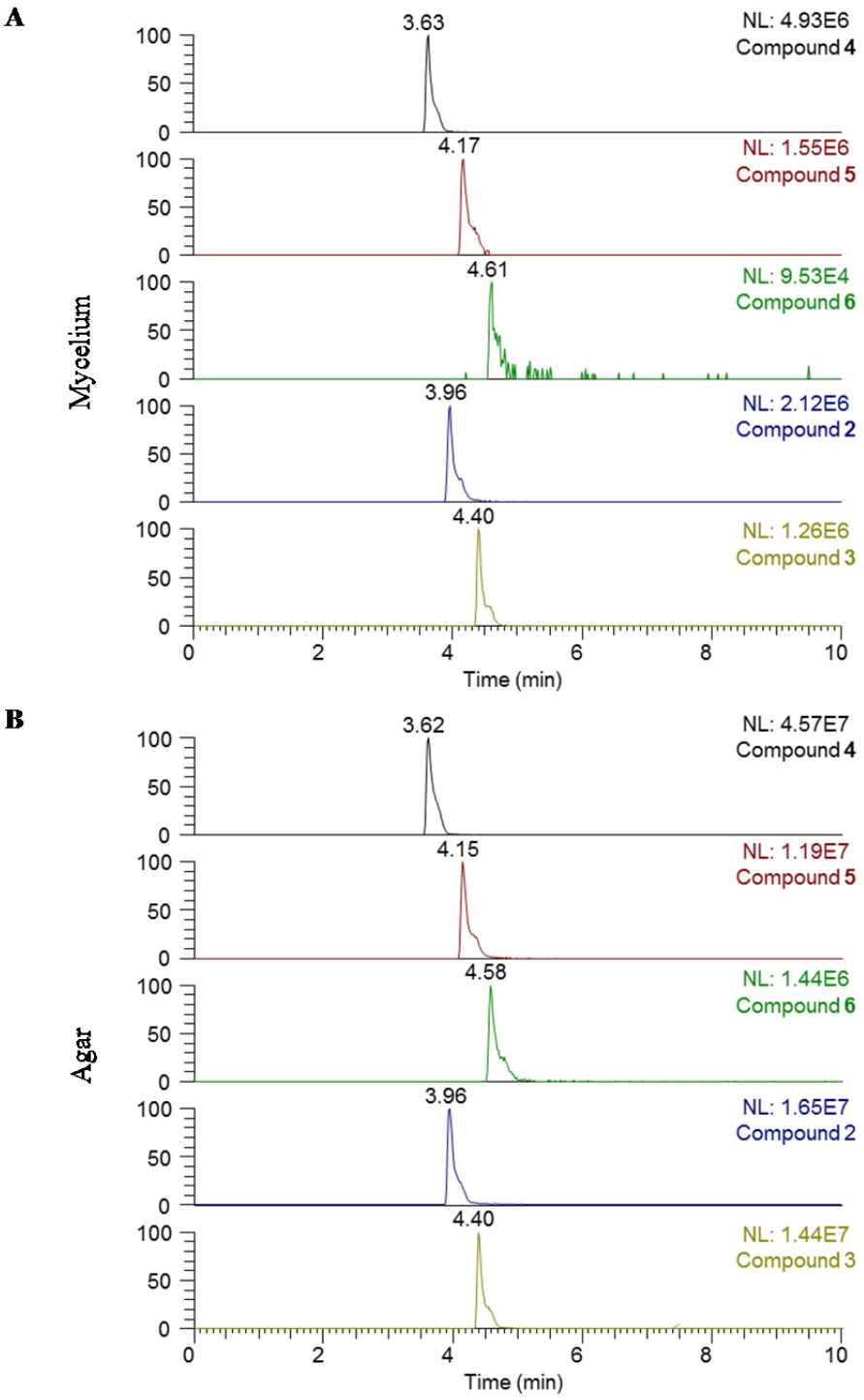

Figure S21. Secondary Metabolites (2-6) of *P. restrictum* After 5.5 Weeks on the (A) Mycelium and (B) Agar.

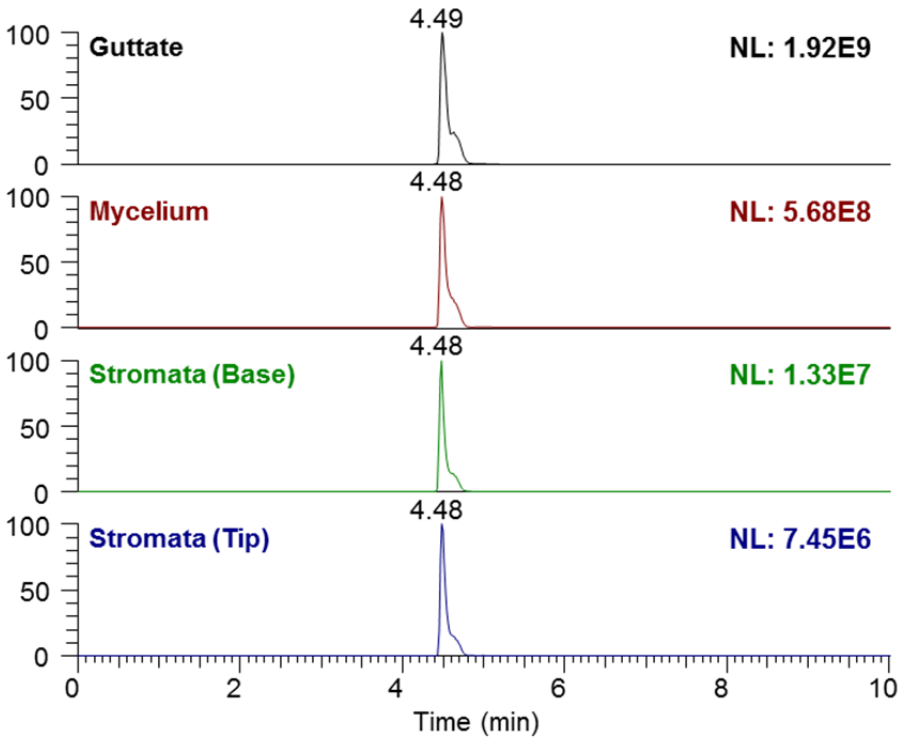

Figure S22. Detection of Griseofulvin (33) on the Surface of a Guttate, Mycelium, and Stromata (Base and Tip) for *X. cubensis*.

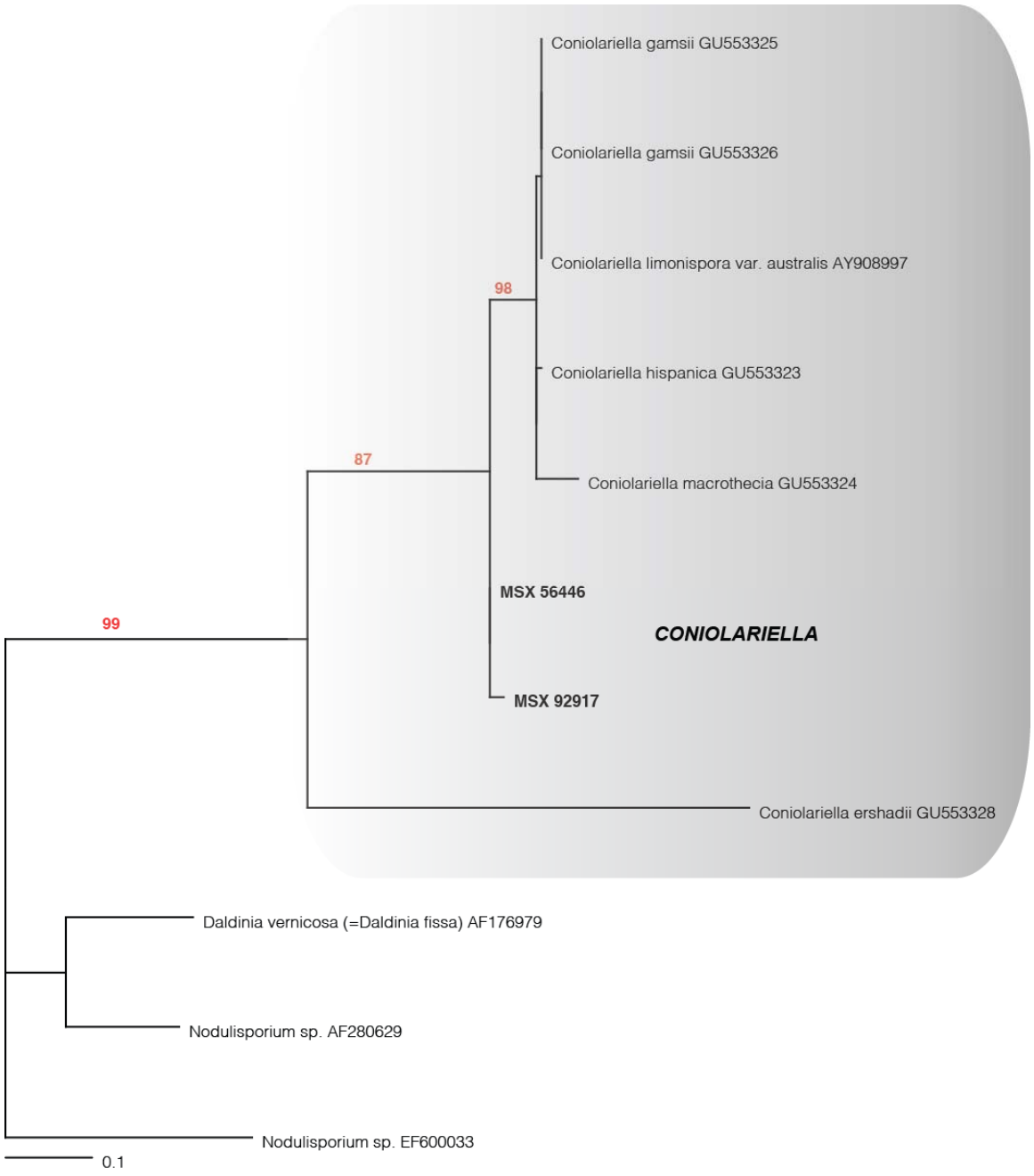

Figure S23. Phylogram of the Most Likely Tree (-lnL = 1766.4) from a PHYML Analysis of 18 Sequences Based on Complete ITS rDNA (467 bp). Numbers refer to PHYML bootstrap support values based on 1000 replicates. MSX strains used in the present study are nested within the *Coniolariella* clade with the type species, *C. gamsii*. The *Coniolariella* clade is highlighted in gray. Bar indicates nucleotide substitutions per site.

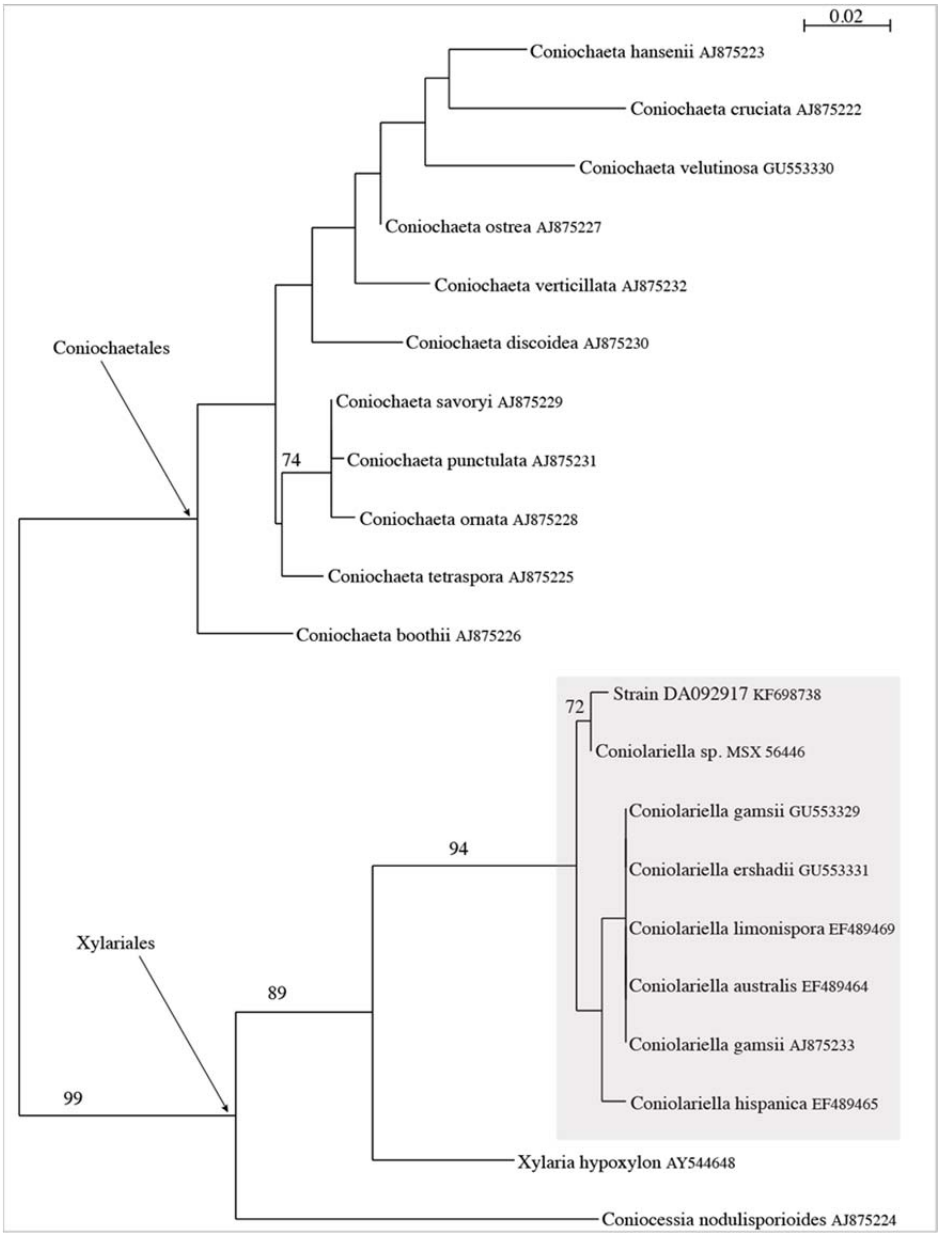

Figure S24. Phylogram of the Most Likely Tree (-lnL = 1461.94) from a PHYML Analysis of 21 Sequences Based on a Portion of the D1/D2 Divergent Domains of the 28SrDNA (396 bp). Numbers refer to PHYML bootstrap support values based on 1000 replicates. MSX56446 nested within the Coniolariella clade with the type species, *C. gamsii*, highlighted in gray.
Note: Gerwick et al. [13] sequenced DA092917_KF698738 and DA056446_KF698737 for D2 region of the 28S, which is a small portion about 300 bp. We compared, MSX56446, which we sequenced for the complete ITS region and partial D1/D2 regions as a single contig using primers ITS4-LR3. We then compared the D2 region of MSX56446 with both DA092917 and DA056446. MSX56446 was <1% different compared to the D2 region of DA092917, but was 16% different compared to D2 region of DA056446. Additionally, the ITS region of both MSX92917 and MSX56446 was identical.

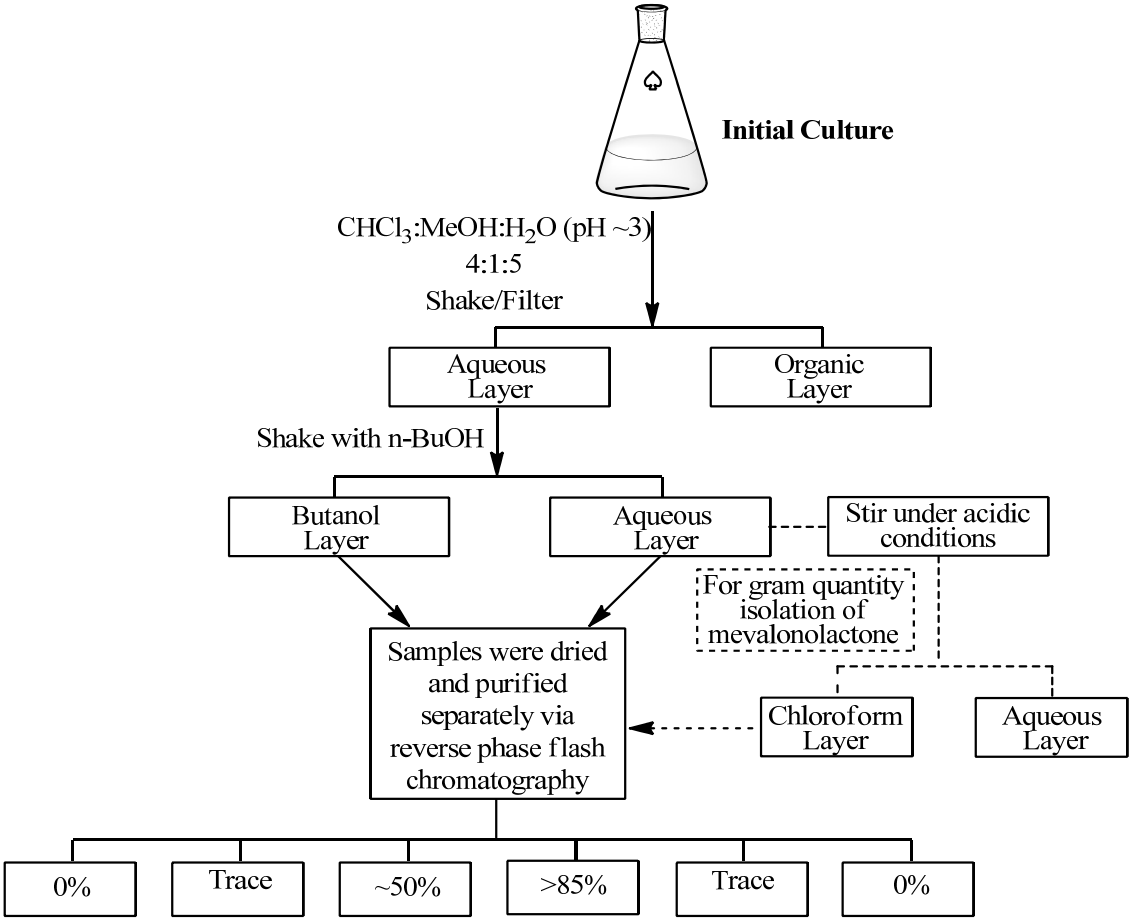

Figure S25. General Procedure for the Extraction, Fractionation, and Initial Chromatography Utilized for the Isolation of Mevalocidin and/or Methylidene Mevalonolactone. The percentages refer to the approximate amount of mevalocidin in each fraction as monitored by ^{1}H NMR. The dashed route is an addition to the isolation procedure to convert mevalocidin to methylidene mevalonolactone.

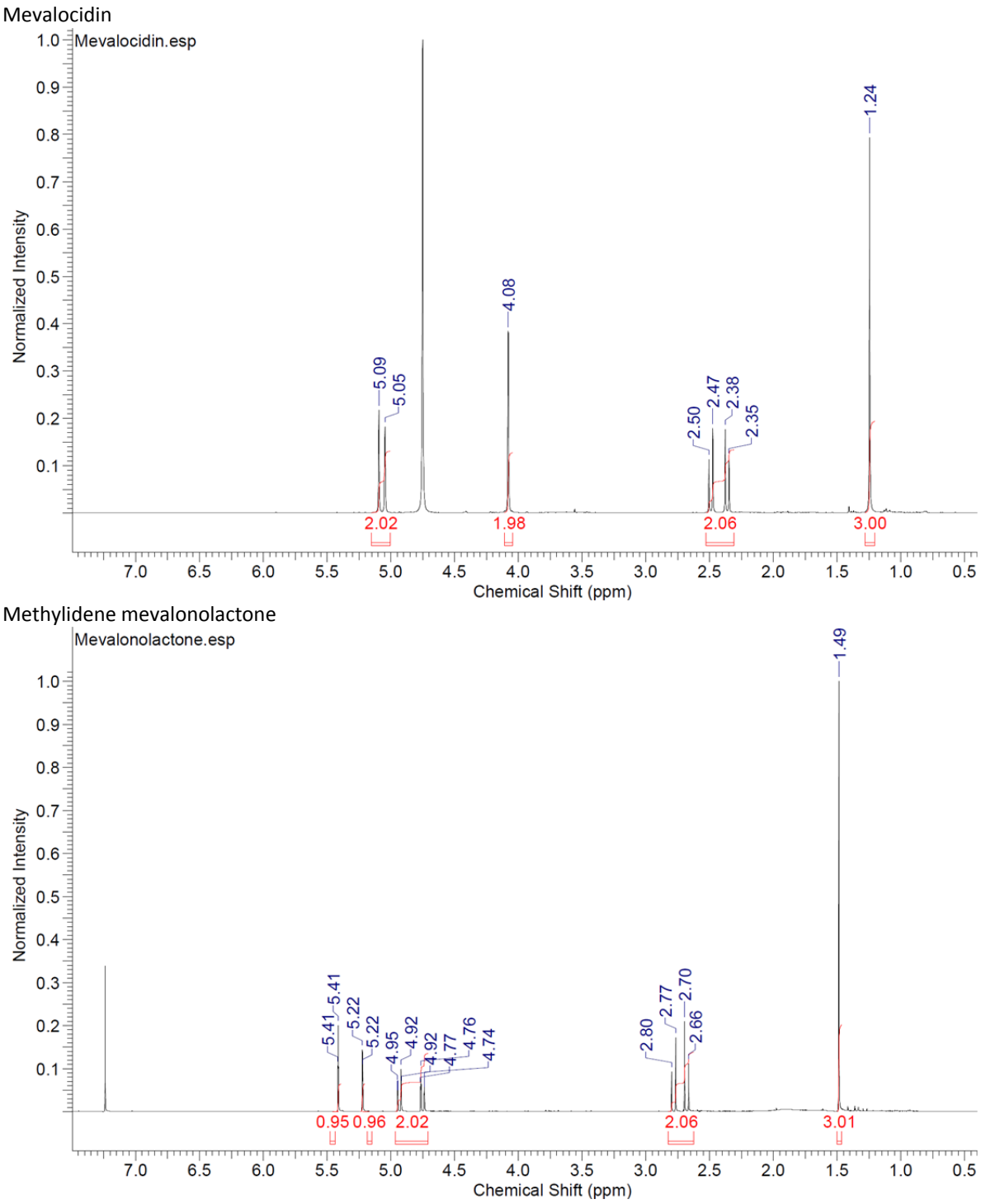

Figure S26. ^{1}H NMR Spectrum of Mevalocidin (39; top) [400 MHz, D_2O]. ^{1}H NMR spectrum of methylidene mevalonolactone (**40**; bottom) [400 MHZ, $CDCl_3$].

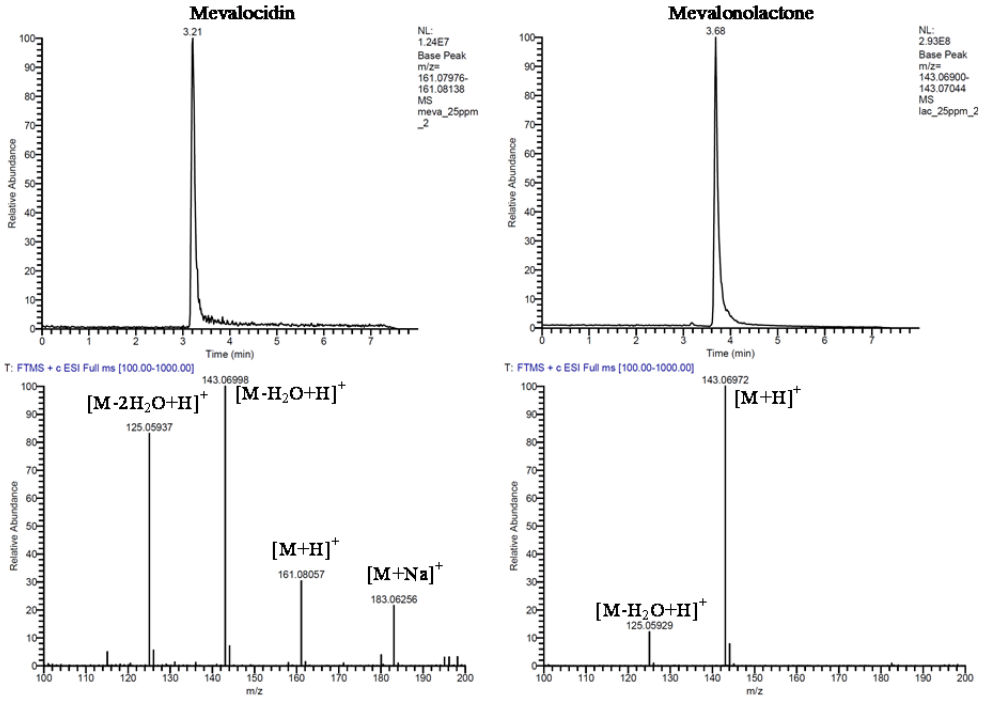

Figure S27. The Base Peak Chromatograms (Top) of Both Mevalocidin (39) and Methylidene Mevalonolactone (40) for Their Accurate (±5 ppm) Molecular Ion Peaks of 161.0808 and 143.0703, Respectively. The accurate mass spectra (bottom) for both compounds with labeled ions including $[M+H]^+$, $[M+Na]^+$, $[M-H_2O+H]^+$, and $[M-2H_2O+H]^+$ where appropriate.

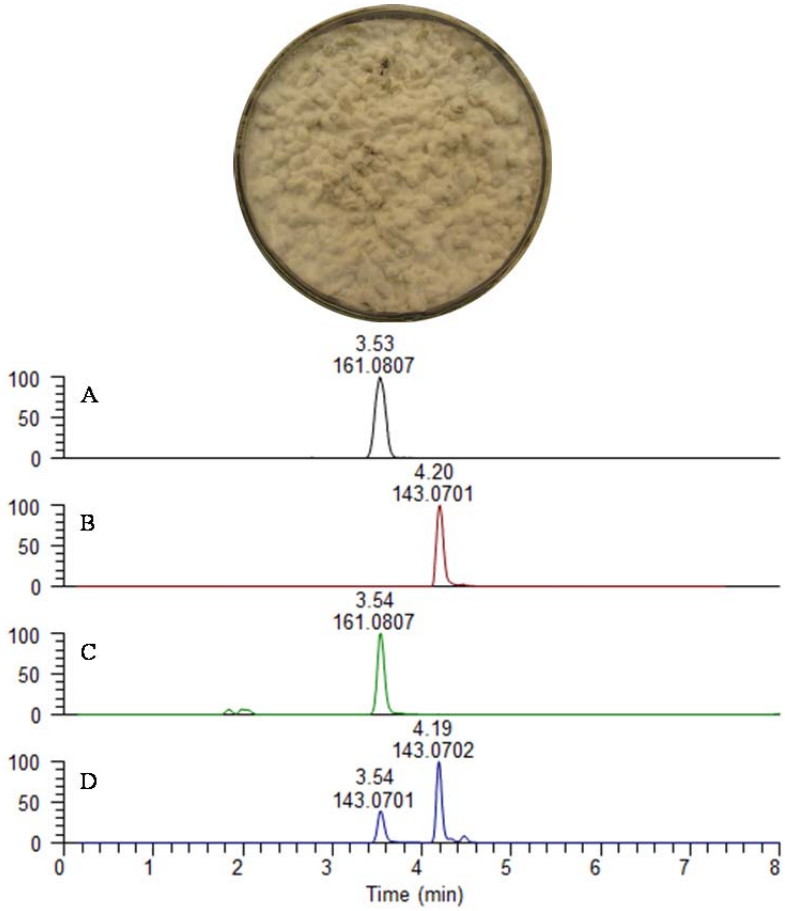

Figure S28. (A) The Extracted Ion Chromatogram (XIC) of *m/z* 161.0808 (±5 ppm) for the Mevalocidin (39) Standard. (B) The XIC of *m/z* 143.0703 (±5 ppm) for the methylidene mevalonolactone (40) standard. The XIC for (C) *m/z* 161.0808 (±5 ppm) and (D) *m/z* 143.0703 (±5 ppm) of the direct fungal culture extraction *via* the droplet–LMJ–SSP. The peak at 3.54 min in chromatogram D is a result of the loss of water on mevalocidin due to in source fragmentation.

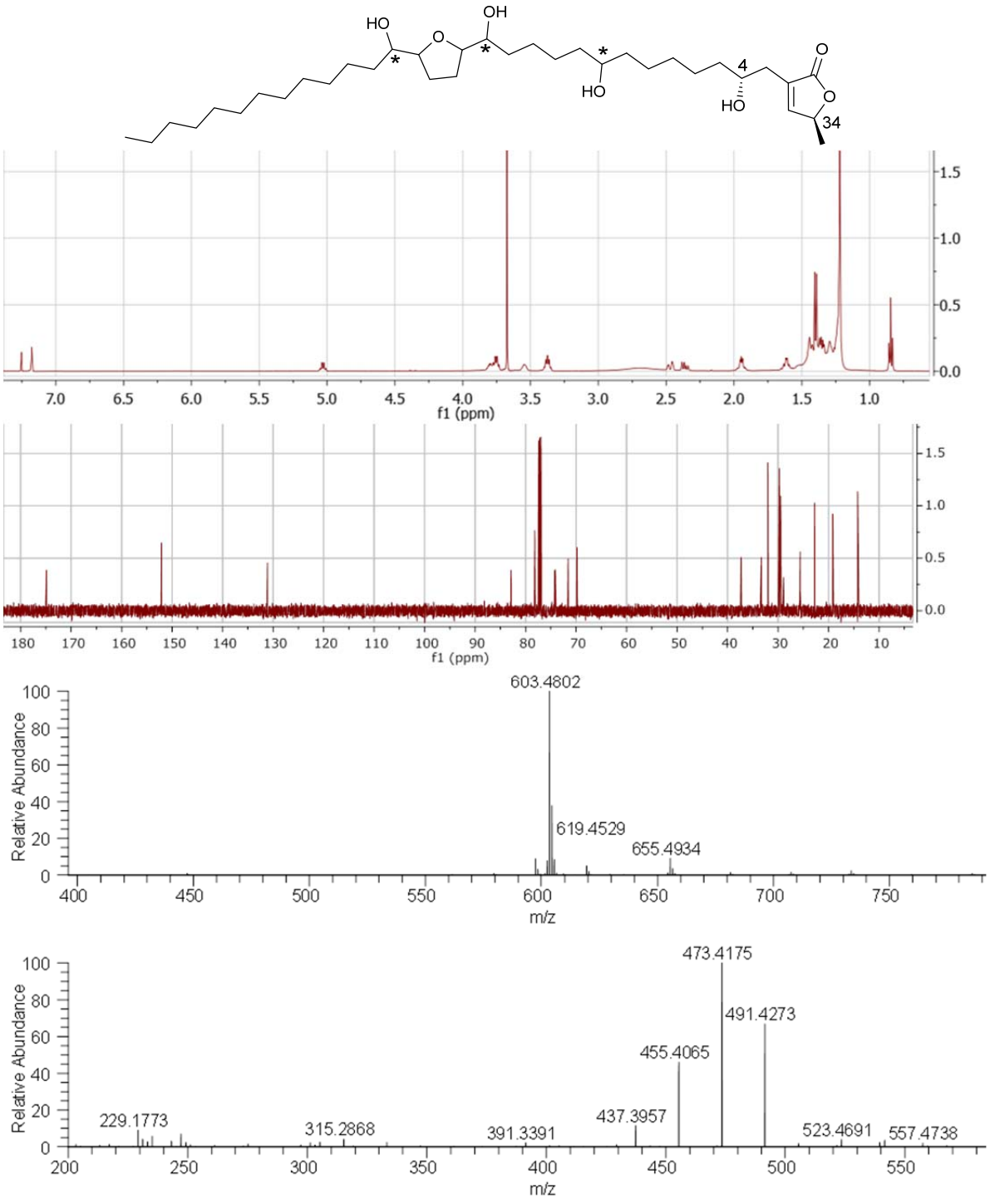

Figure S29. The Structure, the ^{1}H NMR (400 MHz, $CDCl_3$), ^{13}C NMR (100 MHz, $CDCl_3$), HRMS and MS/MS Spectra for Annonacin. The stereocenters were determined by preparing Mosher ester derivatives and the compound was identified as annonacin.[51]

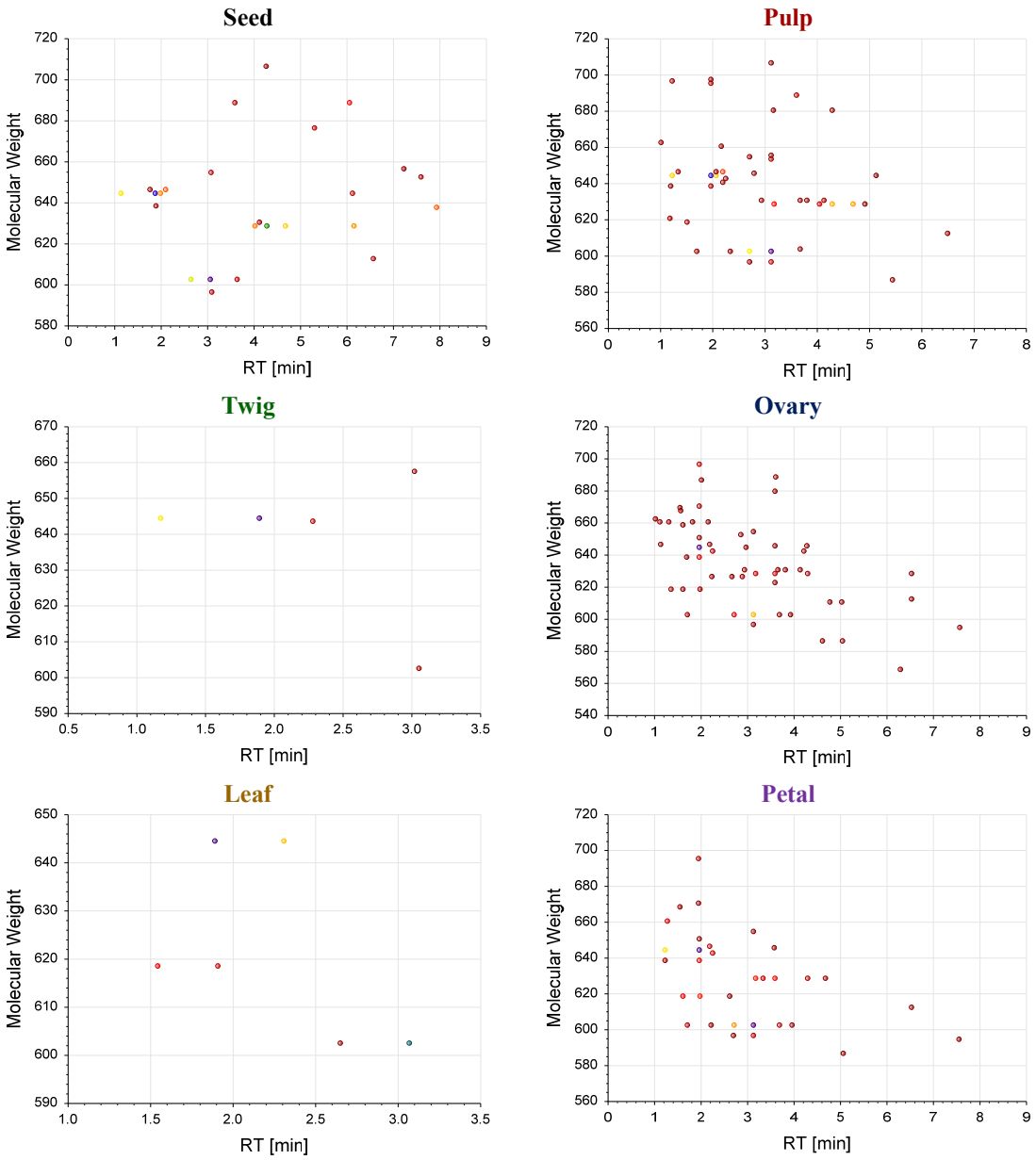

Figure S30. The generated plots of mass defects for *m/z* 603.4807±100 Da with a mass defect of ±25 mDa.

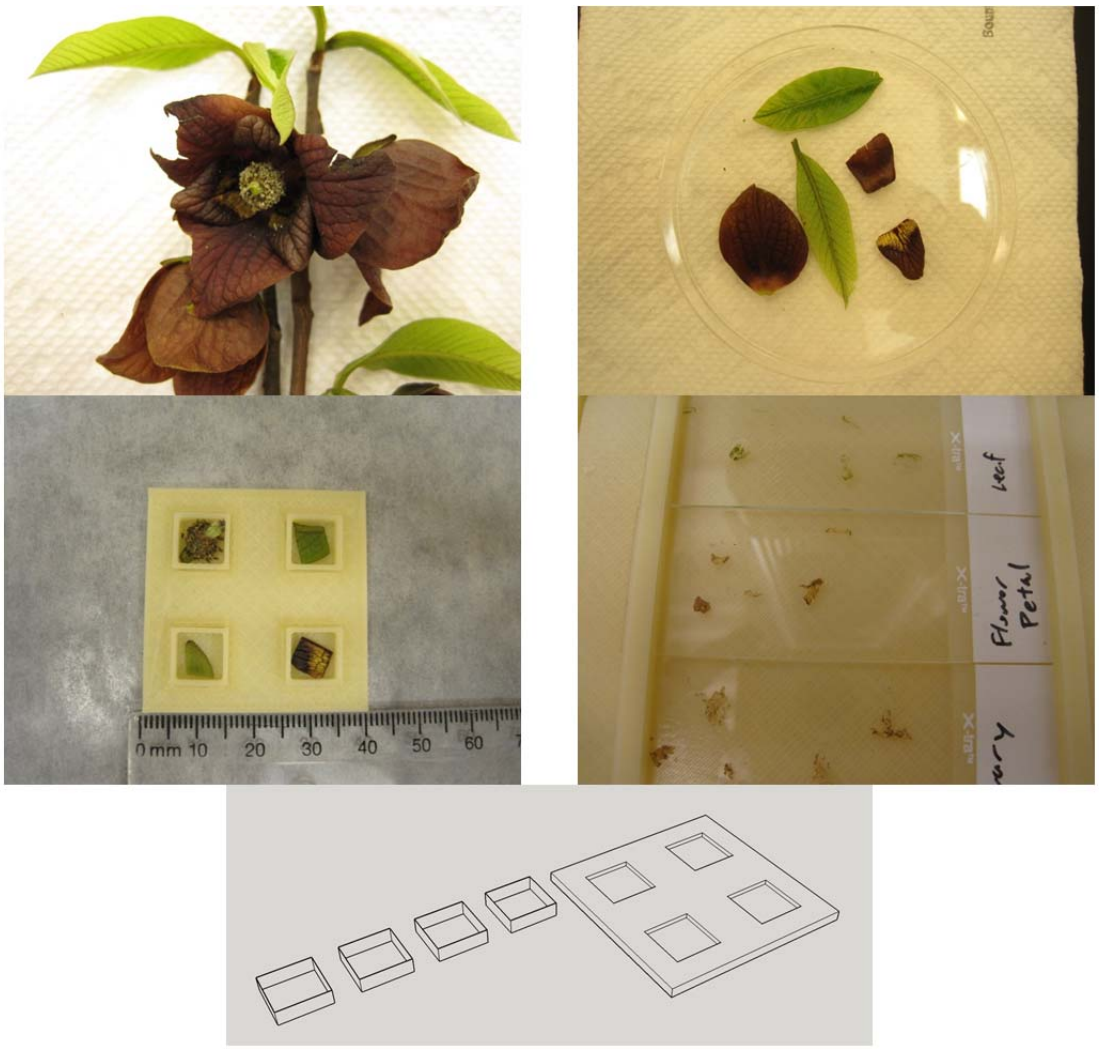

Figure S31. The Leaves and Flowers of *Asimina triloba* as They Were Prepared for Cryotome Cross-Sectioning. A 3D printed tray was created for the application of the optimum cutting temperature (O.C.T.) embedding medium prior to cross-sectioning. This tray was created using SketchUp Make and printed on an F306 3D printer.